UNIVERSITY OF LEON

FACULTY OF BIOLOGICAL AND ENVIRONMENTAL SCIENCES
MOLECULAR BIOLOGY DEPARTMENT
CELL BIOLOGY AREA

THE ROLE OF THE AUTOPHAGY IN THE DIFFERENTIAL VULNERABILITY AND THE INTEGRATED STRESS RESPONSE TO THE CEREBRAL ISCHEMIA

EL PAPEL DE LA AUTOFAGIA EN LA VULNERABILIDAD DIFERENCIAL Y EN LA RESPUESTA INTEGRADA AL ESTRÉS EN LA ISQUEMIA CEREBRAL

Memoria para optar al Grado de Doctor con Mención Internacional que presenta **Diego Pérez Rodríguez**

León, junio de 2017

*'The broadly dynamic nature of life becomes
more and more apparent with every advance
in scientific understanding'*
Yoshinori Ohsumi

*"O verdadeiro heroísmo consiste en trocar
os anceios en realidades, as ideas en feitos"*
Alfonso Daniel Rodríguez Castelao

Memory for opting to the PhD degree

The studies summarized in this memory were made under the supervision of the Professor Dr. Arsenio Fernández López, Área de Biología Celular, Dpto. Biología Molecular, Universidad de León, Spain.

Experimental procedures were performed in the Animal House, the laboratories of Biología Molecular, Medicina, Anatomía y Cirugía Veterinaria and Instituto de Biomedicina in Universidad de León. Complementary assays were made in the Dipartimento di Scienze della Salute, Sezione di Farmacologia Clinica e Oncologia, Università degli Studi di Firenze, Italy, under the supervision of Dr. Domenico Pellegrini-Giampietro.

Index

SUMMARY

Summary

There is an increasing burden of the stroke worldwide and low chances of reducing the mortality and disabilities derived from this pathology. Therefore, there is urgent need for the identification of novel stroke targets for clinical use. Here we investigate autophagy response to ischemia and its relationships with reticulum stress. Our aim is to gain insight into these mechanisms as potentially useful target pathways against stroke.

In the first chapter, a comparative study of the autophagy response in structures with different vulnerability to ischemia (cerebral cortex and hippocampus) was performed using brain slices; an *ex vivo* animal model of stroke. This model allows the comparison of various structures under identical conditions (namely, maintained for 30 min under oxygen and glucose deprivation [OGD], followed by 3 h under normoxic conditions that simulates the reperfusion that follows ischemia *in vivo* [RL, reperfusion-like]). Various markers for both autophagy induction and autophagy flux were measured to characterize the whole autophagy process. We conclude that OGD induces a rapid autophagy response in the cerebral cortex that plays a neuroprotective role, but this could not be demonstrated in the hippocampus. Polyubiquitination levels and control of the glutamate release appear to be involved in the neuroprotective role of autophagy.

The second chapter compares the *in vivo* autophagy response using a global cerebral ischemia model. This model allows the analysis of the *in vitro* response of the structures studied in the previous chapter. The whole autophagy process in response to ischemia was also studied, as well as its links with the unfolded protein response (UPR) induced by endoplasmic reticulum (ER) stress. Both cerebral cortex and CA1 presented an autophagy response that could not be detected in CA3. Autophagy response in CA1 is unable to counteract the ER stress, which leads to the presence of sequestosomes in this structure. The enhancement of UPR increased the autophagy response and eliminates sequestosomes, as well as providing neuroprotection for this area.

The third chapter analyzes the relationships between the UPR-PERK pathway and autophagy in a model of organotypic hippocampal slice culture under OGD and RL

conditions. This model allows the maintaince of concentrations of the UPR modulators and immediate sampling to measure changes in these pathways. OGD-induced eIF2α phosphorylation in this model presented a quick and short response. Moreover, when this phosphorylation was enhanced, there was a rapid and significant neuroprotective effect through the activation of transcription factor 4 (ATF4), which elicits a cytoprotective response called integrated stress response (ISR). This response includes autophagy activation and increases in the anti-oxidant response. In this model, ATF4 neuroprotective response seemed to be mediated by the control of oxidative stress, rather than autophagy in contrast with other hypoxia models. We concluded that the weight of the different components of the integrated stress response depends on the cellular context and the experimental model.

Resumen

El coste social y económico del accidente cerebrovascular (CVA) está continuamente en aumento y hasta la fecha hay pocas posibilidades de reducir la mortalidad o la discapacidad derivadas de esta patología. Por ello la búsqueda de nuevas dianas terapéuticas para su aplicación en clínica constituye una necesidad prioritaria. En el presente estudio se estudió la respuesta autofágica a la isquemia cerebral y su relación con el estrés del retículo. El objetivo era profundizar en el conocimiento de estos mecanismos, que constituyen potenciales dianas terapéuticas contra el CVA.

En el primer capítulo, se realizó un estudio comparativo de la respuesta autofágica entre dos estructuras cerebrales (corteza cerebral e hipocampo) que presentan una vulnerabilidad diferencial a la isquemia. Para ello, se utilizó un modelo *ex vivo* de isquemia basado en el uso de secciones cerebrales. Este modelo permite la comparación de respuestas de diferentes estructuras en idénticas condiciones experimentales (en particular, se utilizaron 30 minutos de privación de oxígeno y glucosa [OGD] seguido de 3 horas en condiciones normóxicas [RL, *reperfusion like*]. Para caracterizar la actividad autofágica se midieron los niveles tanto de marcadores de inducción de autofagia como de sustratos específicos de autofagia (estimando así el flujo autofágico). Los resultados obtenidos permitieron concluir que la OGD induce una respuesta autofágica rápida en la corteza cerebral que no se observó en el hipocampo. El papel neuroprotector de la autofagia en la corteza cerebral parece implicar el control de los niveles de poliubiquitina y de la liberación de glutamato.

El segundo capítulo compara la respuesta autofágica entre estructuras utilizando un modelo de isquemia cerebral global. Este modelo permitió extender los resultados descritos en el capítulo anterior a un modelo *in vivo*. Se analizó tanto la respuesta autofágica a la isquemia como su relación con la respuesta a las proteínas mal plegadas (UPR) inducida por el estrés de retículo endoplásmico. Tanto en la corteza cerebral como en la estructura hipocampal CA1 se observó actividad autofágica que no pudo ser detectada en la región hipocampal CA3. La respuesta autofágica en CA1 no parece suficiente para combatir el estrés de retículo, lo que explica la presencia de

secuestosomas (agregados de proteínas mal plegadas) observados en las neuronas de esta estructura. La activación farmacológica de la UPR incrementó la actividad autofágica, eliminando los secuestosomas y reduciendo el daño isquémico.

El tercer capítulo analiza la relación entre autofagia y la vía PERK de la UPR en un modelo de cultivos organotípicos de hipocampo sometidos a OGD y RL. Este modelo permite controlar la concentración de fármaco que llega a las neuronas y obtener muestras de una forma rápida, lo que permite estudiar diferencias en las respuestas entre tiempos muy cortos. El estudio mostró que la fosforilación de eIF2α (marcador de la activación de la vía PERK) presentó una respuesta rápida y de corta duración. Cuando está fosforilación se mantuvo a lo largo de la RL, se produjo un efecto neuroprotector mediado por ATF4 (a*ctivating transcription factor 4*). Se ha descrito que ATF4 es capaz de producir una respuesta citoprotectora conocida como respuesta integrada al estrés (ISR, *integrated stress response*). La ISR incluye la activación de la autofagia y el aumento de la actividad antioxidante. Al contrario de lo observado en otros modelos de hipoxia, en el modelo aquí utilizado el efecto neuroprotector de ATF4 se debe a una respuesta antioxidante más que a una activación de la autofagia. Esto permitió concluir que el peso específico de los distintos componentes de la ISR depende del contexto celular y del modelo experimental.

ABBREVIATIONS

2VO: 2-vessel occlusion

3-MA: 3-methyladenine

4VO: 4-vessel occlusion

A

AMPA: alpha-amino-3-hydroxy-5-methyl-4 isoxazole propionate

AMPK: Adenosine monophosphate-activated protein kinase

ASK1: Apoptosis signal-regulating kinase 1

ATE: 3-aminopropyl trithoxysilane

ATF2: Activating transcription factor 2

ATF3: Activating transcription factor 3

ATF4: Activating transcription factor 4

ATF6: Activating transcription factor 6

atg: autophagy –related gen

ATP: Adenosine 5'-triphosphate

B

BCL2: B-cell lymphoma 2

BIM: BH3-only protein

BSA: Bovine serum albumin

bZIP: Basic leucine zipper

C

CA1: Cornu Ammonis 1

CA3: Cornu Ammonis 3

CARE: C/EBP-ATF response element

CBF: Cerebral blood flow

CHOP: C/EBP homologous protein

CMA: Chaperon-mediated autophagy

CVA: Cerebrovascular accident

Cvt: Cytoplasm to vacuole targeting

D

DALYs: Disability-adjusted-life-years

DFCP1: Double FYVE domain-containing protein 1

DNP-hydrazone: 2,4-dinitrophenylhydrazone

DNPH: 2,4-dinitrophenylhydrazine

E

eiF2α: Eukaryotic initiation factor 2 α-subunit

EM: Electron microscopy

ER: Endoplasmic reticulum

ERAD: ER associated degradation

ERSE: ER-stress response element

F

FDA: Food and drug admnisnitration agency

FJ-B: Fluorojade-B

G

GABARAPs: gamma-aminobutyric acid receptor-associated proteins

GADD34: grow arrest and DNA damage-inducible protein 34

GCLM: glutamate-cysteine ligase regulatory subunit

GCN2: General control nonderepressible 2 kinase

GRP78/Bip: Glucose-related protein 78/binding inmunoglobulin protein

GRP94: Glucose-related protein 94

GSA: Glucose induced selective autophagy

H

HMOX1: Heme oxygenase 1

HRI: Heme-regulated eIF2α kinase

I

IL-1β: Interleukin-1β

IP₃PR: Inositol 1,4,5-triphosphate receptor

IRE1: Inositol requiring enzyme 1

J

JIK: c-jun-N-terminal-inhibiting kinase

JNK: c-jun kinase

K

KEAP1: Cullin3-ubiquitin E3 ligase complex adaptor protein

L

LAMP 1/2: Lysosome-associated membrane glycoprotein 1/2

LC3: Microtubule associated protein 1 light chain 3

LDH: Lactate dehydrogenase

LIR: LC3 interacting region

M

MCAO: Middle cerebral artery occlusion

MIQE: Minimal information for publication of quantitive real-time PCR experiments

MMP-9: Matrix metalloproteinase-9

MPTP: Mitochondrial permeability transition pore

MRI: Magnetic resonance imaging

mTOR: Mammalian target of rapamycin

mTORC1: mTOR complex 1

MTT: Thiazolyl blue tetrazolium bromide

N

NF-κB: Nuclear factor kappa-light-chain-enhancer of activated B cells

NMDA: N-methyl-D-aspartate

NOS: Nitric oxide synthase

NQO1: NAD(P)H quinone dehydrogenase 1

NRF2: Nuclear factor (erythroid-derived 2)-like 2

NVU: Neurovascular unit

O

OGD: Oxygen and glucose deprivation

OHSC: Organotypic hippocampal slice culture

ORF: Open reading frame

P

P62/SQSTM1: Sequestosome 1

PAG: Peroxisome degradation via autophagy

PAZ: Pexophagy zeocin-resistant

PB1: Phax and Bem1 domain

PBS: 50 mM phosphate buffered saline

PDD: peroxisome degradation deficient

PDI: Protein disulfide isomerase

PE: Phosphatydil ethanolamine

PERK: Double-stranded RNA-activated protein kinase-like ER kinase

PI3K: Phosphatidil inositol 3 phosphate kinase

PI3P: Phosphatidil inositol 3 phosphate

PKR: Protein kinase R

PP1: Protein phosphatase 1

PSI: Protein synthesis inhibition

PVDF: Polyvinylidene difluoride

R

RL: Reperfusion-like

RT-qPCR: Real-time quantitative polymerase chain reaction

rt-PA : Recombinant tissue plasminogen activator

RyR: Ryanodine receptor

S

SDS: Sodium dodecyl sulphate

SEF: Second energy failure

SERCA: Sarcoplasmic/endoplasmic reticulu calcium ATPase pump

SNARE: Soluble N-ethylmaleimide-sensitive factor activating protein receptor

SOD: Superoxide dismutase

T

TBS: 50 mM Tris buffered saline pH 7.4

TBST: 0.2% Tween-20 in TBS

TIA: Transient ischemic accident

TRAF2: Tumor necrosis factor receptor associated factor 2

U

UBA: Ubiquitin-associated domain

UPR: Unfolded protein response

UTR: Untranslated region

UVRAG: UV radiation resistance-associated gene

V

Vps34: Vacuolar protein sorting 34

W

WHO: World health organization

X

XBP1: X-box binding protein 1

INTRODUCTION

Basics of stroke

According to the World Health Organization (WHO) criteria, the definition of **cerebrovascular accident (CVA)** or **stroke** is 'the rapid developing clinical signs of focal (at times, global) disturbances of cerebral function, lasting more than 24 h or leading to death with no apparent cause other than that of vascular origin'. Additionally, WHO defines **Transient Ischemic Accident (TIA)** as 'a brief episode of neurologic dysfunction caused by focal brain or retinal ischemia, with clinical symptoms typically lasting less than 1 h, and without evidence of acute infarction'.

Costs of stroke

In developed countries, stroke is the second leading cause of death, the main cause of permanent disability, and the second most common cause of dementia after Alzheimer's disease (Olesen et al., 2012). However, the burden of a specific disease is better estimated by the disability-adjusted-life-years (DALYs) (Murray, 1994), which takes into account the years of healthy life lost both by premature mortality and by disability. In this regard, stroke is the third leading cause of DALYs worldwide, only surpassed by ischemic heart disease and respiratory infections (Murray et al., 2012). Overall, stroke has a strong negative impact on quality of life, since it results in hemiplegia, facial paralysis, aphasia, and other temporal or permanent disabilities that affect walking, talking, speech, balance, co-ordination, vision, spatial awareness, swallowing, bladder control, and bowel control. Additionally, almost 50% of the patients suffer from depression in the first year after stroke and 30–92% suffer from fatigue (Béjot et al., 2015). Despite rates of stroke mortality decreasing in the last two decades, the absolute number of people who suffer a stroke every year has increased, as well as the stroke-related deaths and the overall burden of stroke (DALYs lost) (Feigin et al., 2015; Hankey, 2013).

In Spain, stroke represents 7% of the total number of deaths, making it the third most common cause of mortality, behind cancer and heart diseases (**Table 1**).

Table 1. Mortality causes in Spain in 2014. (Instituto Nacional de Estadística [INE] 2017)

Range	Cause of death	Death number	% of deaths
	All causes	*395.830*	*100*
1	Cancer	106.269	26.9
2	Heart attack	79.707	20.2
3	Cerebrovascular diseases	27.579	7
4	Chronic diseases of the lower respiratory tract	15.546	3.9
5	Alzheimer disease	14.022	3.5
6	Unintentional accidents	10.313	2.6
7	Diabetes mellitus	9.625	2.4
8	Pneumonia and influenza	8.825	2.2
9	Nephritis, nephrosis and nephrotic syndrome	6.556	1.7
10	Hypertensive disease	4.533	1.1
	Rest of causes	98563	28.6

Social and sanitary costs of stroke have been estimated to account for 6% of the total Spanish Health expenditure (Spanish Neurology Society, 2015). The total cost per patient in Spain is estimated as €13,329 (€3,461 direct medical costs, €9,032 direct non-medical costs, and €835 indirect costs, **Figure 1**) (Parés-Badell et al., 2014).
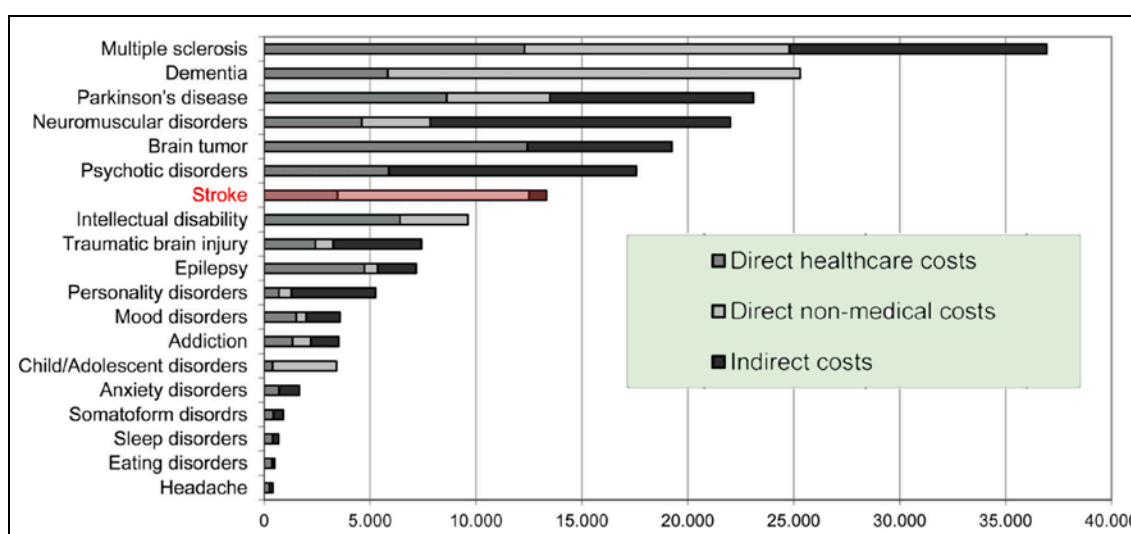
Figure 1. Per patient costs by disorder in Spain in 2010 (*modified from Parés-Badell et al., 2014*)

Risk factors and stroke prevention

CVAs can appear at any age, but their incidence starts to be relevant from the age of 60 and exponentially increases from the age of 65 (**Figure 2**). This makes aging as the most important risk factor for stroke (Baltan et al., 2008; Broderick, 2004; Seshadri and Wolf,

2007). However, other main risk factors for stroke are directly related to lifestyle habits. The INTERESTROKE study for 2016, carried out in 32 countries including more than 25,000 stroke patients, revealed that 10 potentially modifiable risk factors account for 88.1% of all strokes: hypertension, smoking, high waist-to-hip ratio, unhealthy diet, insufficient regular physical activity, diabetes, excessive alcohol consumption, psychosocial factors such as stress, cardiac pathologies, and high ratio of proatherogenic lipoproteins measured either as apolipoprotein B (ApoB) to ApoA1 or the cholesterol ratio (total cholesterol:high-density lipoprotein cholesterol) (O'Donnell et al., 2016).
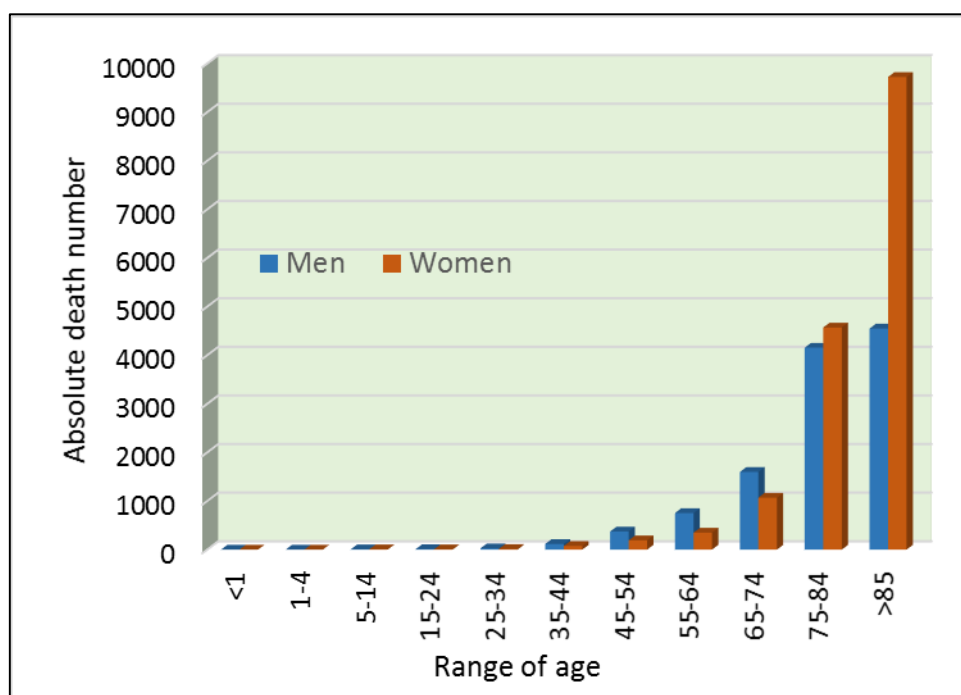
Figure 2. Absolute deaths in 2014 in Spain caused by cerebrovascular diseases (INE, 2017)

Types of human stroke

Two main types of stroke (depending on their origin) are usually distinguished: hemorrhagic and ischemic strokes. **Hemorrhagic stroke** is defined as the spontaneous leaking of blood into the brain and extravascular spaces and can be elicited by several pathologies, such as hypertension, vascular malformations, and amyloid angiopathy or coagulation problems (Mayer, 2003). This type of CVA accounts for 15% of all strokes and presents the highest mortality and disability rates. **Ischemic stroke** accounts for approximately 85% of all strokes and is defined as a blood flow decrease in the brain

tissue. Ischemic stroke can be further subdivided into three categories: thrombosis, embolism, and decreased systemic perfusion (Caplan, 2009).

1. <u>Thrombosis</u> is the obstruction of blood flow by a localized occlusive process within one or more blood vessels. The lumen of the vessel is narrowed or completely occluded by alterations in the vessel wall or by an overlaid clot formation. Atherosclerosis is the most common cause of thrombosis (Elkind, 2010).

2. <u>Embolism</u> is defined as the blockage of a blood vessel by a material formed elsewhere, in contrast to thrombosis where the blockage is originated in the blocked vessel (Broussalis, Killer, et al., 2012a). The material comes from the neighborhood of the occlusion, especially from the heart, and have multiple origins, such as pieces of atheromatous plaque, clots, fibrin, fat, air, and tumors (Dudney and Elliott, 1994).

3. <u>Decreased systemic perfusion</u> is the reduction in blood flow to the brain caused by low blood pressure. The most common causes of decreased systemic perfusion are heart failure (due to myocardial infarction or arrhythmia) and systemic hypotension (due to blood loss or hypovolemia) (Jovićević et al., 2010). Although hypoperfusion affects the whole brain, the greatest damage appeared in the watershed area, localized between the territories of the major cerebral and cerebellar arteries.

According to the size of the brain region affected, ischemic stroke is considered as **focal** when the reduction in blood supply is limited to a discrete region in the brain or **global** when blood flow decreases affect the whole brain (Traystman, 2003). Thrombotic and embolic strokes can be focal or multifocal, while decreased systemic perfusion is usually a global ischemia.

Current stroke treatments

Stroke treatments aim for a rapid recovery of cerebral blood flow to the damaged area and the neuroprotection of the neural parenchyma after the ischemic insult. To date, the most effective treatment of the ischemic stroke is rapid thrombus removal, either

by endovascular intervention or using drug-mediated thrombolysis. The mechanical intervention for removing the clot is intra-arterial. Two types of devices are used: **clot retrieval devices** that physically grasp the cerebral thrombus and pull it out of the cerebral circulation; and **suction thrombectomy devices** that aspirate occlusive material from the vessel (Broussalis, Killer, et al., 2012a).

For thrombolysis, the **recombinant tissue plasminogen activator (rt-PA)** is the only drug approved by the US Food and Drug Administration (FDA) for the treatment of acute stroke (Hacke et al., 1995). However, this treatment is only effective in the first 4–5 h after stroke onset. However, the use of this molecule is currently controversial due to its deleterious effects on neural N-methyl-D-aspartate (NMDA) channels promoting excitotoxicity (Nicole et al., 2001). In addition, rt-PA upregulates plasma matrix metalloproteinase-9 (MMP-9) levels, which is correlated with haemorrhagic conversion after thrombolysis (Ning et al., 2006).

The basic aim of **neuroprotection** is to prevent the death of brain cells, and the main targets explored are related to the ischemic cascade events (O'Collins et al., 2006). However, most of the promising molecules in animal models of stroke have failed in clinical trials. Several hypotheses have been put forward to account for this (Broussalis et al., 2012b):

1. <u>Time window</u>*:* In animal models, the neuroprotective drug is administered shortly after, or even before, the onset of stroke, contrasting with longer times between stroke onset and drug administration in patients.
2. <u>Outcome measurement</u>*:* Monitoring of the damage evolution in preclinical trials is shorter and use magnetic resonance imaging (MRI) or histology, in contrast with long-term monitoring in patients mainly based on behavioral tests such as Rankin Scale and Bartel Index.
3. <u>Differences in comorbidities</u>*:* Animal models use young healthy animals, which is in contrast with normal aged patients, which usually present additional pathologies (comorbidities) and are under different medications.

4. <u>The diversity of stroke types</u>: Models of stroke do not completely mimic the pathophysiological complexity in patient stroke types, which also has higher variability in extent and severity.

5. <u>Differences in physiological variables</u>: Laboratory animals are tightly controlled regarding blood pressure, temperature, and metabolic factors, which is not the case for human patients.

Thus, the high incidence of stroke, its social and medical costs, and the lack of effective therapies have created an urgent need for effective neuroprotective therapies.

Experimental models of stroke

Experimental models of stroke allow us to gain insight into the pathophysiology mechanisms of ischemia, to look for possible therapeutic targets, and to check the neuroprotective effects of different compounds as potential medicines. The main requirement in the experimental models of stroke is obtaining reproducible lesions in the brain, with little variability among individuals. In this regard, a strict control of the physiological parameters involved in the tissue damage (e.g., the age and sex of animals) is crucial (Prieto-Arribas et al., 2011, 2008).

Two main categories are considered in experimental stroke models: *in vivo* assays, closer to human stroke and more used for studies of damage or neuroprotection; and *ex vivo* assays, using tissues or cells, used to gain insight into the specific mechanism since they allow a strict control of experimental conditions, such as oxygen and glucose levels, temperature, and drug concentration.

For this study, various models of global ischemia (both *in vivo* and *ex vivo*) were used. ***In vivo* models of global ischemia** are usually considered as complete or incomplete ischemia. Complete ischemia is defined as a complete stop of the blood flow into the brain, whereas, in incomplete ischemia, global blood flow is severely reduced to levels insufficient to maintain cerebral metabolism and function (Traystman, 2003). There are multiple models of **complete global ischemia**, including:

1. Cardiac arrest: This model of cardiac arrest is performed by ventricular fibrillation or cardioplegic agents and is usually followed by cardiopulmonary resuscitation (Hossmann and Hossmann, 1973; Kofler et al., 2004).

2. Aortic occlusion: To perform this model, simultaneous clamping of the aorta and inferior cava vein is carried out, thus blocking blood flow through the three major vessels supplying the brain (Jackson and Dole, 1979).

3. Neck cuff: This model consists of the use of a neck tourniquet or an inflatable neck cuff. In this model, the vertebral arteries, encapsulated by vertebrae, must be occluded separately (Kabat and Schadewald, 1941; Siemkowicz and Hansen, 1978).

4. Decapitation: This model is carried out by connecting the head to an extracorporeal perfusion system (Hinzen et al., 1972).

The most common models of **incomplete global ischemia** are:

1. 2-vessel occlusion (2VO): The 2VO model consists of the bilateral common carotid artery occlusion coupled with systemic hypotension, reached either by bleeding or by pharmacological agents (Eklöf and Siesjö, 1972; Smith et al., 1984).

2. 4-vessel occlusion (4VO): The 4VO model is performed by the bilateral common carotid artery occlusion after the electro-cauterization of the vertebral arteries (Pulsinelli and Brierley, 1974).

Ex vivo **models of ischemia** are based in the incubation of brain sections in physiological solutions in the absence of both oxygen and glucose; a condition referred to as oxygen and glucose deprivation (OGD), which mimics the main effects of the lack of blood supply to the brain. *In vivo* ischemia is followed by recanalization and reperfusion of blood into the tissue, which is mimicked by the return of tissues to normoxic and normoglycemic conditions. This condition is usually referred to as reperfusion-like (RL) (Dos-Anjos et al., 2009). Some *ex vivo* models can only be performed in short-time experiments (e.g., **acute brain slices**) (Whittingham et al., 1984). Longer experiments require some type of stabilization, such as the model of **organotypic hippocampal cultures** (Vornov et al., 1994). The main advantages of *ex vivo* models compared to *in*

vivo models are: 1) better control of parameters affecting to ischemic injury; 2) easier analysis of the molecular pathways activated during and after the ischemic insult; 3) lower costs; 4) lower number of animals used; and 5) less ethical concerns. Compared with cell culture, the *ex vivo* assay presents the advantage of having a similar structure and connections to those observed in the *in vivo* models. However, *ex vivo* models also present some disadvantages, such as: 1) intrinsic tissue damage during the process of obtaining sections; 2) differences between the incubation medium and the endogenous extracellular medium; 3) absence of blood flow and blood brain barrier protection; 4) absence of oedema pressure; and 4) limitations in the age of the animals useful to obtain proper sections.

Pathophysiology of stroke

The brain has a high demand for oxygen and glucose which makes it extremely sensitive to decreases in blood flow. In an ischemic stroke, cerebral blood flow (CBF) decreases from physiological values (50 – 60 ml/100 g/min) to less than 7 ml/100 g/min (Baron, n.d.). Brain areas under this reduction suffer a quick and irreversible cellular damage, mainly mediated by necrosis, and are usually referred to as the **ischemic core** (Mehta et al., 2007) (**Figure 3**).
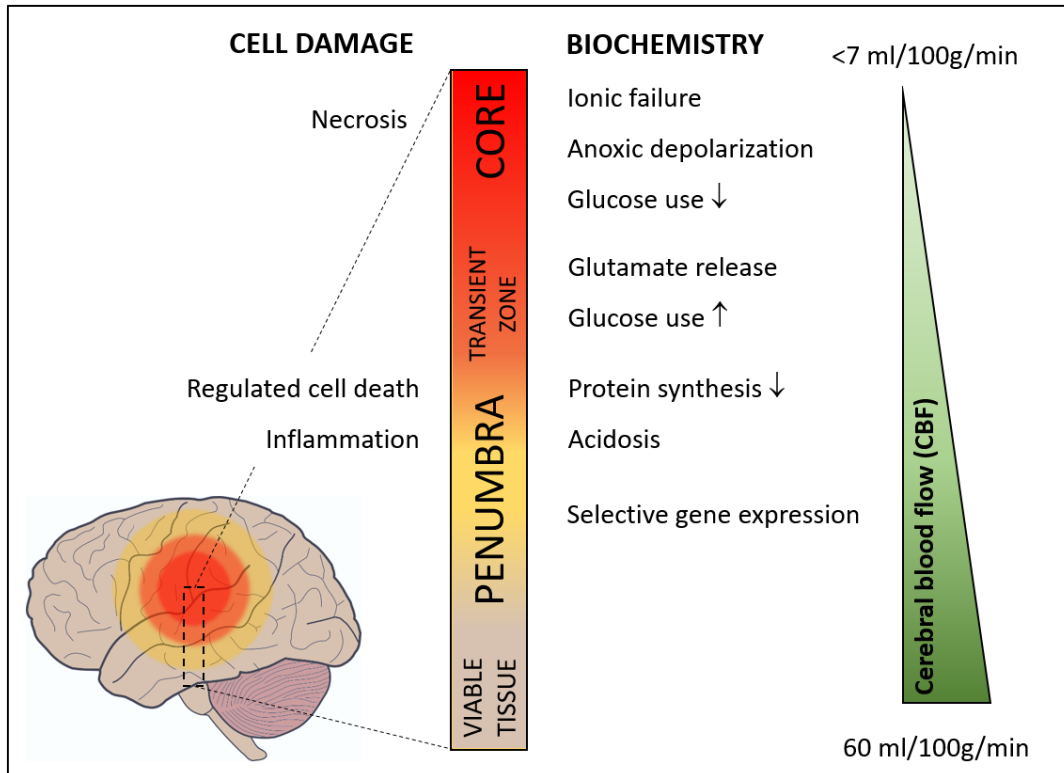
Figure 3. Brain damage areas after ischemic stroke (*modified from Dirnagl et al., 1999).*

The ischemic core is surrounded by an area called the **ischemic penumbra (Figure 3)**. Ischemic penumbra is defined as the region of ischemic tissue potentially destined for infarction but not yet irreversibly injured (Ma et al., 2011). CBF in the ischemic penumbra ranges from 7 to 22 ml/100 g/min, which gives the tissue enough oxygen to keep metabolically active (Mehta et al., 2007). If ischemic penumbra is not controlled, most of it becomes irreversibly ischemic in the first days after ischemic insult (Hossmann, 1994). The mechanisms of cell damage in the ischemic penumbra are mainly mediated by regulated cell death subroutines. The recovery of the ischemic penumbra is considered the main target for acute stroke therapies (Ma et al., 2011).

The ischemic cascade

The decrease in blood flow results in an energy depletion that elicits a complex, coordinated, and interrelated cascade of molecular events (**Figure 4**) that affects several cellular processes involved in cellular homeostasis and can result in different types of cell death, either necrotic or regulated cell death (Liu et al., 2012; Mehta et al., 2007; Pundik et al., 2012). Ischemia depletes adenosine 5'-triphosphate (ATP) levels within

minutes and low oxygen levels activate anaerobic glucose metabolism, triggering the accumulation of lactic acid (Nowicki et al., 1988). **Lactic acidosis** during the early ischemic stages inhibits oxidative phosphorylation, thus contributing to energy failure and increasing both cytotoxic oedema and intracellular Ca^{2+} concentrations (Kimelberg, 2005). Low energy levels impair the function of membrane ATP-dependent Na^+/K^+ pumps, resulting in a massive influx of Na^+, efflux of K^+, and membrane depolarization. In turn, the membrane depolarization opens voltage-sensitive Ca^{2+} channels, which triggers a **massive release of glutamate** to the extracellular space. This accumulation of glutamate results in the activation of glutamate receptors, mainly the ionotropic receptors N-methyl-D-aspartate (NMDA), alpha-amino-3-hydroxy-5-methyl-4 isoxazole propionate (AMPA), and kainate glutamate receptors, which results in an additional Ca^{2+} influx, thus enhancing cell injury (Mehta et al., 2007).

The massive influx of Ca^{2+} disrupts the mitochondrial electron transport chain and opens the **mitochondrial permeability transition pore (MPTP)** (Liu et al., 2009). The massive opening of the MPTP is considered a non-return point in the neuronal death pathway and results in mitochondrial swelling, inner membrane depolarization, uncoupling of oxidative phosphorylation, increased superoxide radical (O_2^-), and production and release of pro-apoptotic proteins (cytochrome c, apoptosis inducing factor-AIF- and caspases) (Sims and Muyderman, 2010). High levels of cytosolic Ca^{2+} also promotes the activation of nitric oxide synthases (NOS) and the release of nitric oxide (NO), which results in the formation of O_2^-, peroxynitrite ($ONOO^-$), and hydroxyl (OH^-) radicals (Beckman et al., 1990). The increased free radical formation, together with the reduction of energy-dependent scavenger enzymes, leads the cell to this unbalanced state, called **oxidative stress**. Oxidative stress damages all the cell components, protein, lipid and nucleic acids, which in turn exacerbates the cell stress (Karsy et al., 2017; Slemmer et al., 2008).
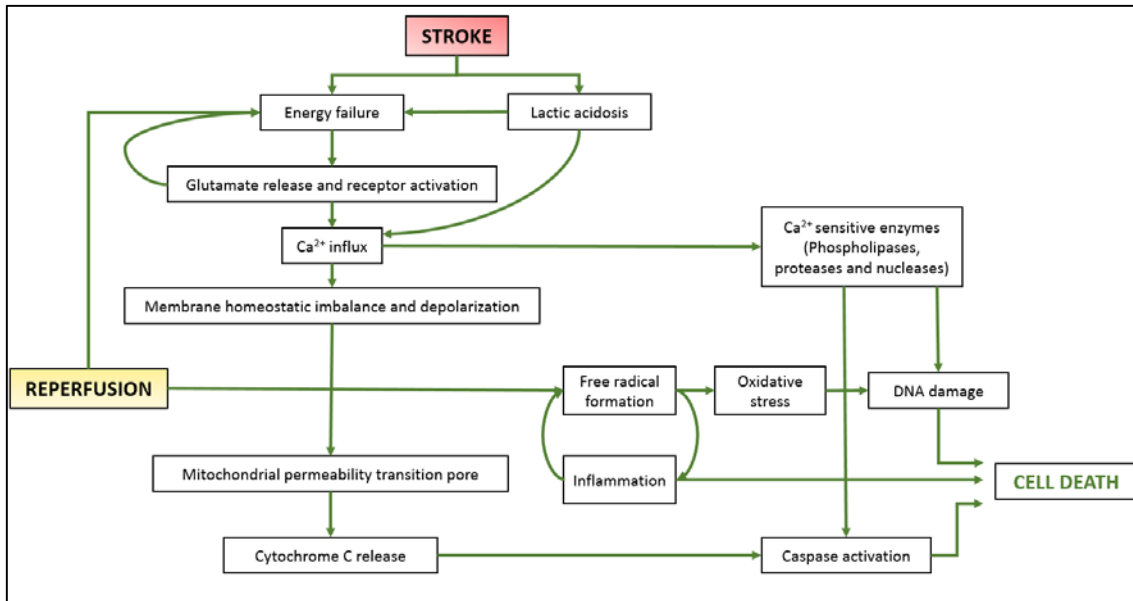
Figure 4. Schematic view of ischemic cascade (*modified form Mehta et al., 2011*)

High concentrations of Ca^{2+} also activate proteases, lipases, and endonucleases, which lead to the disruption of the cell membrane, cytoskeleton, and the genomic DNA. Protease activation plays a critical role in triggering different **subroutines of regulated cell death**, such as apoptosis, necroptosis, and autophagic cell death (Fakharnia et al., 2017; Mehta et al., 2007; Shi et al., 2012; Wang et al., 2011; Zhu et al., 2005).

Free radicals and Ca^{2+} also induce pro-inflammatory cytokines, chemokines, endothelial cell adhesion molecules, and pro-inflammatory genes, leading to a long-term inflammatory response (del Zoppo et al., 2000). All components of the neural parenchyma are involved in this inflammatory response, which leads to the permeability of the blood-brain barrier, allowing the infiltration of leukocytes into the brain (Pundik et al., 2012).

Reperfusion restores cerebral blood flow, which is obligatory for the tissue survival. However, reperfusion enhances the tissue damage since it provides oxygen as a substrate for several enzymatic oxidation reactions that produce ROS and mitochondrial dysfunction. In fact, reperfusion leads to a transient mitochondrial impairment causing a secondary energy failure (SEF) (Pundik et al., 2012). Reperfusion also increases prostaglandin synthesis and inflammation (Fraser, 2011).

Selective vulnerability of hippocampal CA1 pyramidal neurons

One of the unsolved paradigms in cerebral ischemia is the higher vulnerability of Cornu Ammonis 1 (CA1) pyramidal neurons, which, together with some hilar neurons, are considered the most sensitive neurons of the whole forebrain to the ischemic insult (Sanganalmath et al., 2017). In this regard, models of transient global brain ischemia carried out in gerbil, mouse, and rat show a predominant damage in the CA1 hippocampal area (Birch et al., 1991; Hatakeyama et al., 1988; Pulsinelli et al., 1982), which correlates with the findings obtained in post-mortem analysis of human brains suffering from cardiac arrest (Petito et al., 1987).

Multiple molecular studies have been carried out with the aim of explaining the mechanisms involved in the selective vulnerability of CA1 neurons. The **neuronal theory** assumes that the disruption of blood flow equally affects all hippocampal neurons, and differential vulnerability is dependent on intrinsic differences (Schmidt-Kastner, 2015). The preservation of this selective vulnerability in *ex vivo* models of ischemia (Gerace et al., 2012), where blood flow is absent, provides additional support to this hypothesis. Many hypotheses have been proposed to account for this selective vulnerability, including glutamate excitotoxicity (Pellegrini-Giampietro et al., 1992), protein synthesis inhibition (Hossmann, 1993), susceptibility to calpain-caspase activation (Ayuso et al., 2010), and differences in kinase and phosphorylase activities (Pieper et al., 2001), but none of these has been universally accepted.

An alternative theory to explain differential vulnerability is the **vascular theory**, assuming that intrinsic neuron properties and differences in the vascular system are involved in the higher sensitive CA1 hippocampal. The differential expression of angiogenesis-related genes (Schmidt-Kastner, 2015) and the differential response of the neurovascular unit (NVU) to global ischemia (Anuncibay-Soto et al., 2014, 2016) are evidence for this theory.

ER-stress and stroke

Endoplasmic reticulum (ER) is a highly specialized organelle in the synthesis and proper folding of proteins destined to be secreted out of the cell or addressed to different cell compartments, either in their lumen or integrated into their membranes, including the plasmatic membrane (Sanderson et al., 2015). Post-translational modifications in the nascent peptides (such as disulfide bond formation, glycosylation, controlled proteolysis, and chaperone-mediated folding) are ATP- and Ca^{2+}-dependent (Kaufman, 1999). To carry out this plethora of functions, ER requires an oxidizing environment, elevated Ca^{2+} concentration, as well as molecular chaperones, isomerases and glycosylation enzymes that aid polypeptides to achieve their final functional conformation (Chapman et al., 1998). In this regard, the ER is the main intracellular calcium store.

When neuron homeostasis is impaired, ATP levels drastically decrease, and Ca^{2+} is released from the ER (Mehta et al., 2007). The activation of ryanodine receptors (RyR) and inositol 1,4,5-triphosphate receptors (IP_3R), as well as the inhibition of sarcoplasmic/endoplasmic reticulum calcium ATPase pump (SERCA) in the ER membrane, are crucial in the release of Ca^{2+} to the cytosol (Bodalia et al., 2013).

The impairment of the proper ER functions, by pathologies as ischemia, leads to the accumulation of damaged and misfolded proteins in the cytoplasm and ER lumen, a situation known as **ER-stress** (Bodalia et al., 2013; Kumar et al., 2003; Raghubir et al., 2011). ER-stress has been reported in different models of global and focal ischemia (Chen et al., 2015; Osada et al., 2010; Wu et al., 2013; Zhang et al., 2015), as well as in cultured neurons subjected to OGD (Badiola et al., 2011; Kumar et al., 2003). Thus, the first evidence of ER-stress following brain ischemia was observed in neurons by electron microscopy (EM), in which it was observed that the ER and Golgi lost their normal morphology of "flattened pancake" to became rounded vesicles (Petito and Pulsinelli, 1984). Also, these vesicles accumulate products of lipid peroxidation (White et al., 1993). Also, neurons of the CA1 pyramidal layer accumulate protein aggregates after ischemia/reperfusion (Hu et al., 2000). These results correlate with direct evidence of ischemic-dependent ER dysfunction. For example, the decrease in SERCA activity in

microsomes from the ischemic brain (Parsons et al., 1997), as well as reductions in the ER Ca^{2+} levels in reperfused neurons (Kohno et al., 1997).

In summary, multiple causes of ER-stress have been concluded to converge in neurons subjected to ischemia/reperfusion, including depletion of ER Ca^{2+}, aggregation of proteins, decreased protein degradation, and accumulation of lipid peroxidation products in the ER and Golgi structures (DeGracia and Montie, 2004).

Unfolded protein response (UPR)

In response to ER-stress, cells ignite an adaptive response known as **unfolded protein response (UPR)**. The first evidence of UPR was reported by Kozutsumi et al. (1988), but the term 'unfolded protein response' appeared for the first time in the 1990s (Mori et al., 1992). UPR includes multiple cellular mechanisms aimed at: 1) reducing the rate of protein synthesis; 2) upregulating the expression of genes encoding ER chaperones, enzymes, and structural components to increase the processing protein capacity; 3) activating degradation pathways that overcome the excess of misfolded/damaged proteins; and 4) initiate programs of delayed cell death, such as apoptosis, if the stress cannot be overcome (Sanderson et al., 2015).

In the ER membrane, three transmembrane proteins involved in eliciting UPR have been described (known as '**UPR sensors**'): inositol-requiring enzyme 1 (**IRE1**); double-stranded RNA-activated protein kinase-like ER kinase (**PERK**); and activating transcription factor ATF6 (**ATF6**) (Walter and Ron, 2011). An schematic overview of tue UPR in shown in **Figure 5**. The key UPR initiator is the ER molecular chaperone glucose-related protein 78/binding immunoglobulin protein (GRP78/BiP). Under physiological conditions, the ER lumen presents GRP78 constitutively bound to the luminal domains of PERK, IRE-1, and ATF6. GRP78 are dissociated of these sensors to bind the exposed hydrophobic residues of misfolded proteins as they accumulate in ER lumen. The release of GRP78 from IRE1 induces oligomerization and activation of this sensor (Chapman et al., 1998). This mechanism of activation, involving GRP78 dissociation to bind misfolded proteins, is assumed to occur in the three UPR sensors, although it has not been proven for PERK and ATF6 since no alternative mechanisms have been proposed. However, the

mechanism of UPR-sensor activation is probably more complex than just GRP78 dissociation, since recent findings in yeast have shown that hydrophobic residues of unfolded proteins could directly activate the UPR sensors in a GRP78-independent manner (Gardner and Walter, 2011).
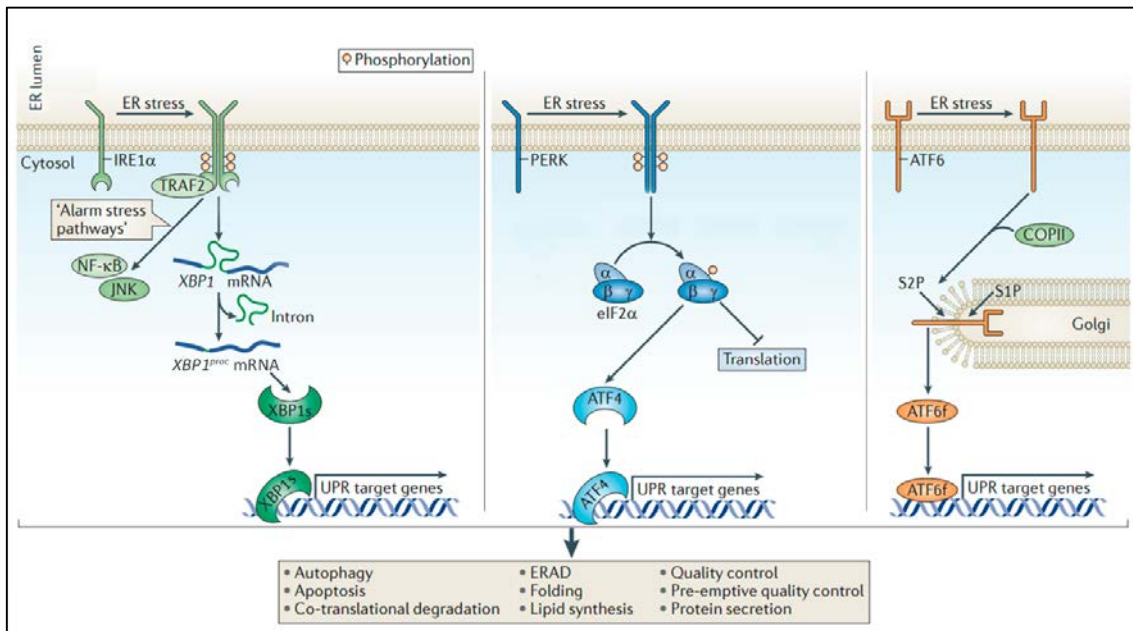

Figure 5. UPR signaling pathways (*modified from Hetz, 2012*)

Inositol Requiring Enzyme 1 (IRE1)

IRE1 protein can work as an UPR sensor through two different cytosolic domains: a serine-threonine kinase domain and an endoribonuclease domain (Tirasophon et al., 1998). After GRP78 release, IRE1 subunits form dimers that phosphorylate each other, thus activating its endoribonuclease activity. Autocatalytically activated IRE1 can eliminate a 26 nucleotide sequence in the coding region of X-box binding protein 1 (XBP1) mRNA. In normal conditions, the product of XBP1 mRNA is a 33 kDA XBP1 protein, but in stress conditions, the alternative splicing of XBP1 mRNA, promoted by IRE1, results in a 54 kDa protein known as processed XBP1 (XBP1[proc]). The resulting XBP1[proc] acts as a transcription factor, up-regulating the expression of molecular chaperones and components of the ER-associated degradation (ERAD) system (Walter and Ron, 2011). Thus IRE1 activation primarily constitutes a pro-survival response mechanism that alleviates the accumulation of misfolded proteins in the cell. However, active IRE-1 has also been shown to bind to tumor necrosis factor receptor-associated factor 2 (TRAF2). This IRE1-TRAF2 complex can elicit apoptotic cell death through the activation of

caspase-12 and the Jun kinases (JNK) pathway (Kaneko et al., 2003). Nevertheless, the regulatory mechanisms that select between pro-survival and pro-apoptotic functions of IRE1 activation are, to date, totally unknown.

Activating Transcription Factor-6 (ATF6)

Inactive ATF6 is a 90 kDa ER-membrane protein that, after cleavage, act as a transcription factor. The pathway starts with dissociation from GRP78, which allows ATF6 to translocate from the ER to the Golgi apparatus. There, two proteases, S1P and S2P, cleave ATF6 into a 50 kDa protein able to translocate to the nucleus as an active transcription factor. There, ATF6 makes a complex with several co-activators and binds to ER-stress response elements (ERSE), thereby upregulating the expression of molecular chaperones (GRP78, GRP94, PDI), as well as C/EBP homologous protein (CHOP). Additionally, ATF6 has also been reported to increase the mRNA levels of XBP1. Cleaved-ATF6 has a short half-life (less than 2 h) (Morishima et al., 2011).

Double-stranded RNA-activated protein kinase-like ER kinase (PERK)

The UPR-sensor PERK follows the same activation mechanism as IRE1. After GRP78 dissociation, PERK homodimerizes and activates itself by autophosphorylation. Active pPERK, in turn, phosphorylates the α-subunit of the elongation initiation factor 2 (eIF2α) at serine 51. Phosphorylated eIF2α prevents the translation of most of proteins, decreasing ER overload. Interestingly, the translation of some mRNAs is promoted by eIF2α phosphorylation by a mechanism known as 'by-pass scanning' (Young and Wek, 2016), activating transcription factor 4 (ATF4) being the most relevant. ATF4 is a transcription factor that translocates to the nucleus and promotes the expression of both pro-survival and pro-apoptotic genes. The pro-survival response triggered by ATF4 includes antioxidant enzymes, autophagy enhancement, and expression of genes related to amino acid metabolism. In 2003, the pro-survival response triggered by ATF4 was named the **integrated stress response** (Harding et al., 2003), which is describe in detail below. ATF4 also increases the expression of CHOP, which lead to apoptosis (Hetz, 2012)

UPR-induced cell death

ER stress and the subsequent UPR can lead to either survival or death. The pro-apoptotic mechanism of UPR is based on three signaling pathways (**Figure 6**), mediated by CHOP, JNK, and caspase-12 respectively (Xin et al., 2014).
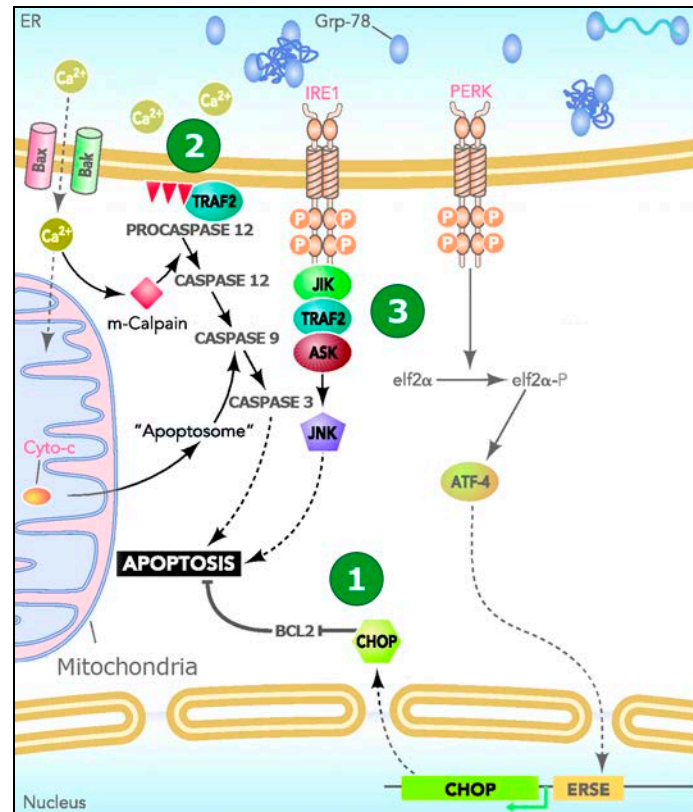

Figure 6. Signaling pathways of UPR-induced cell death: CHOP (1), CASPASE 12 (2) and JNK (3) (*modified from Hetz, 2012*)

CHOP, also known as GADD153, is a member of the CCAAT/enhancer-binding protein family of transcription factors and was the first protein described to promote apoptosis under ER stress conditions. CHOP is induced by both the UPR PERK and ATF6 (Ron and Walter, 2007) pathways and is reported to induce apoptosis by decreasing the levels of the antiapoptotic factor B-cell lymphoma 2 (BCL-2). In fact, CHOP$^{-/-}$ mice are more resistant to ischemic insult than wild-type animals (Tajiri et al., 2004).

The second apoptotic signaling pathway is mediated by **CASPASE-12**, which is bound to the ER membrane in unstressed cells. The activation of m-calpain, a Ca^{2+}-dependent cysteine protease, due to cell calcium imbalance, has been shown to play a key role in generating active caspase-12 after ischemic brain injury. This activated caspase, in turn,

activates downstream caspases, such as caspase-9 and caspase-3, which results in apoptosis (Rao et al., 2001).

The third apoptotic signaling pathway, mediated by **JNKs**, is a common response to many forms of stress (Nickischer et al., 2006) and not exclusively induced by UPR (as CHOP and caspase-12 are). UPR-mediated JNK activation involves IRE1, which activates c-Jun-N-terminal-inhibiting kinase (JIK), leading to the phosphorylation of TRAF2. Under physiological conditions, TRAF2 is bound to procaspase-12. Phosphorylated TRAF2 (pTRAF2) binds to IRE1 and detaches from procaspase-12, which oligomerizes and becomes active. The pTRAF2-IRE1 complex interacts with apoptosis signal-regulating kinase 1 (ASK1), which, in turn, activates the JNK pathway (Tanoue and Nishida, 2002). JNK induces the expression and further phosphorylation of pro-apoptotic BH3-only protein (BIM), as well as the phosphorylation of c-fos and c-Jun, to initiate apoptosis regulated by death receptors (extrinsic apoptosis) (Putcha et al., 2003).

UPR in global cerebral ischemia

UPR activation following brain ischemia leads to protein synthesis inhibition (PSI), which occurs in the first hours of reperfusion due to PERK-mediated eIF2α phosphorylation. After global ischemia, PSI initially affects the whole brain but then returns to normal translation levels, except in the highly vulnerable CA1 region (Hossmann, 1993). However, the CA1 maintained PSI does not correlate with levels of p-eIF2α. Levels of p-eIF2α fall after 6 h of reperfusion, thus indicating that PSI maintenance is independent of UPR activation (Althausen et al., 2001).

IRE1 activation, without ATF6 activation, has been shown to last for 90 min after 10 min of global ischemia (Kumar et al., 2003). Processing of *xbp-1* mRNA after 2 h of reperfusion was reported in focal and global ischemia, and consistent increase of XBP-1 protein was observed in focal, although not in global ischemia (Paschen et al., 2003). These data suggest that the time course for UPR depends on the experimental model.

Increases in transcript levels of the UPR-related genes *chop* and *grp78* have been described after global cerebral ischemia in mice. Additionally, increases in CHOP protein have been described in hippocampal neurons (Tajiri et al., 2004). The same report shows

an attenuation of cell death in the hippocampus of CHOP knockout mice after ischemia, providing additional support to the notion that CHOP induction elicits cell death after UPR activation. Also, structure-dependent increases in transcript levels of *grp78*, *grp94*, *pdi*, and *chop* have been reported in the rat model of cerebral ischemia after 48 h of reperfusion (Llorente et al., 2013a).

Autophagy and stroke

Autophagy (in Greek 'to eat' -*phagy* 'oneself' -*auto*) is a homeostatic mechanism conserved from yeast to mammals, which consists of the lysosomal degradation of old, supernumerary or damaged cytoplasmic entities (Galluzzi et al., 2016). Three types of autophagy that converge in the lysosomal degradation and recycling are described: microautophagy, chaperon-mediated autophagy, and macroautophagy (**Figure 7**). **Microautophagy** relies on the engulfment of small cytosolic portions directly by the lysosomal membrane (Mijaljica et al., 2011). **Chaperon-mediated autophagy** is a specific mechanism that degrades proteins containing a specific amino acid sequence that targets them directly to the lysosomal through transporters located in the lysosomal membrane (Kaminskyy and Zhivotovsky, 2012). **Macroautophagy** (hereafter referred to as 'autophagy' since it constitutes the main topic of this dissertation) is characterized by the formation of a new membrane compartment, the autophagosome, which engulfs a portion of cytoplasm (Galluzzi et al., 2016). Autophagosome formation involves a series of dynamic membrane events: first, a small flat membrane cistern wraps around a portion of cytosol and organelles (the phagophore or isolation membrane). It progressively extends to form a closed double-membrane bound vacuole containing a part of the cytoplasm, the autophagosome. The autophagosome fuses with the lysosome forming the so-called autolysosome, allowing its inner membrane and content to be degraded by lysosomal enzymes. Finally, the autophagolysosome becomes a residual body, and degradation products are transported back to the cytosol to be reused (Eskelinen, 2005; Klionsky et al., 2014).
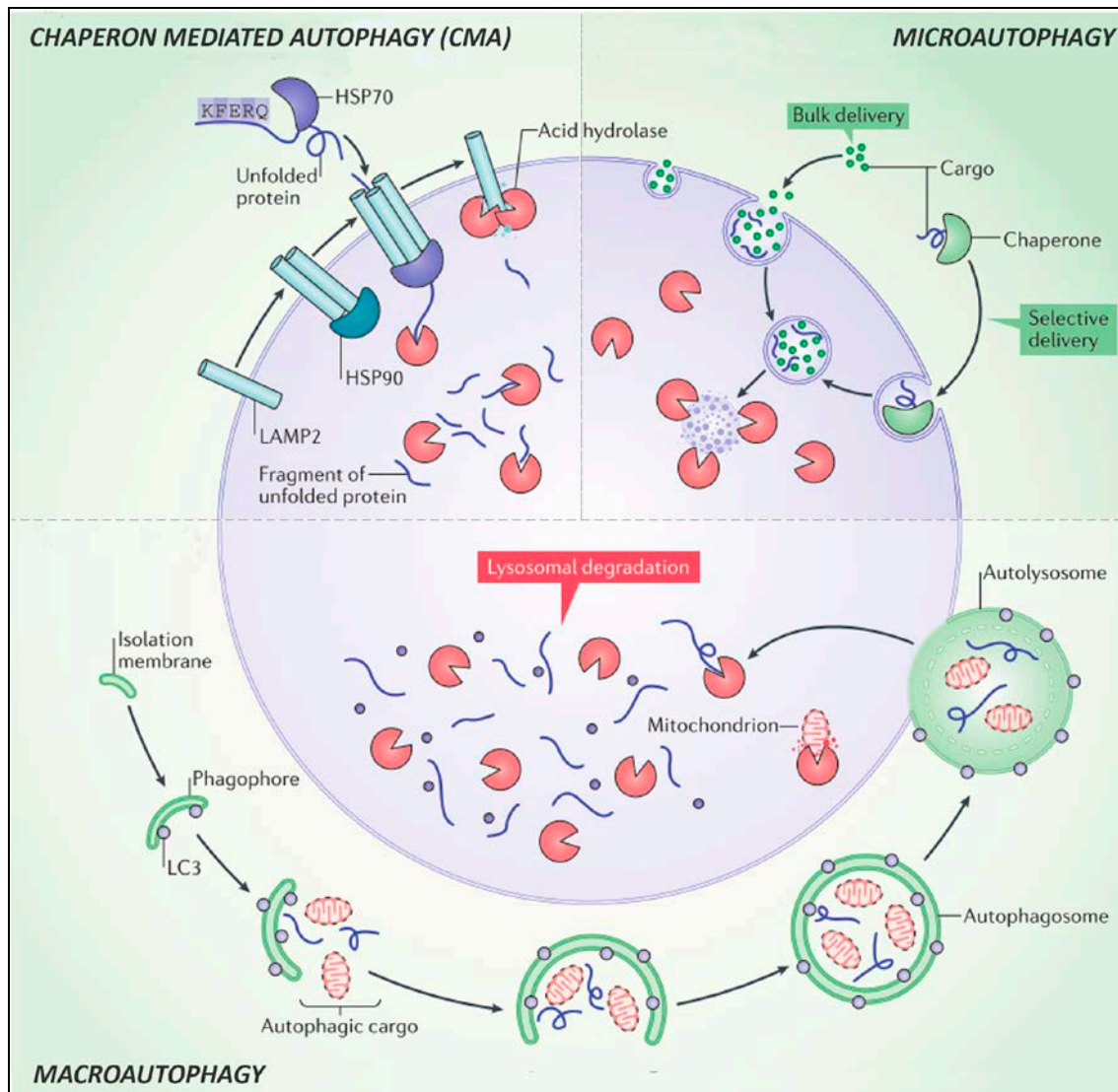
Figure 7. Main features of the three different types of autophagy (*modified from Galluzzi et al., 2016*)

A brief history of autophagy

The word autophagy was firstly coined in 1963, as part of a lysosome-related nomenclature by Christian de Duve (Klionsky, 2008), the lysosome discoverer who was awarded the Nobel Prize in Physiology and Medicine in 1974. However, the phenomenon of 'self-eating' of the cells was previously reported in rat liver cells (Ashford and Porter, 1962). Two different temporal stages in understanding autophagy can be distinguished: before the discovery of autophagy-related genes (*atg*s) and after their discovery. Before the discovery of *atg*s, the first evidence of the physiological role of autophagy, elucidated by de Duve and others, were based on the glucagon-induced autophagy in the liver (Deter et al., 2014). Autophagy-dependent degradation of long-

lived proteins and their strict control by nutrient conditions, especially amino-acid levels, was independently discovered by multiple research teams (Dice et al., 1978; Pfeifer and Strauss, 1981).

First, approaches to understand the mechanism of autophagy were based on morphological approaches of EM, characterized through autophagosomes and autolysosomes. Lysosome-related membrane structures, which are heterogenous in shape and content, required long-term experience for a proper image interpretation. The observation of ribosomes, mitochondria, and other organelles in the autophagosome led to the notion of autophagy as a mechanism for degrading large supramolecular structures and organelles in a non-selective way (Ohsumi, 2014).

Several autophagy modulators were discovered during the 1980s, pushing the research in this field. First, modulators were used to raise the lysosomal pH, thus impairing its function, such as ammonium ions and chloroquine. However, these compounds affect a range of cellular components, which limited the studies of the autophagy regulation (Ohsumi, 2014). The discovery in 1982 of the autophagy inhibitor 3-methyladenine (3-MA) (Seglen and Gordon, 1982) was a milestone in autophagy studies. In fact, this inhibitor is still used in autophagy research. 3-MA was demonstrated to act as an inhibitor of protein phosphorylation (Holen et al., 1992, 1993), although the targets and kinases involved remained unknown for a long time.

Yeast vacuoles are equivalent to mammalian lysosomes, and autophagy research drastically changed in 1992 when membrane-bound vesicles were observed in the vacuoles of *Saccharomyces cerevisiae* after starvation (Takeshige et al., 1992). These vesicles were termed 'autophagic bodies' and contained ribosomes and diverse cytoplasmic structures (Baba et al., 1994). Further EM studies revealed double membrane structures, autophagosomes, which fused to the yeast vacuoles (Baba et al., 1995) in a process morphologically identical to autophagy in mammals.

These discoveries allowed a genetic approach to gain insight into the autophagy process in yeast. Genetic approaches led to the identification of almost one hundred autophagy-deficient mutants, and their genetic analysis revealed 15 complementation groups (i.e., groups with different mutations but similar phenotype) (Tsukada and Ohsumi, 1993). At

the same time, six isolated autophagy-defective (*aut*) mutants (Thumma et al., 1994), as well as several *cvt* mutants defective in the cytoplasm to vacuole targeting (Cvt) pathway (Harding et al., 1995), were identified. The Cvt pathway is highly selective and follows the same membrane dynamics as autophagy, which led to the discarding of the idea of autophagy as a non-selective pathway (Baba et al., 1997). An increasing number of researchers have been analyzing autophagy in yeast species others than *S. cerevisiae,* obtaining mutants arbitrarily given names such as peroxisome degradation via autophagy (*pag*)*,* pexophagy zeocin-resistant (*paz*), peroxisome degradation deficient (*pdd*) and glucose-induced selective autophagy (*gsa*). To avoid confusion, a unified nomenclature was adopted in 2003, using the terms **ATG or *atg* for 'autophagy-related' protein and genes** respectively (Klionsky et al., 2003).

ATG includes a range of more than 34 gene products responsible for the core machinery of autophagosome formation, as well as those genes required for selective modes of autophagy (Weidberg et al., 2011). In yeast, each single gene encodes an Atg protein with a specific function. In contrast, different ATG proteins in higher eukaryotes coded by different genes originated by duplication can present a similar function (paralog genes) (Ohsumi, 2014). This phenomenon may reflect the increased complex nature of autophagy in mammalian cells, where paralog gene products plays a specific regulatory role in the diverse modes of autophagy in the various tissue and cell types.

Molecular machinery of autophagy

Five sequential steps are involved in autophagy degradation: 1) autophagy induction, 2) vesicle nucleation, 3) autophagosome elongation, 4) autophagosome maturation, and 5) lysosomal fusion and degradation of the autophagosome cargo. An overview of this process is shown in **Figure 8**.
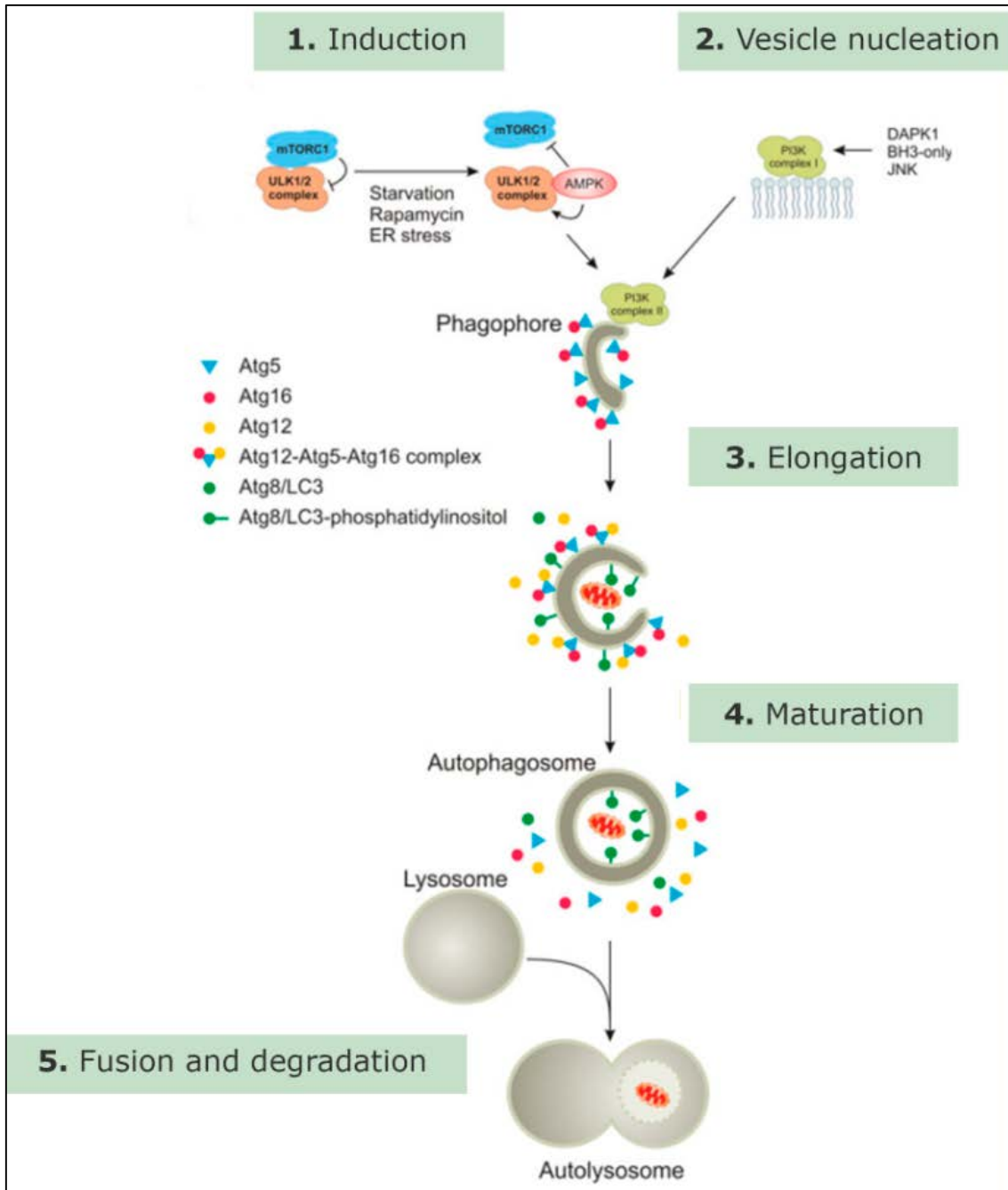
Figure 8. Overview of the different stages of the autophagy process (*modified from Deegan et al., 2013*)

Autophagy induction

Autophagy aims to maintain the cell homeostasis and always presents a basal level of activity. The level of autophagy activity is increased in response to multiple physiological stresses, such as nutrient starvation, oxidative stress, accumulation of unfolded proteins, and microbial infection (He and Klionsky, 2009).

The key step in the induction of autophagy is the activation of the **ATG1/ULK complex,** which is made of four proteins: ULK1/2 (mammalian homologous of Atg1), mATG13, FIP200, and ATG101. This complex promotes the formation of the **phagophore**, also known as isolation membrane (Weidberg et al., 2011). The activation of this complex depends on the adenosine monophosphate-activated protein kinase **(AMPK)** which enhances autophagy, while the ATG1/ULK complex inactivation depends on mammalian target of rapamycin (mTOR) complex 1 **(mTORC1),** which suppresses autophagy (Kim et al., 2011). In fact, AMPK is considered the main sensor of intracellular energy under starvation or stress conditions (Hardie, 2007). The activation of the ATG1/ULK complex involves a sequential series of phosphorylation events (**Figure 9**).
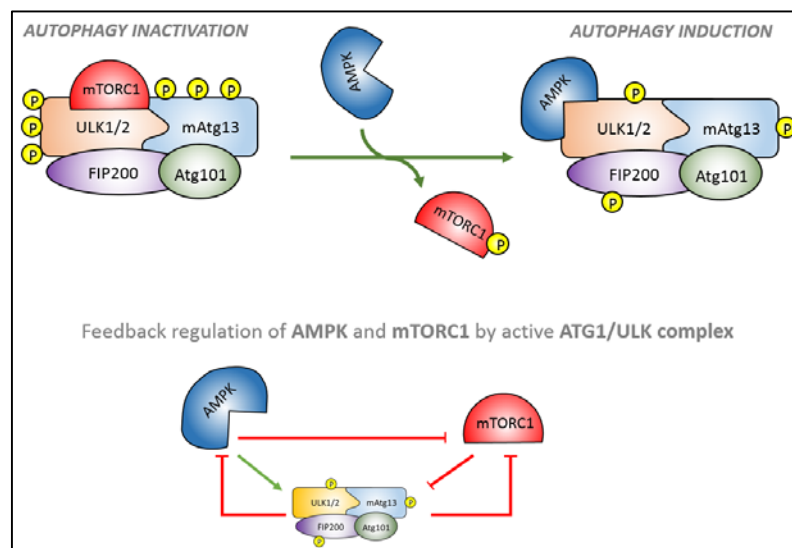
Figure 9. Regulation of ATG1/ULK complex by phosphorylation events.

First, mTORC1 is inactivated by phosphorylation, which allows the dephosphorylation of ULK1 that then facilitates the AMPK binding to the complex. Then, AMPK activates ULK1 by phosphorylating it in multiple residues. The activated ATG1/ULK1 complex provides a positive feedback on mTORC1 and negative feedback on AMPK. Thus, ATG1/ULK1 phosphorylates mTORC1, amplifying the activation of ULK1, but also phosphorylates and inactivates AMPK, which decreases ATG1/ULK1 activity (Weidberg et al., 2011). This mechanism is complex and different stress stimuli lead to different phosphorylation states, which allow a fine tuning of autophagy activity (Chan, 2012).

Vesicle nucleation

A process of vesicle nucleation, expansion, and curvature of the membrane occurs after activation of the ATG1/ULK complex and formation of the isolation membrane, which involves the synthesis of phosphatidylinositol 3 phosphate (PI3P). The vesicle nucleation requires the activation of the **(PI3P) kinase (PI3K) class III/Vps34 (vacuolar protein sorting 34) complex (PI3K complex)** (Weidberg et al., 2011)**.** In mammals, there are two PI3K complexes, I and II, with different functions. Both complexes present three common components (Vps34, p150, and Beclin1) and an exclusive component (ATG14L for PI3K-I or ultraviolet radiation resistance-associated gene [UVRAG] for PI3K-II), each type presenting different functions related to PI3P synthesis (Itakura et al., 2008). **PI3K complex I** regulates vesicle nucleation since ATG14L recruits the PI3K complex I to the isolation membrane (Matsunaga et al., 2009). **PI3K complex II** is involved in the expansion and curvature of the membrane, where UVRAG is proposed to recruit BIF1, which plays a role in binding membranes and promoting its curvature (Liang et al., 2008).

How these complexes regulate autophagy remains unclear, but PI3Ps are crucial in the recruitment of essential proteins to the phagophore. In fact, inhibitors of PI3K complexes, such as 3-MA, wortmannin, and LY294002, result in complete inhibition of autophagosome formation (Pasquier, 2016).

The origin of the phagophore membrane also remains unclear. Early biochemical studies on autophagosome-enriched fractions failed to identify protein markers of different membrane structures. This led to the notion that phagophore membranes were generated via *de novo* synthesis. However, advances in microscopy assays and identification of new autophagy markers showed that structures in the ER membrane, known as **omegasomes**, as well as mitochondria and the plasma membranes, could originate the phagophore in a PI3P-dependent manner (Weidberg et al., 2011). In fact, both the PI3K complex I, which is directed to the ER by ATG14L and double FYVE domain-containing protein (DFCP1), which binds PI3P, have been shown to be involved in omegasome formation (Polson et al., 2010).

Autophagosome elongation

The elongation of the phagophore to form an autophagosome requires two ubiquitin-like conjugation systems, the ATG12-ATG5 and ATG8 conjugation systems (Ohsumi, 2001). **Figure 10** shows the similarity between ATG12, ATG8 and ubiquitin molecules.
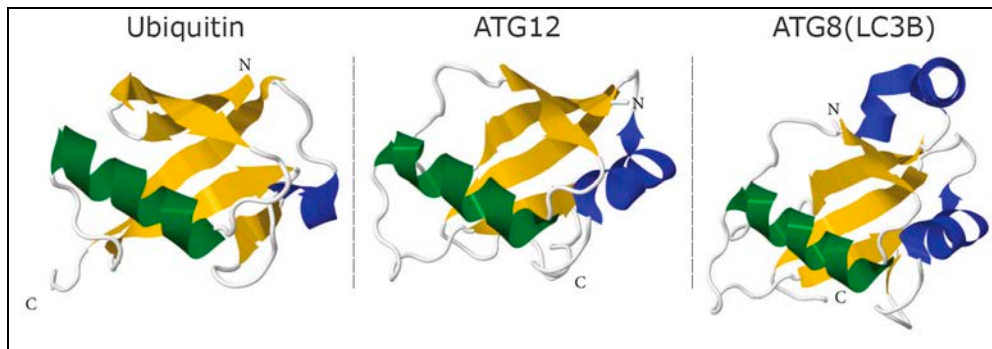
Figure 10. Ribbon diagrams showing structures of ubiquitin and ubiquitin-like proteins (Ubls) ATG12 and ATG8. Notice how the three proteins share a β-sheet with four antiparallel β-strands (yellow) and a helical segment (green). Other helical structures are represented in blue. (*modified from Lippai and Low, 2014*)

The **ATG12-ATG5 conjugation system** is formed by the covalent binding of ATG12 and ATG5 (**Figure 11**), which is catalyzed by ATG7 and ATG10. This conjugation system can recruit ATG16L through its interaction with ATG5. ATG16L is thought to serve as a scaffold for protein-protein interaction in the autophagosomal membrane (Kuma et al., 2002; Ohsumi, 2001). The recruitment of the ATG12-ATG5-ATG16L complex to the autophagosome membrane also depends on the synthesis of PI3P by PI3K complexes, although the exact mechanism remains unknown (Weidberg et al., 2011).

Figure 11. ATG12-ATG5 and AT8 conjugation systems. (*modified from Geng and Klionsky, 2008*)

Some differences between yeast and mammals have been described in the **ATG8 conjugation system**. Thus, only the ATG8 prote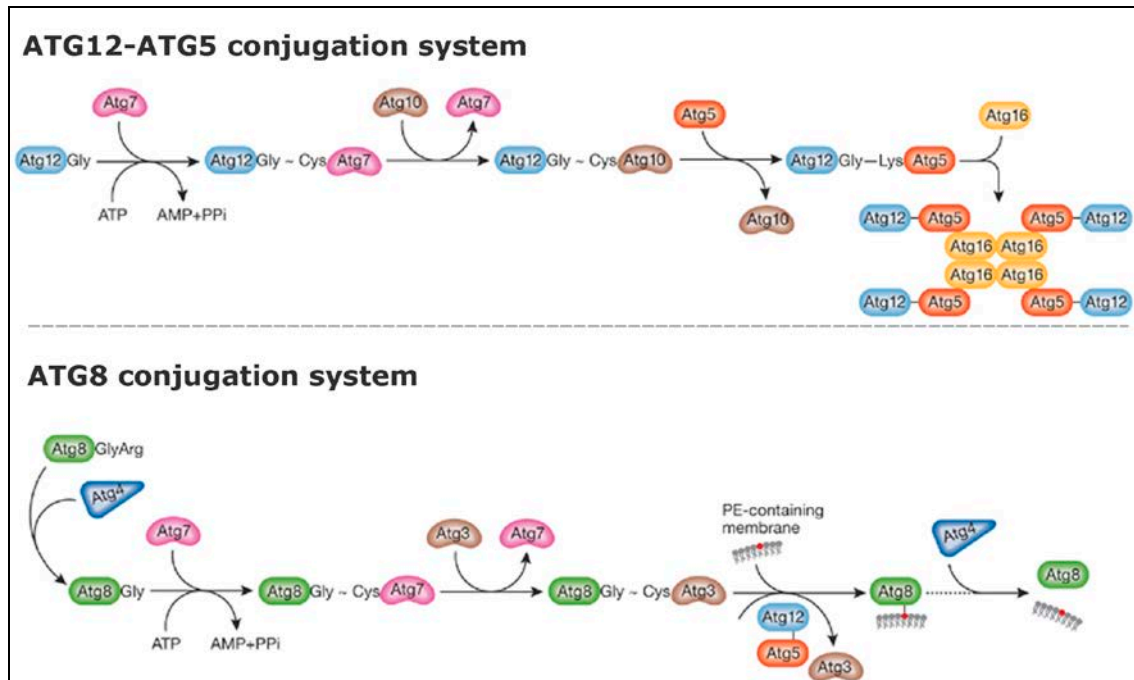in is described in yeast, while mammals express a family of mATG8 proteins subdivided into microtubule-associated protein 1 light chain 3 proteins (LC3s) and gamma-aminobutyric acid receptor-associated proteins (GABARAPs) (Weidberg et al., 2010). Members of the ATG8 family are translated as pro-forms, which are subsequently cleaved at the C-terminal region by the protease ATG4, thus exposing a glycine residue (**Figure 11**). This step is followed by the binding of a phosphatidylethanolamine (PE) to the exposed glycine residue, a process mediated by ATG7 and ATG3. The lipidated form of ATG8 can be then recruited to the autophagosome membrane, a process that requires the AT12-ATG5-ATG16 complex as a platform (Tanida et al., 2004, 2008).

The mAtg8 proteins play a role in autophagosome biogenesis. Thus, a role of ATG8 in the determination of autophagosome size has been demonstrated (Xie et al., 2008). Moreover, both the LC3 and GABARAP proteins play essential roles in autophagosome formation, but they operate at different steps in this process. LC3 mediating the elongation of the autophagic membranes and GABARAPs in the sealing of autophagosome (Nakatogawa et al., 2007; Weidberg et al., 2011). Moreover, ATG8 also plays a role in autophagosome cargo recruitment that will be discussed in the *Selectivity*

in the autophagy process section. Thus, a dual role for ATG8 in autophagy provides new examples of the paralog genes in autophagy.

Autophagosome maturation

The sealing of the autophagosomal membranes is considered the autophagosome maturation process (Eskelinen, 2005). This sealing originates the characteristic closed double-membrane autophagosomes that are targeted to the lysosomal system. The autophagosome maturation process remains poorly characterized. Autophagosomes converge with the endocytic pathway, which results in the fusion of autophagosomes and endosomes to form organelles, referred to as **amphisomes** (Klionsky et al., 2014). Amphisomes present factors from endosomes that facilitate the targeting and fusion with lysosomes (Simonsen and Tooze, 2009).

The mechanisms that lead to the fusion with lysosomes relies on cytoskeletal networks since, unlike phagophores (that are immobile organelles), autophagosomes present mobile properties (Fass et al., 2006; Jahreiss et al., 2008). Two populations of microtubules related to the autophagic process have been described: a labile population that recruits early autophagic factors and a stable, acetylated population that binds mature autophagosomes (Geeraert et al., 2010). The autophagosome transport requires a protein complex in the autophagosome/amphisome membrane formed by the FYVE proteins FYCO, PI3P, Rab7, and LC3. FYCO is an adaptor between the autophagosome and kinesins of the microtubule network, and Rab7 promotes microtubule plus-end-directed transport of autophagosomes (Weidberg et al., 2011). The complex also plays a role in the fusion with the lysosome, where Rab7 is the responsible for the binding between autophagosome/amphisome and lysosome, recognizing and binding to lysosome-associated membrane glycoprotein 1/2 (LAMP1/2) on the lysosomal membrane (Jäger et al., 2004).

Fusion and degradation

Fusion of the autophagosome/amphisome and lysosome membrane relies on members of the classic membrane fusion soluble N-ethylmaleimide-sensitive factor activating protein receptor (SNARE) protein machinery (Furuta et al., 2010; Moreau et al., 2013),

as well as the ATG8 proteins (Yu and Melia, 2017). Once inside the lysosome, substrates are degraded by lysosomal enzymes, such as nucleases, phosphatases, proteases (cathepsins), and glycosidases (Yamashima and Oikawa, 2009).

When analyzing autophagy, it is crucial to consider that increases in autophagosome formation do not imply an increase of the whole autophagic process. Thus, an increase in **autophagy induction** must be accompanied by the proper lysosomal degradation of autophagy substrates (**autophagy flux**) (Klionsky et al., 2016; Mizushima and Yoshimori, 2007). In fact, increases in autophagy induction without lysosomal degradation has been described and associated with neuronal cell death in a model of traumatic brain injury (Sarkar et al., 2014).

Selectivity in the autophagic process

Autophagy was initially considered as a non-selective process. However, evidence of a high selective autophagy of the Cvt pathway were outlined in the 1990s (Baba et al., 1997; Harding et al., 1995) and it has been confirmed in autophagy of mitochondria (mitophagy), ER (ER-phagy/reticulophagy), ribosomes (ribophagy), peroxisomes (pexophagy), Golgi (crinophagy), endosomes (heterophagy), pathogens (xenophagy), aggresomes (aggrephagy), and lipids (lipophagy) (Klionsky et al., 2016). This selectivity is evidenced by the identification of autophagy receptors for specific autophagosome cargo.

Autophagic receptors (such as P62/SQSTM1, NBR1, NIX and NDP52) are proteins required for the selective recruitment of specific substrates in the autophagosome (Fujita et al., 2013; Katarzyna and Suresh, 2016; Lippai and Low, 2014). All of them present a domain for recognizing specific substrates to be degraded, as well as the LC3-interacting region (LIR) domain. LIR interacts with the different subfamilies of mATG8 (LC3 and GABARAP) anchored in the membrane of the autophagosome. Autophagy receptor proteins are well characterized, both structurally and functionally. However, their regulation and the functional consequence of their absence in response to different stress stimuli is largely unknown (Weidberg et al., 2011).

Selective clearance of Cytosolic Proteins: P62/SQSTM1

Sequestosome 1 (P62/SQSTM1) was the first protein reported as an autophagy receptor (Bjørkøy et al., 2005). This ubiquitin-binding protein specifically interacts with mAtg8s (LC3B and GABARP). Experiments with knockout mice have shown that P62/SQSTM1 is required for the aggregation of ubiquitinylated proteins and plays essential roles in its autophagic clearance (Komatsu et al., 2006) and, usually, the levels of P62/SQSTM1 inversely correlate with autophagic degradation (Ichimura et al., 2008; Mizushima and Yoshimori, 2007). P62/SQSTM1 present three different domains related with autophagic degradation of polyubiquinilated proteins (**Figure 12**): 1) **ubiquitin-associated domain (UBA)** in the C-terminus, which can recognize polyubiquitin tags in proteins; 2) The **LIR** domain, common to autophagic receptors, located between Ser334 and Ser344. The two main features of this domain are the presence of acidic amino acids (Asp337 and Asp339), which interact with basic groups in the N-terminal region of LC3B, and two 'hydrophobic pockets' (Trp340 and Leu343), which interact with the ubiquitin domain of LC3B; and 3) The **Phax and Bem1 (PB1) domain** in the N-terminal region, which allows self-oligomerization of P62/SQSTM1. This oligomerization enhances the recruitment of ubiquitinated proteins (Lippai and Low, 2014).
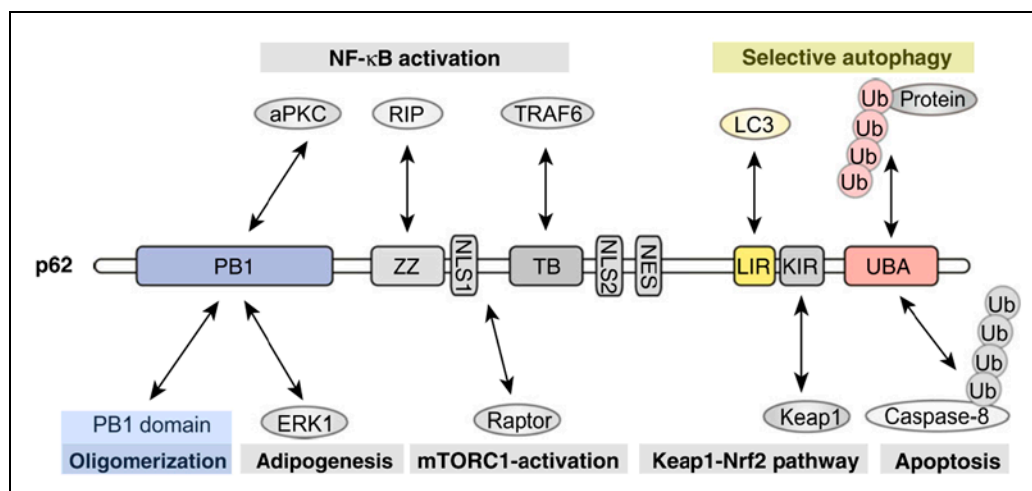

Figure 12. Domain structure of P62/SQSTM1 and its binding partners. Domains involved in selective autophagy are highlighted in color. *(Modified from Katsuragi et al., 2015)*

Other roles of P62/SQSTM1 in autophagy

The single view of P62/SQSTM1 as a receptor protein linking ubiquitinylated protein aggregates to LC3B has drastically changed in recent years. Recently, cytoplasmic

protein aggregates containing P62/SQSTM1 and ubiquitinylated proteins, have also been shown to be used as a scaffold for autophagosome biogenesis, interacting with multiple upstream ATG proteins (Fujita et al., 2013; Nagy et al., 2014). A functional role of P62/SQSTM1 as a shuttle exporting ubiquitinylated substrates from the nucleus into the cytosol has also been reported (Pankiv et al., 2010).

The role of P62/SQSTM1 in autophagy regulation is controversial. This protein has been reported to inactivate autophagy promoting mTORC1 activation (Moscat and Diaz-Meco, 2012). However, P62/SQSTM1 increases autophagy in cultured cells by releasing BECLIN1 from BCL2 (Zhou et al., 2013). In carcinoma cells, P62/SQSTM1 silencing induces autophagy, but autophagosomes become abnormal leading to autophagic cell death (Nihira et al., 2014). Thus, the role of P62/SQSTM1 in regulating autophagy seems complex and probably context-dependent.

P62/SQSTM1 is involved signaling pathways others than autophagy

P62/SQSTM1 was originally described as a scaffold protein able to form signaling hubs interacting with several enzymes through its different domains (**Figure 12**). The role of P62/SQSTM1 in inflammation is well known; this protein can promote the pro-inflammatory interleukin-1β (IL-1β) production and activate the inflammatory-related nuclear factor kappa-light-chain-enhancer of activated B cells (NF-κB) pathway (Laurin et al., 2002; Sanz et al., 1999).

P62/SQSTM1 is also involved in the regulation of extrinsic apoptosis since it is required for the caspase-8 activation (Jin et al., 2009). It also plays a role in oxidative stress since it promotes the translocation of the nuclear factor (erythroid-derived 2)-like 2 (NRF2) transcription factor to the nucleus, blocking its regulator Cullin3-ubiquitin E3 ligase complex adaptor protein (KEAP1). This allows the induction of NRF2-dependent anti-oxidant gene products. In turn, the P62/SQSTM1 gene is also controlled by NRF2 (Jain et al., 2010).

When autophagy becomes excessive: autophagic cell death

Autophagy is essentially a mechanism for cytoprotection. However, an excessive autophagy activation can lead to a regulated cell death characterized by the unspecific

and massive degradation of large cytoplasmic entities. This type of death was described during animal development, tissue homeostasis, and in several diseases, as well as in cultured mammalian cells treated with chemotherapeutic agents or toxic compounds.

For many years, the type II autophagic cell death was described based on morphological criteria, including plasma membrane rupture, enlargement of Golgi, mitochondria, and ER, numerous autophagosomes and autolysosomes and depletion of cytoplasmic organelles (Denton et al., 2012). However, further research revealed that different subroutines of cell death could lead to these morphological characteristics. Thus, in 2015, the Nomenclature Committee on Cell Death (NCCD) redefined the term '**autophagic cell death**' to describe cell death that: 1) occurs independently of apoptosis; 2) present an increase in autophagy markers and autophagy flux; and 3) is prevented by the genetic or chemical suppression of autophagy (Galluzzi et al., 2014).

Thus, excessive autophagy can elicit differently regulated cell death subroutines, and not all of them result in the morphological autophagy cell death. The best characterized is the molecular interaction between autophagy and apoptosis through the antiapoptotic or proapoptotic protein family of BCL2, which can lead either to inhibition autophagy or inhibition of apoptosis (Eisenberg-Lerner et al., 2009; Gump and Thorburn, 2011). This dual regulation of BCL2 family members evidences the need of cells to simultaneously regulate and coordinate these two pathways. However, the practical implication of this dual regulation is not well understood (Denton et al., 2012). Other death subroutines, such as necroptosis (Bonapace et al., 2010), pyroptosis (Suzuki et al., 2007) and entosis (Florey et al., 2011) have been related to autophagy, but the relationships are mostly unknown.

The use of autophagy inducer peptides has led to the definition of a new form of autophagy gene dependent cell death, referred to as **autosis** (auto, autophagic, tosis, death) because it can be prevented by inhibiting autophagy. Autosis is mediated by the Na^+, K^+-ATPase pump with unique morphological features: focal plasma membrane rupture, nuclear membrane shrinkage, focal swelling of the perinuclear space, numerous autophagosomes and autolysosomes in early stages that disappear in final stages, dilated and fragmented ER that, in late stages, disappear, and enhanced cell-

substrate adhesion (Liu and Levine, 2015). Autosis has been described in hippocampal CA3 neurons of neonatal rats subjected to cerebral hypoxia-ischemia (Liu et al., 2013).

Autophagy and stroke

Constitutively active autophagy at low levels is important for maintaining homeostasis and protein quality control under normal conditions in neurons. The first evidence of the involvement of autophagy in stroke relied on the increased number of autolysosomes in hippocampal neurons after transient global cerebral ischemia (Nitatori et al., 1995). Further studies described an autophagic role in global and focal cerebral ischemia during the first 48 h of reperfusion, reporting changes in markers of both autophagy induction marker (BECLIN1 and LC3B, as well as autophagosome number) and autophagy flux (P62/SQSTM1), as well as in lysosome-related enzymes (Cathepsin B, Cathepsin D and LAMP1) (Descloux et al., 2015). However, the role of autophagy in ischemic damage is controversial and largely unknown since there are reports describing both neuroprotective and detrimental effects that involve different subroutines in the cell death.

Results using autophagy modulators to assess its neuroprotective or detrimental role after ischemia are not conclusive. **Table 2** summarizes a bibliography search about the role of autophagy during reperfusion in different *in vivo* models of stroke.

Table 2. Published reports about neuroprotective and detrimental autophagy in *in vivo* models of stroke.

Neuroprotective		Detrimental	
Reference	Stroke model*	Reference	Stroke model*
Carloni et al., 2014	Neonatal H-I	(Adhami et al., 2006)	pRCCAO
(Wang et al., 2014)	tMCAO	(Rami et al., 2008)	tMCAO
(Papadakis et al., 2013)	BCCAO	(Qin et al., 2010)	pMCAO
(Carloni et al., 2010)	Neonatal H-I	(Shi et al., 2012)	pRCCAO
(Liu et al., 2010)	BCCAO	(Jiang et al., 2012)	tMCAO
		(Xu et al., 2013)	tMCAO
		(Cui et al., 2013)	2-VO

BCCAO: bilateral common carotid artery occlusion; H-I: hypoxia-ischemia; pMCAO: permanent middle cerebral artery occlusion; pRCCAO: permanent right common carotid artery occlusion; tMCAO: transient middle cerebral artery occlusion; 2-VO: two-vessel occlusion.

The use of neuroprotective agents was unable to clarify this controversial role. Thus, the neuroprotective effects of lithium chloride (Li et al., 2010), 2-methoxyestradiol (Xin et al., 2011) and NAD$^+$ (Zheng et al., 2012) against stroke have been related to their ability

to decrease autophagy activity. In contrast, other neuroprotective agents, such as pinocembrin (Zhao et al., 2014) or melatonin (Guo et al., 2010), increase autophagy. Ischemic preconditioning studies, where a short time of ischemia previous to the full ischemic insult decreases the extension of the damage, have also been used to analyze autophagy. The neuroprotective effect has been hypothesized to rely on autophagy enhancement in the preconditioning stimulus (Gao et al., 2015; Su et al., 2014).

The neuroprotective effect of the autophagy in stroke has been linked to the prevention of protein aggregation (Liu et al., 2010), the removal of damaged mitochondria (Zhang et al., 2013), and increased ribosome turnover (Carloni et al., 2014).

The controversial role of autophagy in stroke has been proposed to depend on differences in the severity of the ischemic insult. In this regard, a comparative study in $atg7^{-/-}$ mice demonstrated the beneficial role of autophagy after transient middle cerebral artery occlusion (MCAO) but a detrimental role after permanent MCAO (Zhang et al., 2013). Detrimental or beneficial autophagy effects have also been reported when administering pre- or post-ischemia inhibitors of autophagy respectively (Wang et al., 2011). Autophagy response to ischemic insult also depends on age and sex. Thus, neonate female rats present higher levels of LC3B after hypoxia-ischemia than males (Weis et al., 2014). Moreover, autophagy response after cerebral ischemia is higher in adult than in immature brains (Zhu et al., 2005).

Autophagy responses to ischemic challenge are not only related with ischemic-reperfused neurons, but it is also modified in other cell populations, such as astroglia (Qin et al., 2010) and vascular endothelial cells (Li et al., 2014).

Crosslink between autophagy and UPR: the integrated stress response

Two main degradation pathways regulate protein homeostasis in mammals, the ubiquitin-proteasome system and autophagy. Both of these rely on polyubiquitin tags for recognizing protein to be degraded. However, the proteasome has been related to

the degradation of soluble misfolded proteins while autophagy is the responsible for the clearance of large insoluble cytosolic protein aggregates (Ohsumi, 2006). In fact, differences in polyubiquitin tag, lys48 linked ubiquitin and lys63 linked ubiquitin, have been described to tag proteins for proteasomal or autophagy degradation respectively (Kirkin et al., 2009).
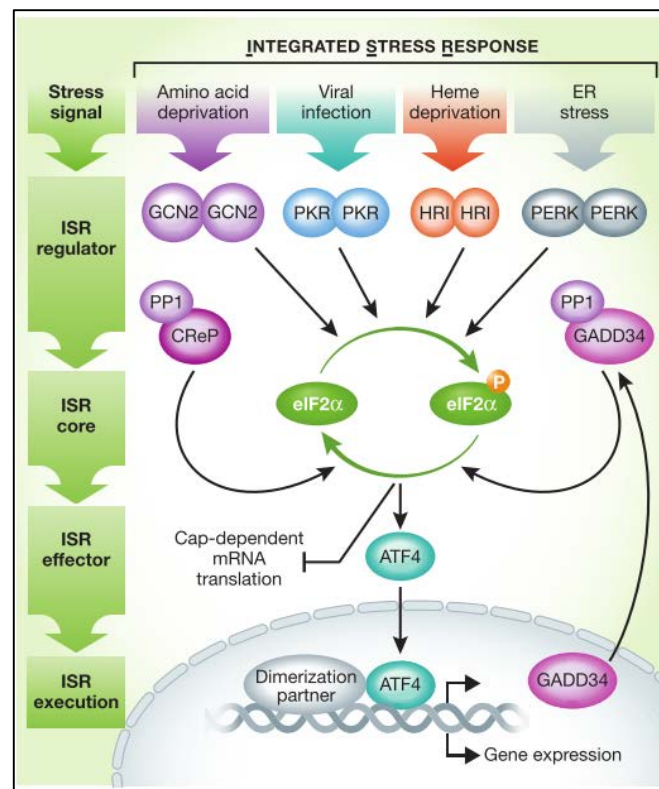
Figure 13. Overview of the integrated stress response mediated by ATF4 (*modified from Pakos-Zebrucka et al., 2016*)

ER-stress ignites autophagy through the activation of UPR (Hetz, 2012). The key event that linked both pathways is the phosphorylation of eiF2α (Deegan et al., 2015; Rzymski et al., 2010). Four different kinases are responsible for eiF2α phosphorylation in mammals: general control nonderepressible 2 kinase (GCN2), protein kinase R (PKR), heme-regulated eIF2α kinase (HRI), and PERK (Taniuchi et al., 2016) (**Figure 13**). As explained above, p-eiF2α inhibits the 5'cap-dependent mRNA translation, thus impeding the synthesis of most proteins, but promotes selective translation of some mRNAs, such as ATF4 by the 'by-pass scanning' mechanism that involves two open reading frames (ORF) in the 5'-untranslated region (UTR) (**Figure 14**) (Jackson et al., 2010; Young and Wek, 2016). ATF4 initiates a cytoprotective transcriptional response known as

integrated stress response (ISR) that involves autophagy and antioxidant responses (Harding et al., 2003). ATF4 is a member of the ATF subfamily of the basic leucine zipper (bZIP) transcription factor superfamily able to bind to C/EBP-ATF Response Element (CARE) sequences of a subset of specific target genes (**Figure 13**). The interaction of ATF4 with other transcription factors, such as activating transcription factor 2 (ATF2), activating transcription factor 3 (ATF3), CHOP, and NRF2, modifies ATF4 affinity for different CARE sequences and, thus, contributes to the different responses elicited by different stress stimuli (Pakos-zebrucka et al., 2016). In this regard, ATF4 has been reported to be essential for autophagy gene expression induction in response to ER-stress in mammalian cells (B'chir et al., 2013; Deegan et al., 2015) , as well as to mediate the resistance of tumors to hypoxia (Rzymski et al., 2009, 2010). In brain disorders, several inhibitors of eiF2α dephosphorylation, such as salubrinal (Anuncibay-Soto et al., 2016; Nakka et al., 2010), guanabenz (Way et al., 2015) and sephin1 (Das et al., 2015), have shown a neuroprotective effect. This has leading some to consider the integrated stress response as a promising therapeutic target for central nervous system injuries (Romero-Ramírez et al., 2017).
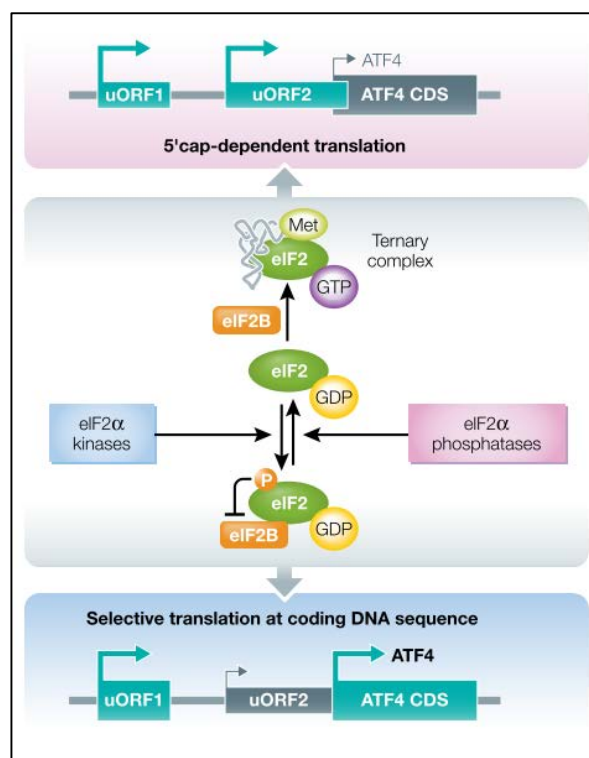

Figure 14. P-eiF2α control of mRNA translation (*modified from Pakos-Zebrubcka et al., 2016*)

AIMS

Work hypothesis and aims

Despite the many successful approaches in experimental models to alleviate the ischemic damage, there have as yet been no successful clinical trials. The increasing incidence of stroke and the corresponding growth in social and medical costs have created an urgent need of new targets or therapeutic strategies against this pathology. Stroke elicits the so called integrated stress response which includes modifications in the autophagy response whose role is controversial. **Our work hypothesis assumes that autophagy plays a crucial role in neuroprotection, responsible for the differential vulnerability, the role of which possibly differs in different experimental models**.

To test this hypothesis, we proposed the following objectives and questions:

1) Are there local structural differences in the autophagy response to stroke? To answer this question, the autophagy response between structures (cerebral cortex and hippocampus) with different vulnerability to the ischemia was compared using the *ex vivo* brain slice model, which allows us to obtain and maintain these structures under identical conditions.

2) Are structure-dependent differences in autophagy are involved in differences in vulnerability? Structures with different vulnerability correlate with different UPR responses, whose enhancement results in a neuroprotective effect. Since autophagy is a homeostatic mechanism to decrease ER stress, we analyzed autophagy response in different vulnerable structures treated with a neuroprotective agent that enhances UPR.

3) Is the autophagy response similar in different models of ischemia and what is its relevance in the integrated stress response elicited by UPR? The hippocampal CA1 region is the most ischemia-vulnerable structure and seems an appropriate focus for an analysis performed in another model of ischemia, such as organotypic hippocampal slice culture. The effects of autophagy and anti-oxidant responses in the neuroprotective effect of UPR enhancement were analyzed

CHAPTER 1

Hippocampus and cerebral cortex present a different autophagic response after oxygen and glucose deprivation in an ex vivo rat brain slice model

Background

Stroke is one the leading causes of death as well as the main cause of permanent disability and the second cause of dementia in developed countries. This results in dramatic social costs and in European countries represents up to 4% of the total medical budget (Creutzfeldt and Holloway, 2012; Olesen et al., 2012). Stroke, also called cerebrovascular accident, is a failure in the brain function as a consequence of the partial or total interruption of blood supply. It results in a lack of glucose and oxygen and therefore to an energy failure and homeostatic imbalance that damages the cells and can elicit their death (Fisher and Bastan, 2008; Mehta et al., 2007). The return to normoxic conditions, as a consequence of the reperfusion, is required for the tissue to survive but increases the glutamate release and elicits an excitotoxic cascade that increases the damage and cell mortality (Lobo et al., 2011; Luccini et al., 2010). Rescue of the damaged cells is considered to play a crucial role in the degree of patient recovery and therefore the mechanisms involved in this process may be important therapeutic targets (Mehta et al., 2007).

Autophagy is a crucial mechanism involved in the processes that follow ischaemia (Xu et al., 2012). In this regard, the reports on this topic have extraordinarily increased in the last 5 years and different animal models have proved the relationship between autophagy and stroke. Thus, the roles of autophagy present some differences depending on the structure, model or time after stroke (Carloni et al., 2008; Cui et al., 2013; Ginet et al., 2009; Qin et al., 2010; Rami et al., 2008; Shi et al., 2012; Smith et al., 2011), but the autophagy that follows stroke seems to play a neuroprotective role, removing damaged proteins and organelles (Reggiori et al., 2012; Smith et al., 2011). In addition, autophagy gives metabolic support to apoptosis and delays necrosis (Balduini et al.,

2009) and could prevent the extension of the damage if massive necrosis exists. Autophagy has been suggested to be involved in the delayed cell death (Puyal and Clarke, 2009) and could facilitate the recovery of the less-damaged cells. On the other hand, excessive autophagy leads to autophagy cell death and cross talks with other programmed cell death types (Chaabane et al., 2013).

Early stages in autophagy are characterized by phagophore formation (Burman and Ktistakis, 2010; Devenish and Klionsky, 2012). However, increases in phagophore formation do not implies an increase of the whole autophagic process and therefore the two stages of autophagy, induction and flux of autophagy, have to be analysed (Klionsky et al., 2016).

To our knowledge, there are no data on the autophagic response at under 6 hours after ischaemia either in *in vivo* or *ex vivo* models, a period that can be crucial in the recovery of the damaged cells. Thus, we analysed for the first time the autophagic stages at 3 hours of RL after OGD in the hippocampus and cerebral cortex, two structures with different ischaemic vulnerability (Kirino, 1982; Zhu et al., 2012).

Methods

Animals

Sixteen male, 2-month-old, Sprague-Dawley rats were housed at 22±1oC in a 12 h light/dark controlled environment, with free access to food and water. Two rats were used in each assay to obtain the number of slices necessary for the different conditions assayed and eight assays were carried out. All the experimental procedures were carried out following the Guidelines of the European Union Council (86/609/EU) and Spanish regulations (RD 53/2013, BOE 8/2/2013) for the use of laboratory animals, and were approved by the Ethics Committee of the University of Leon. All efforts were made to minimize animal number and suffering.

Experimental procedure

Solutions

Four different solutions were employed to obtain brain slices and to perform OGD assays: <u>Cutting Solution</u> (120 mM NaCl, 2 mM KCl, 0.5 mM CaCl2, 26 mM NaHCO3, 10 mM MgSO4, 1.18 mM KH2PO4, 11 mM glucose and 20 mM sucrose); <u>Pre-incubation Solution</u> (120 mM NaCl, 2 mM KCl, 0.5 mM CaCl2, 26 mM NaHCO3, 10 mM MgSO4, 1.18 mM KH2PO4, 11 mM glucose); <u>Incubation Solution</u> (120 mM NaCl, 2 mM KCl, 2 mM CaCl2, 26 mM NaHCO3, 1.19 mM MgSO4, 1.18 mM KH2PO4, 11 mM glucose) and <u>OGD Solution</u> (120 mM NaCl, 2 mM KCl, 2 mM CaCl2, 26 mM NaHCO3, 1.19 mM MgSO4, 1.18 mM KH2PO4). Osmolarity of all solutions was 300 mOsm and pH 7.4. OGD solution was aerated with 95% N_2 at least 1 hour prior to the start of the experiment to reach an oxygen concentration lower than 5%.

OGD assays

OGD assays were performed modifying a previous protocol (Dos-Anjos et al., 2009). After decapitation, the forebrain was rapidly removed while dripping on it cold (4°C) cutting solution. Rostral, caudal and lateral portions to the hippocampus were removed with a surgical blade and the remaining portion divided sagitally along the interhemispheric fissure. The resulting blocks (containing the hippocampus and the region of cerebral cortex above it) were fixed to a vibratome stage (VT100S, Leica Microsystems, Wetzlar, Germany) and then placed in the vibratome chamber filled with cold cutting solution aerated with 95% O_2 and 5% CO_2, This process was performed in less than 4 minutes to ensure cell viability. Vibratome slices, 350 μm thick, were dissected in the cerebral cortex and hippocampus and transferred into a Petri dish filled with pre-incubation solution aerated with 95% O_2 and 5% CO_2. Hippocampus and cerebral cortex sections were processed independently using four sections for each condition. When required, sections were placed into cell strainers to avoid mechanical damage due to bubbling. The incubation step was performed in a 12-well plate, each well containing 3 ml of the incubation solution and four sections. This plate was maintained in a chamber saturated with 95% O_2 and 5% CO_2 for 15 minutes.

OGD assays were performed by placing the cell strainers with the slices in OGD solution aerated with 95% N_2 5% CO_2 for 30 minutes and then transferring them back into the incubation solution maintained in an O2-saturated chamber for 3 hours (OGD/RL condition). Equal amounts of slices were kept for 3.5 hours in oxygenated incubation solution as controls (normoxic condition).

Slices from each experimental condition were frozen in RNAse-free tubes on dry ice for posterior real time quantitative polymerase chain reaction (RT-qPCR and Western blot assays. Moreover, samples of incubation solution were assayed for cell mortality and glutamate release.

Pharmacological agents

Autophagy inhibition assays were performed both in the OGD/RL and normoxic conditions in the presence of 5 mM 3-MA (Acros Organics, Cat. No. 379791000).

Real-time quantitative PCR (RT-qPCR) assays

All the RT-qPCR assays were performed in accordance with the Minimal Information for Publication of Quantitative Real-Time PCR Experiments (MIQE) guidelines (Taylor et al., 2010).

RNA extraction

Frozen slices from the different experimental conditions were homogenized in Tripure Isolation Reagent (Roche, Cat. No. 11667157001) and total RNA was extracted following the manufacturer's instructions. RNA integrity was determined using Experion^{TM} Automated Electrophoresis System (BioRad, Hercules, CA, US). RNA concentration and purity were determined using a NanoDrop ND-3300 spectrophotometer (NanoDrop Technologies, Wilmington, DE, US). Isolated RNA was maintained in diethylpyrocarbonate (DEPC)-treated water at -80ºC.

Reverse transcriptase reaction

Equal amounts (600 ng) of RNA from each experimental condition were reverse transcribed using the High Capacity cDNA Reverse Transcription Kit (Applied Biosystems, Cat. No. 4368813) following the manufacturer's instructions. Reactions were performed for 10 minutes at 25ºC, 2 hours at 37ºC and 5 seconds at 85ºC in a T-Gradient Thermal

Cycler (Biometra, Gottingen, Germany). Parallel reactions without reverse transcriptase were performed as no-RT controls. Samples of complementary DNA (cDNA) obtained were kept at -20°C until use.

RT-qPCR

RT-qPCR was assayed using transcript-specific primers designed with Primer Express 2.0 software (Applied Biosystems, Foster City, CA, US). Oligonucleotide sequences and GenBank accession numbers are shown in **Table 3**. The 18S ribosomal RNA (rRNA) was used as a housekeeping control. Efficiency of primers was determined from the curve of RT-qPCR amplification of increasing amounts of cDNA using increasing concentrations of primers. Only primers with efficiency values between 90 and 110 were used. Triplicates of 100 ng of cDNA in the presence of 300 nM primers were amplified on a Step-One Plus (Applied Biosystems, Foster City, CA, US) real-time thermal cycler, using SYBR Green PCR Master Mix Kit (Applied Biosystems, Cat. No. 4309155) in the following cycling conditions: 10 min at 90°C and 40 cycles of 15 s at 95°C and 1 min at 60°C.

Table 3. Custom designed primers uses in RT-qPCR assays.

Gene	Primer Forward	Primer Reverse	Gene Bank
beclin1	*5′ctgatggtggcaccatgga*	*5′gccagacatgatgtcaaaaag*	NM_053739.2
p62/sqstm1	*5′ ccatgggtttctcggatgaa*	*5′ ggagggtgctttgaatactgg*	NM_175843.3
atg5	*5′ tggcctactgttcgatcttct*	*5′ acagtgcagaaggtcctttc*	NM_001014250.1
atg7	*5′ cgatggcttcctactgttatt*	*5′ catgacaacaaaggtgbtcaaa*	NM_001012097.1
rna18S	*5′ gattagtccctgcccttgt*	*5′ gatcccgagggcctcaactaaac*	V01270

Changes in the amount of SYBR Green reporter dye fluorescence were analysed with Sequence Detector Software (SDS version 2.2, Applied Biosystems, Foster City, CA, US) obtaining the cycle number (Ct) where the fluorescence signal reaches the designated threshold. Absolute Ct for each transcript to study was normalized with respect to the Ct of the housekeeping control were expressed as 2-ΔCt (Ct target - Ct RNA18S). Fold changes were expressed as $2^{-\Delta\Delta Ct}$, where ΔΔCt represents the transcript increment of OGD/RL with respect to its respective normoxic condition (ΔCt OGD/RL - ΔCt normoxic) (Livak and Schmittgen, 2001).

Western blot analysis

Protein extraction

Total protein was extracted using Tripure Isolation Reagent (Roche, Cat. No. 11667157001) following the manufacturer's protocol and finally dissolved in 8 M urea with 4% SDS. Total protein concentration was determined using the DC Protein Assay Kit (BioRad, Cat. No. 500-0111). Purified protein samples were kept at -20°C.

Electrophoresis and transfer

Sodium dodecyl sulfate-polyacrylamide gel electrophoresis (SDS-PAGE) for p62/SQSTM 1, Beclin 1 and polyubiquitin were carried out in 10% acrylamide while SDS-PAGE for LC3B was carried out in 15% acrylamide. Thirty μg of protein was loaded in each lane and gels were developed during 2 hours at 100 V using a Mini-Protean II system (Bio-Rad, Hercules, CA, US). To detect P62/SQSTM1, BECLIN1 and polyubiquitin, the proteins of the gels were transferred to 0.45-μm nitrocellulose membranes (Life Technologies, Cat. No. IB301001) by dry transfer (7 minutes at 20 V) using an iBlot Gel Transfer System (Invitrogen, Cat. No. IB1001EU). To detect LC3B, the proteins of the gels were transferred to 0.2-μm polyvinylidene difluoride (PVDF) membranes (Bio-Rad, Cat. No. 1620175) during 16 h at 90 mA in a Mini-Protean II tank transfer system (BioRad, Hercules, CA, US). The membranes were stabilized for 10 minutes in 50 mM Tris Buffer Saline pH 7.4 (TBS) and washed three times with 0.2% Tween-20 in TBS (TBS-T).

Protein detection

Membranes were blocked in 5% skimmed milk (for polyubiquitin detection) or 5% bovine serum albumin (BSA, for p62/SQSTM1, BECLIN1 and LC3B) in TBS. Primary antibodies were diluted in 2.5% BSA in TBS-T at the empirically determined optimal concentration (see **Table 4**) and membranes were incubated overnight at 4°C. Primary antibodies were detected using goat anti-rabbit or goat anti-mouse secondary antibodies-HRP conjugated (Dako, Cat. Nos. P0448 and P0447) depending on the primary antibody. Chemiluminiscent reactions were carried out using Pierce ECL Western Blotting Substrate (Thermo, Cat. No. 32106) and detected on Hyperfilm ECL (GE-Healthcare, Cat. No. 28906837). Protein bands were digitalized in a GS-800 Calibrated Densitometer (BioRad, Hercules, CA, US) and the band optical densities were

quantified with Image J Software (NIH, MD, US). Results are expressed as normalized optical density (ratio between optical density (OD) of interest protein and OD of loading control).

Table 4. Antibodies used in Western blot assays.

Protein	Antibody type	Working dilution	Manufacturer	Cat. No.
LC3B	Rabbit polyclonal	0.5 µg/ml	Abcam	Ab48394
P62/SQSTM 1	Mouse monoclonal	0.5 µg/ml	Abnova	H00008878-M01
BECLIN1	Rabbit polyclonal	1 µg/ml	MBL	PD017
Polyubiquitin	Rabbit polyclonal	1 µg/ml	Dako	Z0458
β-ACTIN	Mouse monoclonal	0.2 µg/ml	Sigma	A5316

Cell mortality and cell viability assays

Cell mortality was estimated by cytosolic lactate dehydrogenase (LDH) released into the medium (Decker and Lohmann-Matthes, 1988). LDH activities in the incubation solution in different experimental conditions were quantified in a 96-well plate using the Cytotoxicity Detection Kit (Roche, Cat. No. 11644793001) following the manufacturer's protocol and detecting the iodotetrazolium chloride reduction to formazan at 492 nm in a spectrophotometer (Synergy-HT Microreader, BioTek, Winooski, VT, US). Results are expressed as absorbance units at 492 nm.

Cell viability was measured by mitochondrial reduction of thiazolyl blue tetrazolium bromide (MTT, Sigma, Cat. No. M2128) to purple formazan (Mozes et al., 2012). After OGD/RL, MTT was added to the incubation solution of each condition at a final concentration of 0.5 mg/ml and then maintained for 15 minutes without oxygenation. The slices were then transferred into a 96-well plate with dimethyl sulphoxide (DMSO, 100 µl/well) to dissolve formazan from the slices. The optical densities of extracted formazan were quantified in a spectrophotometer (Synergy-HT Microreader, BioTek, Winooski, VT, US) and data were normalized with the formula OD_{550nm}-OD_{620nm}.

Glutamate Release

The glutamate released into the incubation media was measured by fluorometry using an Amplex Red Glutamic Acid/Glutamate Oxidase Assay Kit (Invitrogen, Cat. No. A12221) following the manufacturer's instructions. Fluorescence emission at 590 nm was read in a Synergy-HT Microreader (BioTek, Winooski, VT, US). Results are expressed as fold change in fluorescence emission.

Statistical analysis

One-way ANOVA analyses followed by Newman-Student-Keuls test were used to compare changes of each variable between different structures in normoxic conditions. Two-way ANOVA analyses followed by the post-hoc Bonferroni test were made to compare the factors OGD and 3MA. Statistics were performed using Graph Pad Prism 5.0 (Graph Pad Software Inc., San Diego, CA, US).

Results

Transcriptional activity

The expression of mRNA levels of *atg5*, *atg7*, *p62/sqstm1* and *beclin1* genes was measured in both cerebral cortex and hippocampus slices at 3 hours of reperfusion following an OGD of 30 minutes. Steady levels of all these transcripts in normoxic conditions were significantly higher in hippocampal than in cerebral cortical slices except for *beclin1* (**Figure 15 A**).

The transcripts of all these markers were significantly higher in the OGD/RL than in the normoxic condition in the cerebral cortex. In contrast, in the hippocampus, the transcript levels of all genes did not change in the OGD/RL with respect to the normoxic condition (**Figure 15 B**).

In the presence of 3-MA in normoxic conditions, we did not detect any differences between the transcript levels of the cerebral cortex and the hippocampus. The presence of 3-MA completely abolished the OGD/RL-induced increases in the cerebral cortex (compare columns 1 and 2 for each gene in **Figure 15 B**).
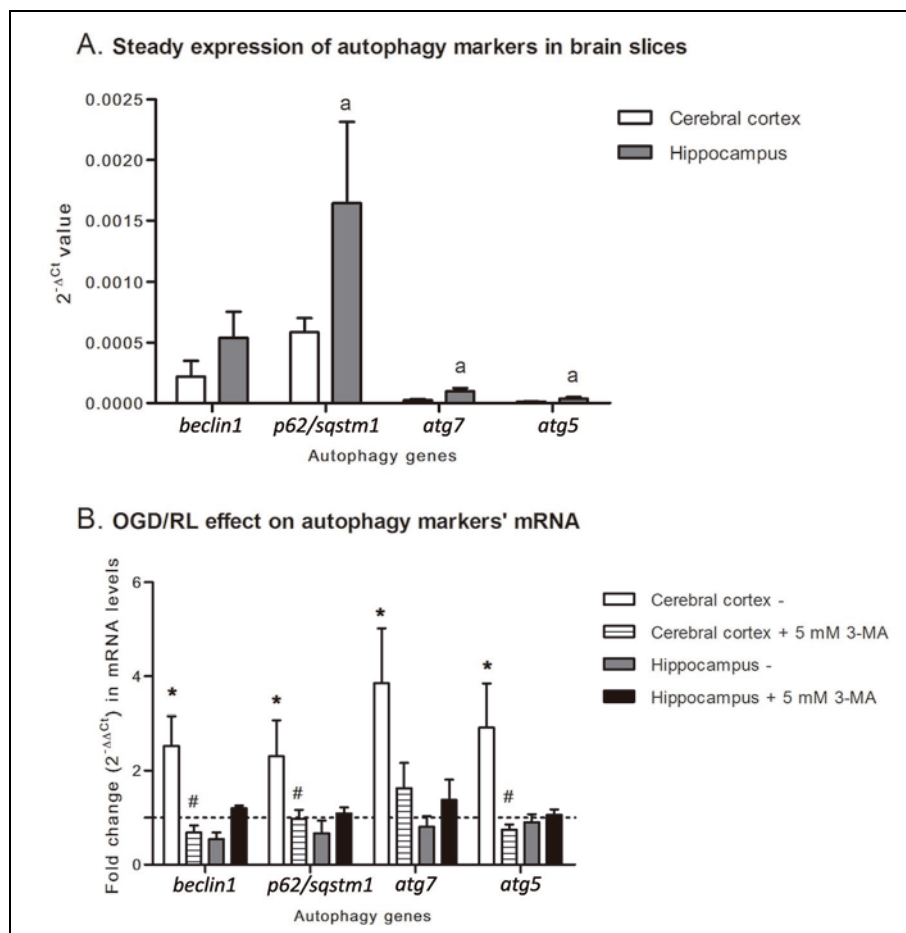
Figure 15. A) Steady state expression. B) OGD/RL effect. Effect of OGD-RL in the presence and in the absence of 3-MA on the transcript levels of autophagy markers. A) Normalized mRNA levels of *Beclin 1*, *P62/SQSTM1*, *Atg5* and *Atg7* with respect to the mRNA levels of RNA 18S in hippocampal and cerebral cortical slices. The figure shows the steady expression (mean ± SEM) of the different mRNAs ($2^{-\Delta Ct}$ values) studied after 3 hours in normoxic conditions. **B)** Columns represent the fold-change ($2^{-\Delta\Delta Ct}$) of mRNA levels due to the OGD/RL with respect to the corresponding normoxic condition (represented by value 1, dotted lines) of the different autophagy markers studied in the presence and in the absence of 3MA in both cerebral cortical and hippocampal slices. [a] indicates statistical differences between the transcript levels of the cerebral cortex and hippocampus ($p < 0.05$, one-way ANOVA followed by Student-Newman-Keuls test, n=5); * indicates statistical differences comparing OGD/RL and normoxic conditions and # indicates significant differences comparing the presence and the absence of 3MA ($p < 0.05$, two-way ANOVA followed by Bonferroni test, n=5).

Phagophore formation

BECLIN1 protein levels in the normoxic condition were significantly higher in the hippocampal slices than in the cerebral cortex. The OGD/RL and normoxic conditions showed similar BECLIN1 protein levels in hippocampal slices. This contrasts with the significantly higher levels of BECLIN1 in the OGD/RL condition observed in the cerebral cortex. In the presence of 3MA, there were no significant differences in BECLIN1 levels

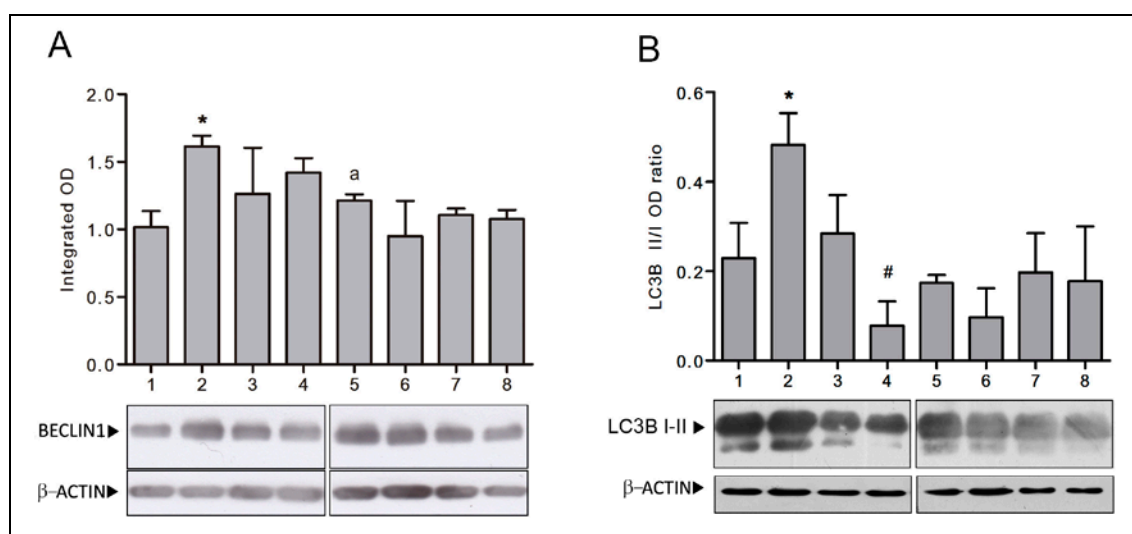between OGD/RL and normoxic conditions, either in the hippocampus or cerebral cortex (**Figure 16 A**).

Figure 16. Effect of OGD-RL in the presence and in the absence of 3-MA on protein levels of phagophore markers. A) Bands and their corresponding optical densities (mean ± SEM) normalized with the β-actin (38 kDa) for Beclin 1 (60 kDa). **B)** LC3BII (16 kDa) and LC3BI (18 kDa) bands and the corresponding ratios LC3BII/LC3BI. Lane 1 (normoxic cerebral cortex), lane 2 (OGD-RL cerebral cortex), lane 3 (normoxic cerebral cortex in the presence of 3MA), lane 4 (normoxic cerebral cortex in the presence of 3MA), lane 5 (normoxic hippocampus), lane 6 (OGD-RL hippocampus), lane 7 (normoxic hippocampus in the presence of 3MA), lane 8 (normoxic hippocampus in the presence of 3MA). [a] indicates statistical differences between protein levels of the cerebral cortex and hippocampus ($p < 0.05$, one-way ANOVA followed by Student-Newman-Keuls test, n=5); * indicates statistical differences comparing OGD/RL and normoxic conditions and # indicates significant differences comparing the presence and the absence of 3MA ($p < 0.05$, two-way ANOVA followed by Bonferroni test, n=5).

The LC3BII/LC3BI ratio was similar in the cerebral cortex and in the hippocampus. This ratio was significantly higher in the OGD/RL condition than in the normoxic condition in the cerebral cortex but there were no differences in the hippocampus. The presence of 3-MA resulted in a decreased LC3BII/LC3BI ratio in the OGD/RL cerebral cortical slices with respect to the normoxic slices. These differences were not found in the hippocampus (**Figure 16 B**).

Autophagy flux

In normoxic conditions, P62/SQSTM1 protein levels were significantly higher in the hippocampal than in the cerebral cortical slices and found no significant changes as a consequence of the presence of 3-MA in any of these structures. The cerebral cortex slices presented significantly lower p62 levels in the OGD/RL condition than those in the normoxic condition (**Figure 17 A**). These decreases were abolished by the presence of

3MA. In the hippocampal slices, there were no significant differences in P62/SQSTM1 levels between the conditions.

In normoxic conditions, no significant differences in the amount of polyubiquitinated proteins were observed between the cerebral cortex and the hippocampus. The OGD/RL assays showed that the amounts of polyubiquitinated proteins in the OGD/RL condition were significantly lower than those observed in the normoxic condition in the cerebral cortex but there were no differences in the hippocampus. In the presence of 3-MA, similar or even higher amounts of polyubiquitinated proteins were observed in the OGD/RL compared to the normoxic conditions in the cerebral cortex. In the hippocampus, the presence of 3-MA resulted in lower but not significant values of polyubiquitinated proteins in the OGD/RL condition than in the normoxic conditions (**Figure 17 B**).
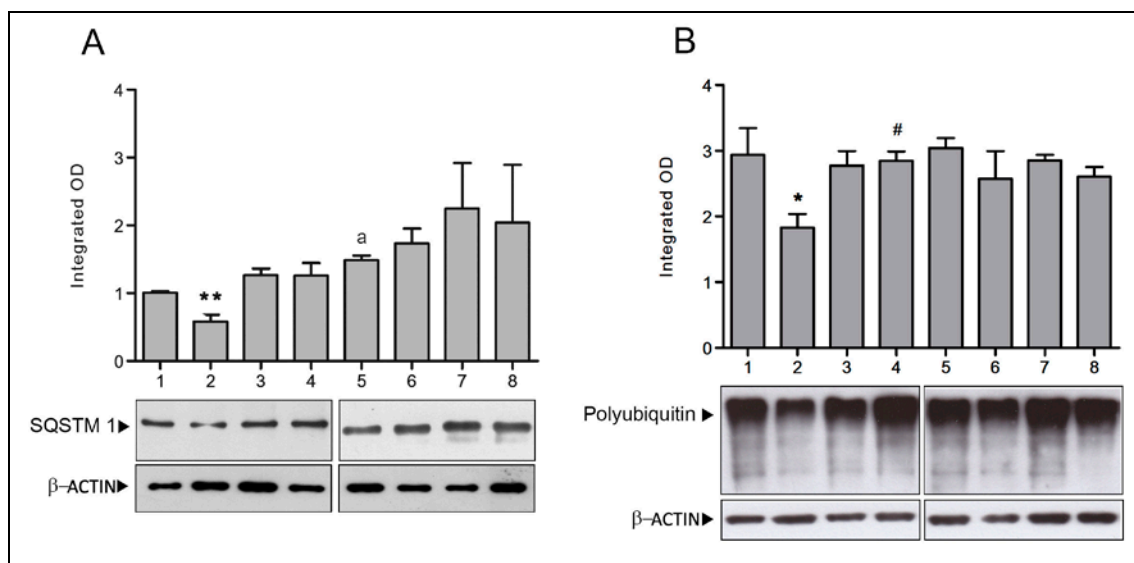

Figure 17. Effect of OGD-RL in the presence and in the absence of 3-MA on protein levels of autophagic flux markers. Bands and their corresponding optical densities (mean ± SEM) normalized with the β-actin for **A)** p62/SQSTM 1 (62 kDa) and **B)** polyubiquitinated proteins (smear from 250 to 130 kDa). Lane 1 (normoxic cerebral cortex), lane 2 (OGD-RL cerebral cortex), lane 3 (normoxic cerebral cortex in the presence of 3-MA), lane 4 (normoxic cerebral cortex in the presence of 3-MA), lane 5 (normoxic hippocampus), lane 6 (OGD-RL hippocampus), lane 7 (normoxic hippocampus in the presence of 3MA), lane 8 (normoxic hippocampus in the presence of 3MA). [a] indicates statistical differences between protein levels of the cerebral cortex and hippocampus ($p < 0.05$, one-way ANOVA followed by Student-Newman-Keuls test, n=5); * ($p < 0.05$) or ** ($p < 0.01$) indicate statistical differences comparing OGD/RL and normoxic conditions and # ($p < 0.05$) indicates significant differences comparing the presence and the absence of 3-MA (two-way ANOVA followed by Bonferroni test, n=5).

Mortality

In the normoxic condition, the presence of 3-MA in the medium significantly increased the mortality compared to its absence in both hippocampal and cerebral cortical slices. In the OGD/RL condition, the presence of 3MA in the medium significantly increased the mortality compared to its absence in the cerebral cortical slices. There were no significant differences between the OGD/RL conditions in the presence or the absence of 3-MA in the hippocampal slices (**Figure 18 A, B**).

MTT assays showed that OGD decreases the viability in both cerebral cortex and hippocampus. The cell viability in the OGD condition in the presence of 3MA was significantly decreased in the cerebral cortex but not in the hippocampus (**Figure 18 C,D**).
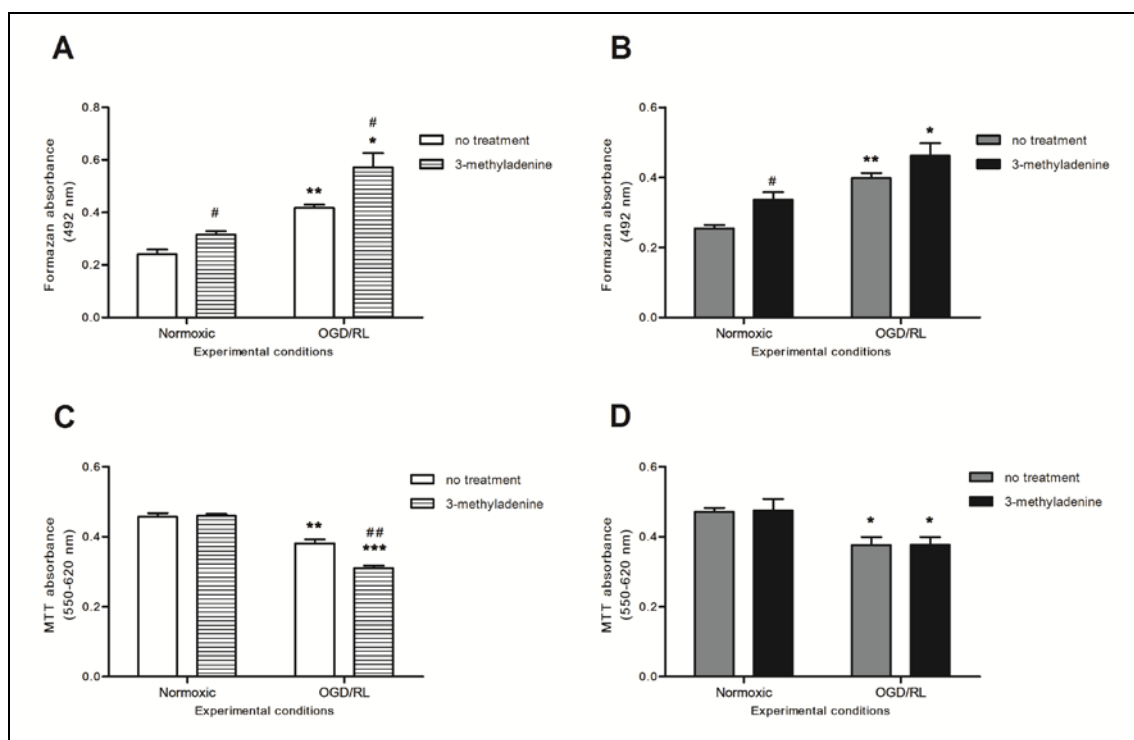
Figure 18. Cell mortality and viability. Release of lactate dehydrogenase (LDH) measured as the absorbance of formazan at 492 nm from A) cerebral cortex and B) hippocampus. Mitochondrial activity measured as the optical density of the formazan extracted from C) cerebral cortex and D) hippocampus. * ($p<0.05$), ** ($p<0.01$) or *** ($p<0.001$) indicate statistical differences comparing OGD/RL and normoxic conditions and # ($p<0.05$) or ## ($p<0.01$) indicate significant differences comparing the presence and the absence of 3MA (two-way ANOVA followed by Bonferroni test, n=5).

Glutamate release

The presence of 3MA in the medium induced the release of glutamate in the normoxic condition in both hippocampal and cerebral cortical slices. In the OGD/RL condition, the presence of 3MA in the medium resulted in a significant increase in the glutamate release when compared with the absence of 3MA. This increase was significantly higher in the cerebral cortex than in the hippocampus (**Figure 19**).

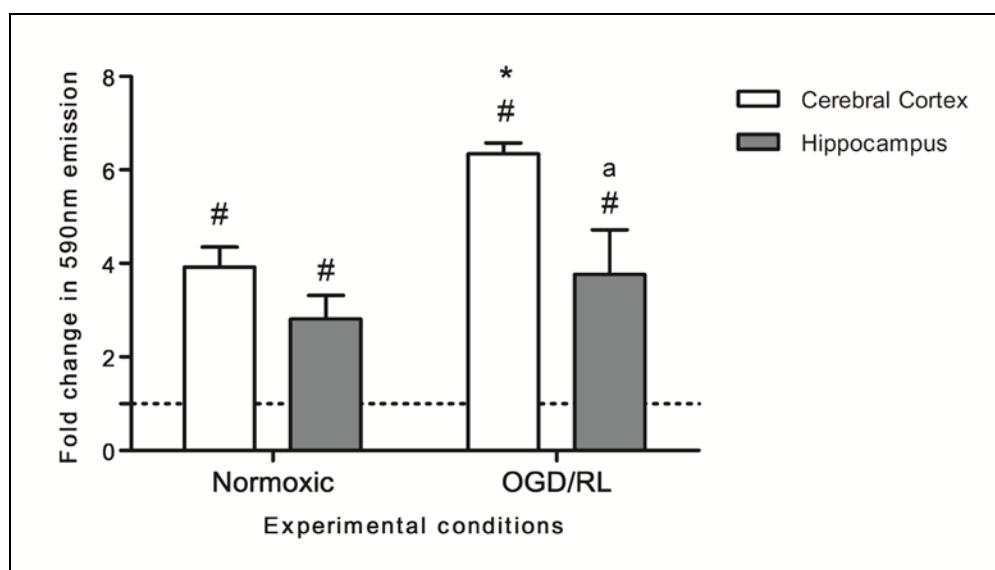**Figure 19. Glutamate release.** Columns show a significant increase of the glutamate release as a consequence of the 3-MA presence in the incubation medium compared to the 3MA absence (indicated by the dotted line, value 1; $p<0.05$, two-way ANOVA followed by Bonferroni test, n=5). The figure also shows that the glutamate release is significantly higher in the cerebral cortex compared with the hippocampus as a consequence of OGD/RL but not in normoxic conditions and is represented by [a] ($p<0.05$, one-way ANOVA followed by Student-Newman-Keuls test, n=5).

Discussion

Limitations and advantages of the brain slice model in quantifying autophagy

Regarding the model of study, the OGD model has been widely used in cultured neurons and in organotypic hippocampal slice culture (Furuichi et al., 2005; Gerace et al., 2012; Huang et al., 2010). The model of brain slices studied herein is widely used for electrophysiology and recently has been used to characterize OGD biochemical responses in different brain structures (Dos-Anjos et al., 2009; Fernández-López et al., 2005; Llorente et al., 2013b; Moro et al., 1998; Richard et al., 2010). This model allows us to compare the response of mature neurons of different structures – such as the

hippocampus or cerebral cortex – in the same experimental conditions. The reliability of this model for mRNA assays is limited to a working window of about 6 hours after obtaining sections (Dos-Anjos et al., 2008) but it represents an unexplored way for the study of the acute autophagy process under different conditions, such as OGD or excitotoxicity.

It must be highlighted that the ex vivo model in normoxic conditions induces an intrinsic stress which elicits an autophagic response that in turn is modified by OGD/RL. In this regard, the use of slices in normoxic conditions in parallel with the OGD/RL condition can be considered equivalent to sham-operated animals. Thus, this study aims to compare how two different brain structures respond in similar conditions to the OGD condition and cannot be considered as representative of the autophagy baseline of these structures *in vivo*. The model provides an accurate measurement of mortality using either LDH release or propidium iodide (Fernández-López et al., 2005; Llorente et al., 2013b). One of the limitations of the model is the number of conditions to assay. Thus, the reduced number of slices that can be obtained (about eight sections from each hemisphere) and the time needed for obtaining them (about 20 minutes per rat) forced us to use a pool of sections from as many as two rats for each experiment. One of the main advantages of the model is that the concentration of oxygen, glucose and pharmacological agents can be controlled as accurately as in cultured cells or hippocampal organotypic cultures. This contrasts with *in vivo* assays where the blood brain barrier and intrinsic properties of each structure (vascularization, diffusion coefficient) modifies the concentration reached by the pharmacological agents (Cavaglia et al., 2001). In addition, unlike the cultured models, the brain slice model retains the structure of the neurons of the different brain regions allowing us to compare them in the same controlled conditions.

Autophagy and OGD/RL

Based on the data of BECLIN1, we found that in normoxic conditions, cerebral cortical and hippocampal slices present different levels of phagophore formation since this marker can be used as a measure of the steady levels of autophagy (Miracco et al., 2007; Sheng Zhang et al., 2013). Therefore it could be stated that hippocampal slices present

higher steady levels than cerebral cortex slices. The rest of the autophagic markers measured in this study also presented higher mRNA expression in the hippocampus than in the cerebral cortex. This supports not only a differential phagophore formation but also the existence of different autophagy levels between slices from these structures, although the autophagy flux cannot be measured without its arrest (Klionsky et al., 2016).

Increases in Beclin1 and the LC3BII/LC3BI ratio in OGD/RL assays in the cerebral cortex add further evidence to the differential autophagy between this structure and the hippocampus found in normoxic conditions. Increases of autophagy dependent on OGD and ischemia have been reported in different models (Carloni et al., 2008; Cui et al., 2013; Qin et al., 2010; Rami et al., 2008; Shi et al., 2012) as well as autophagy differences dependent on the structures. In this regard, different autophagy-induced apoptosis levels in the cerebral cortex and hippocampus have been detected in *in vivo* assays (Ginet et al., 2009).

Considering the time-course of the autophagy, our data allow us to state that in the cerebral cortex the whole autophagic process can be observed 3 hours after OGD. Support for this statement comes from the decrease in the P62/SQSTM1 protein, which would be a consequence of the increase of the autophagy flux that would lead to the P62/SQSTM1 protein being degraded by lysosomes (Mizushima and Yoshimori, n.d.). Additional support for this hypothesis comes from our data of OGD-dependent decreases in the ubiquitination, since P62/SQSTM 1 has been reported to play a link between autophagy and ubiquitinated proteins (Bjørkøy et al., 2005). Variability in the results of hippocampal slices could mask the onset time of the autophagy in this structure and make it difficult to assure its time-course. The autophagy induction in the hippocampus may be undetectable for more than 3 hours. In this regard, some *in vivo* studies detect hippocampal autophagy induction at 12 h (Cui et al., 2013) or 24 h (Ruan et al., 2012) but as far as we know it has not been detected in brain in the first 3 hours.

Autophagy and survival

To what extent does the OGD/RL-dependent autophagy response observed in this model drive survival or programmed cell death? The cerebral cortex has been reported

to present less vulnerability to ischaemia (Jiang et al., 2004; Kirino, 1982; Petito et al., 1987), which could correspond with a protective effect of autophagy following OGD/RL. This would be mirrored by an increase in the phagophore formation in the cerebral cortex. The lesser autophagic hippocampal response could represent a higher sensitivity to OGD or a delayed ability to counteract the OGD-induced stress. In an attempt to prove the hypothesis of differential neuroprotection of autophagy, we used an autophagy inhibitor to check its effect on the cell mortality.

As a first step, we had to choose an inhibitor. Since the assays using this model are limited to a few hours of reperfusion, it is necessary to use autophagy inhibitors able to modulate the response in this period. The inhibitor 3MA has been described to modulate the autophagy response at early timepoints (Wu et al., 2010). In addition, this inhibitor acts on the PI3K class I and class III kinases and therefore modulates both autophagy induction and autophagosome maturation (Shanware et al., 2013; Wu et al., 2010). The presence of 3MA in the medium modified the LC3BII/LC3BI ratio and blocked the decreases in both the P62/SQSTM1 protein and polyubiquitination levels during OGD/RL thus appears to be a reliable inhibitor able to modify the autophagy flux at this early timepoint. These data show that it is possible to analyse both autophagy induction and autophagy flux in the model used herein.

The next step is to answer the question: what are the physiological effects when autophagy is blocked? OGD has been reported to increase mortality in the brain sections as measured by LDH release (Dos-Anjos et al., 2009; Llorente et al., 2013b). In normoxic conditions, the neuroprotective role of the autophagy is evidenced by the mortality elicited by its blocking in both the cerebral cortex and hippocampus. In turn, the OGD/RL assays in which the autophagy was blocked reveals that this neuroprotection is higher in the cerebral cortex than in the hippocampus as revealed both by LDH and MTT assays. In addition, 3MA increases the glutamate release, which results in delayed neuronal death (Arundine and Tymianski, 2004; Caudle and Zhang, 2009). Results of polyubiquitination suggest that, in the cerebral cortex, the increase in the autophagic flux plays a neuroprotective role eliminating the misfolded proteins and this response is lower in the hippocampus. All these data suggest that autophagy is playing a stronger

protective role in the cerebral cortex than in the hippocampus supporting our hypothesis.

In summary, this study shows that, in the cerebral cortex, OGD-induced autophagy flux can be observed at only 3 hours after anoxia and reveals differences between the cerebral cortex and the hippocampus in normoxic conditions. In addition, in the cerebral cortex, autophagy seems to play a neuroprotective role against OGD insult acting on mechanisms such as glutamate release and clearance of misfolded proteins.

CHAPTER 2

Region-specific autophagy response to global cerebral ischemia. The effect of post-ischemic UPR-PERK modulation by salubrinal

Background

Cell insults, such as stroke, result in the excessive accumulation of unfolded proteins, a critical cellular situation called ER stress. To overcome this state, cells ignite a protective response called UPR. This response attenuates general protein translation, activates molecular mechanisms to enhance proper protein folding and increases the activities of two cellular degradation systems, the ER-associated degradation pathway (ERAD) and macroautophagy (B'Chir *et al*., 2013). This latter process (hereafter referred to as autophagy) is characterized by the presence of membrane vesicles, called autophagosomes, which engulf long-lived or damaged proteins and organelles and deliver them to the lysosomes for degradation (He and Klionsky, 2009,Burman and Ktistakis, 2010). Autophagy is a highly selective, tightly regulated process controlled by more than 30 autophagy-related genes (*atg*) that uses specific receptors and adaptors to recognize and eliminate tagged organelles and proteins (Reggiori *et al*., 2012,He and Klionsky, 2009).

Different UPR pathways have been reported to regulate autophagy (Deegan *et al*., 2015) but, in particular, PERK pathway seems to play a neuroprotective role in ischemia (Nakka *et al*., 2010). In this regard, salubrinal, an enhancer of the UPR-PERK pathway that prevents eIF2α dephosphorylation (Boyce *et al*., 2005), has been proven to decrease ischemic-induced damage but only when administered before focal cerebral ischemia (MCAO) (Nakka *et al*., 2010). Recently, we have shown in a previous work that salubrinal also plays a neuroprotective role when administered after global ischemia (Anuncibay-Soto *et al*., 2016).

Ischemic insult elicits an early and strong autophagy activity, reported to appear from the first hours to several days of reperfusion, peaking between 12-48 h(Luo *et al*.,

2014,Yin *et al.*, 2013,Cui *et al.*, 2013,Wiebking *et al.*, 2013,Ruan *et al.*, 2012,Wang *et al.*, 2011). Pharmacological interventions at different times addressed to modulate autophagy result either in exacerbated cell death or neuroprotection (Wang *et al.*, 2011, Cui *et al.*, 2013, Papadakis *et al.*, 2013). This makes it difficult to establish the limits between the neuroprotective and detrimental roles of autophagy. It must be noted that, despite autophagy being one of the main mechanisms involved in cell homeostasis, its role in differential vulnerability to ischemia has scarcely been analysed (Ginet *et al.*, 2009,Perez-Rodriguez *et al.*, 2015).

We wondered if the modulation of the autophagy response to ischemia could also be involved in the previously reported neuroprotective effect of salubrinal. In this study we show the presence of cells with different autophagy response to global ischemia in CA1, CA3 and cerebral cortex and prove, for the first time, that salubrinal modulates this response within the time limits useful in human clinic treatment.

Methods

Animals

Three-month old male Sprague-Dawley rats (350-450 g) were housed at standard temperature (22 ± 1 °C), 12 h light/dark with free access to food and water. A total of 55 rats were randomly divided in the following experimental groups: ischemic animals followed by 24 hours of reperfusion, 5 treated with salubrinal (**24I/R-Sal**) and 5 only treated with vehicle (**24I/R-V**); sham-operated animals sacrificed 24 hours after surgery (**24S-Sal**, n=5 and **24S-V**, n=5); ischemic animals followed by 48 hours of reperfusion, (**48I/R-Sal**, n=10 and **48I/R-V**, n=10); sham-operated animals sacrificed 48 hours after surgery (**48S-Sal**, n=5 and **48S-V**, n=10). Groups of n=5 animals were used only for mRNA and protein sampling, while in groups of n=10, 5 rats were used for microscopy assays and 5 rats for protein and RNA sampling. All experimental procedures were carried out in accordance with the ARRIVE guidelines following the Guidelines of the European Union Council (63/2010/EU) and Spanish regulation (RD 53/2013, BOE 8/2/2013) for the use of laboratory animals and were approved by the Scientific Committee of the

University of Leon. All efforts were made to reduce the number of animals and their suffering.

Transient global cerebral ischemia

Transient global cerebral ischemia was performed using a 2-VO model as previously described (Vieira *et al*., 2014). In brief, animals were anesthetized in an induction box supplied with 4% isoflurane (Abbot Laboratories Ltd, Cat. No. B-PF-013-01) at 3 l/min in 100% oxygen. During surgery, the anesthetized animals received a flux of 1.5-2.5% isoflurane at 800 ml/min in 100% oxygen through a face mask. Body temperature was maintained at $36 \pm 1°C$ using a rectal probe coupled to a feedback regulated heating pad. Both common carotid arteries were exposed and transient global ischemia was induced by clamping them for 15 min with atraumatic aneurysm clips under moderate hypotension conditions (40-50 mmHg) achieved by partial exsanguination. The femoral artery was previously catheterized for permanent monitoring of arterial blood pressure as well as for the extraction and return of blood to the vascular system. About 8 ml of blood were slowly extracted (1 ml/min) through the catheter until the desired hypotension was achieved, which was then maintained by extracting or returning blood through the artery. After ischemia, blood was returned to the animal at 1 ml/min until normal blood pressure was recovered. Then, the catheter was removed and the incisions sutured. Blood clots were prevented by collecting blood in a syringe containing 50 IU heparin (ROVI, Cat. No. 23942-A) in 3 ml of saline solution; moreover, 50 IU heparin/kg were supplied to the animal through the femoral artery. After recovering consciousness the animals were maintained under standard conditions, allowing the reperfusion times desired for each experimental group. Procedures in sham-operated rats were identical to those performed in ischemic animals except for the clamping of the carotid arteries.

Salubrinal treatment

One hour and 24 h after global ischemia, animals received an intraperitoneal dose of 1 mg/kg of salubrinal (TOCRIS, Cat. No. 2347) in a vehicle made of 1 ml of 1.5% DMSO in saline solution, or just the vehicle in the case of untreated animals.

Tissue dissection and total RNA and protein extraction

After decapitation, the brain was quickly removed and placed on a rodent brain matrix (ASI Instruments, Warren, MI, US) at 4°C to obtain 2 mm thick sagittal slices, 1 mm distant from the medial line. In these slices, hippocampal CA1 and CA3 regions, as well as the cerebral cortex (Cx) above the hippocampus were dissected under a light microscope, frozen in dry ice and stored at -80°C. Total RNA and protein from each dissected brain region were extracted using the Tripure® Isolation Reagent (Roche, Cat. No. 11667157001) following the manufacturer's instructions and then stored at -80°C.

Reverse transcriptase reaction and qPCR

All qPCR assays in this study were performed following the MIQE Guidelines (Taylor *et al*., 2010).

RNA sample integrity was confirmed by electrophoresis in 1% agarose gels. Samples whose gels did not show two clear bands, corresponding to 28S and 18S ribosomal RNA (rRNA), were discarded. Possible contamination with genomic DNA was prevented by adding DNase (Thermo, AM2238) to RNA samples. The 260/280 nm absorbance ratio was used to quantify RNA concentrations with a NanoDropND-3300 spectrophotometer (NanoDrop Technologies, Wilmington, DE, US). Six hundred nanograms of total RNA from each sample were reverse transcribed with the High Capacity complementary DNA (cDNA) Reverse Transcription Kit (Applied Biosystems, Cat. No. 4368813) following the manufacturer's protocol. Reverse transcription was performed for 10 min at 25°C, 2 h at 37°C and 5 min at 85°C in a T-Gradient Thermal Cycler (Biometra, Gottingen, Germany) and the cDNA samples were stored at -80°C until use.

Quantitative PCR (qPCR) was carried out in a Step One Plus thermocycler (Applied Biosystems, Foster City, CA, US) using specific primers designed with Primer Express 2.0 software (Applied Biosystems, Foster City, CA, US): *gapdh* (*f5'gggcagcccagaacatca, r5'tgaccttgcccacagcct*, NM_017008); *beclin1* (*f5'ctgatggtggcaccatgga, r5'gccagacatgatgtcaaaaag*, NM_053739.2); *p62/sqstm1* (*f5'ccatgggtttctcggatgaa, r5'ggagggtgctttgaatactgg*, NM_175843.3) and *lc3b (f5'gcgccggagcttcga, r5'gtgctgctcccggatgag,* AY_206669.1). cDNA (100 ng) from each sample was amplified

in triplicate using SYBR Green Master Mix (Applied Biosystems Cat. No 4309155) and 300 nM of each primer, with the following steps: 10 min at 90°C and 40 cycles of 15 s at 95°C and 1 min at 60°C. The *gapdh* housekeeping gene was used as a reference to normalize the Ct values for each gene ($\Delta Ct = Ct_{gen} - Ct_{gapdh}$). Fold changes were analysed following the $2^{-\Delta\Delta Ct}$ method (Livak and Schmittgen, 2001) where $\Delta\Delta Ct$ represents the transcript variation between ischemic and sham animals ($\Delta Ct_{ischemic} - \Delta Ct_{sham}$) or between salubrinal-treated and their respective vehicle-treated animals ($\Delta Ct_{salubrinal} - \Delta Ct_{vehicle}$).

Western blot analysis

Total protein samples were dissolved in 8 M urea in 4% SDS and quantified by a modified Lowry's method using a DC Protein Assay Kit (Bio-Rad, Cat. No. 500-0111). Electrophoresis were performed in SDS-PAGE running 30 µg of protein from each sample in a Mini-Protean II system (Bio-Rad, Hercules, CA, US). The proteins in the gels were transferred to a nitrocellulose membrane (Life Technologies, Cat. No. IB301001) by dry transfer using an iBlot Gel Transfer System (Invitrogen, Cat. No. IB1001EU). Membranes were blocked with 5 % BSA in 0.2 % TBS-T for 1 hour at room temperature. Membranes were incubated overnight at 4°C using one of the following primary antibodies: 1 µg/ml anti-BECLIN1 polyclonal antibody (MBL, Cat. No PD017), 1 µg/ml anti-P62/SQSTM1 monoclonal antibody (AbNova, Cat. No H00008878-M01), or 0.2 µg/ml anti-β ACTIN monoclonal antibody (Sigma, Cat. No A5316). HRP-conjugated anti-mouse or anti-rabbit secondary antibodies (Dako, Cat. Nos. P0448 and P0447) were used. Chemiluminescent visualisation was carried out with Pierce ECL Western Blotting Substrate (Thermo, Cat. No. 32106) and detected on Hyperfilm ECL (Ge-Healthcare, Cat.No. 28906837). The resulting bands were digitalized in a GS-800 Calibrated Densitometer (Bio-Rad, Hercules, CA, US) and band optical densities quantified with ImageJ Software (NIH, Washington, MD, US). The results were expressed as normalized optical density (ratio between the optical density of the target protein band and the optical density of the β-ACTIN loading control band).

Immunofluorescence assays

Rats were euthanized with an intraperitoneal dose of 200 mg/kg sodium pentobarbital and immediately perfused via intra-aortic delivery of RT saline solution, followed by 4%

paraformaldehyde (Fisher, Cat. No. P/0840/53) in 50 mM phosphate-buffered saline pH 7.4 (PBS) at 4°C. Brains were removed, incubated in the same fixing solution during 24 hours at 4°C, cryopreserved in 30% sucrose in PBS and then frozen in dry ice. Forty micron thick coronal sections were obtained with a freezing microtome and stored in 0.025% sodium azide in PBS at 4°C.

An initial epitope-retrieval step was conducted on the sections by incubating them in 0.05% Tween-20 in 10 mM sodium citrate buffer pH 6.0 at 80 °C for 30 minutes. Then sections were blocked in 20% goat serum and 0.2% Triton X-100 in PBS for 1 hour at RT and incubated overnight at 4 °C with the primary antibodies (diluted in 2% goat serum and 0.2% Triton X-100 in PBS). The following primary antibodies were used: 2 µg/ml anti-P62/SQSTM1 (Abnova, Cat. No. H00008878-M01), 2 µg/ml anti-LC3B I/II (Abcam, Cat. No. Ab48394), 1 µg/ml anti-LAMP2A (lysosomal-associated membrane protein 2A) (Abcam, Cat.No. 125068), 1 µg/ml anti-polyubiquitin (Dako, Cat. No. Z0458) and 4 µg/ml anti-NeuN (Millipore, Cat. No. MAB377). Secondary anti-rabbit or anti-mouse IgG antibodies conjugated with Alexa-488 or Alexa-568 (Life Technologies, Cat. Nos. A11008 and A11004, respectively) were used. Nuclei were counterstained with 4', 6-diamino-2-fenilindol (DAPI, Sigma, Cat. No. D9564) and then sections were mounted on 3-aminopropyl trithoxysilane (ATE)-treated glass slides with Fluoromount G Mounting Media (Life Technologies, Cat. No. P36934). Six equidistant non-overlapping sections from rostral to caudal hippocampus were analysed per animal. Image acquisition was carried out in a Nikon Eclipse TE-2000 Confocal Microscope (Nikon Instruments, Amsterdam, Netherlands). Image processing and analysis were performed using ImageJ Software (NIH, Washington, MD, US).

For LC3B quantification, inverted gray scale images were used to count the LC3B puncta in neurons outlined with NeuN labelling (**Figure 20**). These neurons were scored as 0 (no puncta), 1 (very small number of punta), 2 (small number of puncta without aggregates) or 3 (many puncta forming aggregates).

Figures for presentation were filtered with a mean filter and the Sternberg algorithm was used to remove non-specific background (Sternberg, 1983).
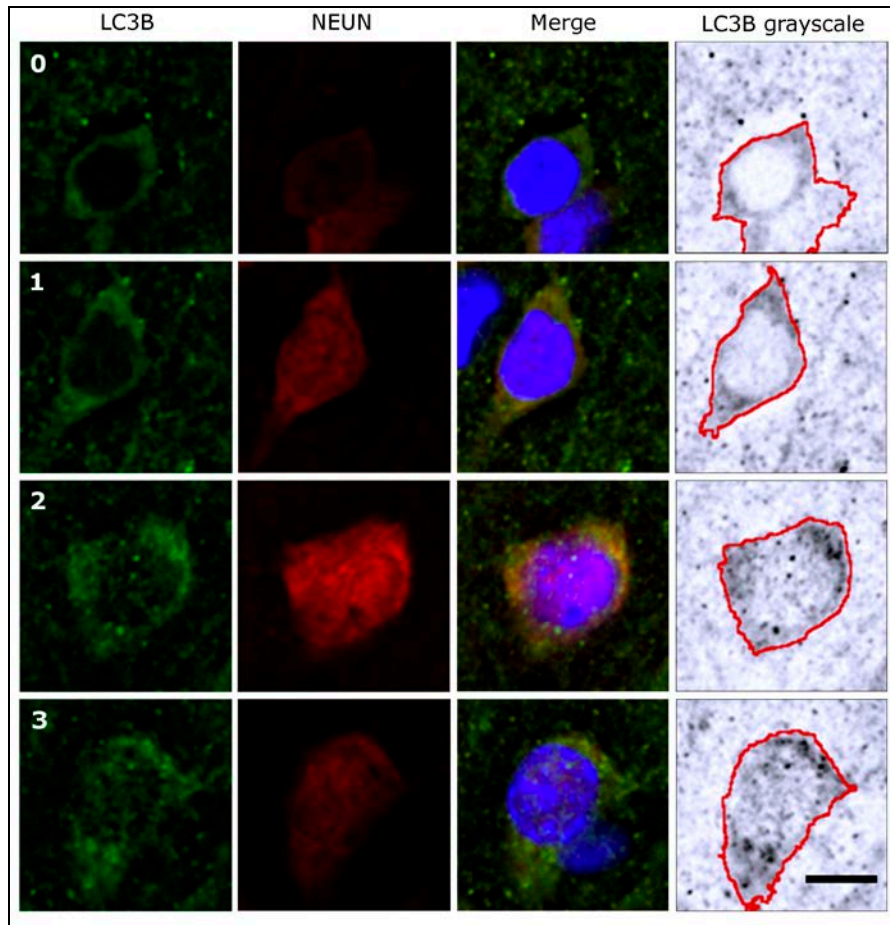
Figure 20. Quantification of LC3B inmunolabelling. Image show pyramidal neurons (stained with anti-NeuN in red) with different amount of autophagosomes (labelled with anti-LC3B in green). Inverted gray images helped to score the neurons as 0 (no puncta), 1 (very small number of punta), 2 (small number of puncta without aggregates) or 3 (many puncta forming aggregates). Bar = 8 µm.

Fluorojade-B staining

Damaged neurons in CA1 pyramidal layer 48 hours after the ischemic insult were stained using Fluorojade-B (FJ-B, Millipore, Cat. No.AG310) which has been reported to specifically stain degenerating neurons (Schmued and Hopkins, 2000).Three equidistant non-overlapping coronal sections of each hemisphere per animal, obtained as above mentioned, were mounted on ATE-treated glass slides and dried at 50 ºC during 1 hour. FJ-B staining was carried out following manufacturer's instructions. In brief, glass slides were immersed 5 min in 5% NaOH in 80% ethanol followed by 2 min in 70% ethanol and 2 min in PBS. Non-specific background was reduced by incubating the slides with 0.06% $KMnO_4$ for 10 minutes. After washing with PBS, slides were incubated in 0.0025% FJ-B in 0.1% acetic acid solution for 20 minutes. Neuronal nuclei were counterstained with 1 µg/ml DAPI in PBS for 20 minutes followed by three washes with PBS. Stained slides

were cleared by immersion in xylene for 2 minutes and mounted with DPX mounting media (Sigma-Aldrich, Cat. No. 44581).Three optical dissectors (255 μm x 255 μm) in CA1 of each section were obtained with a Nikon Eclipse TE-2000 Confocal Microscope (Nikon Instruments, Amsterdam, Netherlands). For quantification, fluorescence average level of each dissector was used as a measure of the Fluorojade B staining.

Double labelling of P62/SQSTM1 and Fluorojade-B

CA1 pyramidal neurons were stained with both P62/SQSTM1 antibody and FJ-B, modifying a previously published protocol (Ehara and Ueda, 2009).After labelling P62/SQSTM1 as explained above, sections were mounted on ATE-treated glass slides, air-dried for 1 hour, immersed for 5 min in PBS, incubated with 0.06% $KMnO_4$ during 5 min and stained for 20 min with 0.0025% FJ-B in 0.1% acetic acid solution. Slides were rinsed three times with PBS and mounted in acidic mounting media (0.1% acetic acid and 80% glycerol). Image acquisition was carried out in a Nikon Eclipse TE-2000 Confocal Microscope (Nikon Instruments, Amsterdam, Netherlands).

Statistical analysis

Statistical analyses were performed with Graph Pad Prism 6.0 Software (Graph Pad Software Inc, La Jolla, CA, US). Parametric variables were analysed with two-way ANOVA followed by Bonferroni post-hoc test. Non parametric variables were analysed with Kruskal-Wallis test followed by the post-hoc Dunn test. A 95% confidence level was stablished to consider significant differences.

Results

mRNA levels of autophagy related genes

A significant increase in transcripts for *beclin1*, *p62/sqstm1* and *lc3b*, representative genes of different steps in autophagy, was observed in cerebral cortex at 24 h and 48 h after ischemic insult. In contrast, no changes were observed in hippocampal structures (**Figure 21 A, C, E**).

Treatment with salubrinal resulted in striking differences in the transcripts of the different genes analysed. Thus, *beclin1* and *lc3b* transcripts were not modulated by salubrinal, except for an increase at 48 h after treatment in Cx of sham animals. (**Figure 21 B, F**). In contrast, salubrinal induced significant increases in *p62/sqstm1* transcripts of sham treated animals in most structures studied at both 24 h and 48 h, except CA3 at 24 h. In injured animals, increases in *p62/sqstm1* transcripts were only observed at 24 h in the CA1 and at 48 h in the Cx after salubrinal treatment. Interestingly, CA3 at 24 h showed decreases in these transcripts as a consequence of salubrinal (**Figure 21 D**).
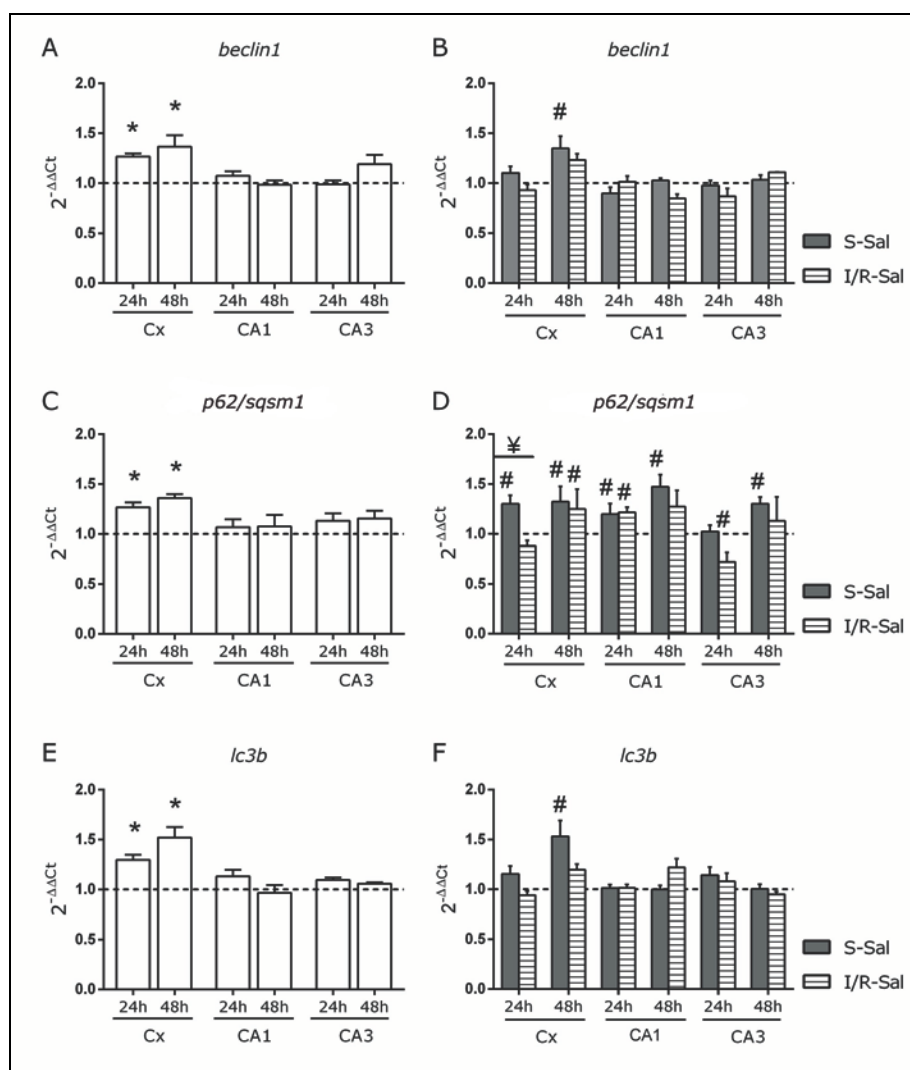

Figure 21. .**Modifications of transcript levels of several autophagy-related genes.** Fold changes in transcript levels of *beclin1* **(A)**, p62/*qstm1* **(C)** and *lc3b***(E)** in animals not treated with salubrinal. White columns represent the values of injured animals (I/R-V) at 24 h and 48 h compared with those of sham animals (S-V) (value 1, dotted line). Salubrinal-induced fold changes in transcript levels for *beclin1***(B)**, *p62/sqstm1* **(D)** and *lc3b***(F)**. Grey columns represent the values of treated sham (S-Sal) and striped columns those of treated injured animals (I/R-Sal) compared with their respective untreated sham (S-V) and untreated injured animals (I/R-V) indicated by a value of 1, dotted line. * represents significant

differences between sham and ischemia, # significant differences elicited by salubrinal treatment and ¥ significant interaction between the factors ischemia and salubrinal treatment. Two way ANOVA followed by Bonferroni test (n=5, p<0.05).

BECLIN1 protein levels

BECLIN1 levels appeared increased in Cx and CA1 24 h after the ischemic insult (**Figure 22 A, B, C**). The treatment with salubrinal increased BECLIN1 protein levels at 24 hours in the injured animals, these increases being significant in all the structures compared with treated sham animals but only significant in Cx when compared with untreated injured animals. After 48 h of reperfusion, no significant changes were observed due to either ischemia or salubrinal (**Figure 22 D, E, F**)
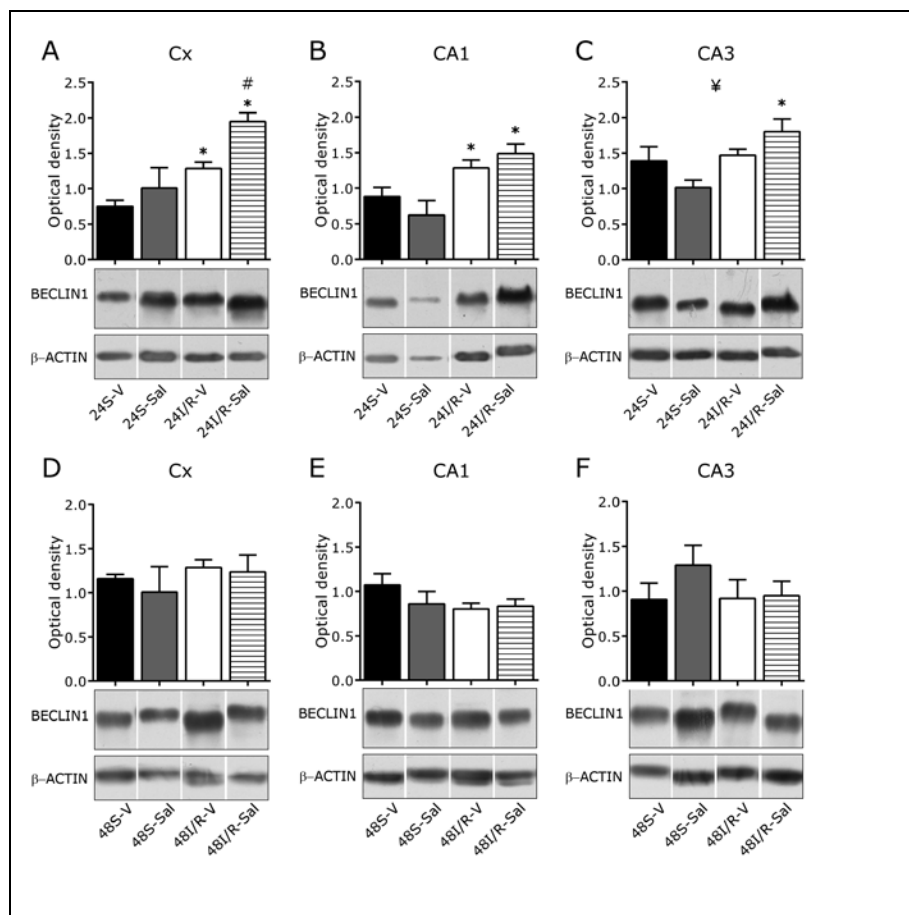

Figure 22. .**Beclin1 protein levels**. Plot shows mean ± SEM of optical density values obtained from Western blot bands normalized with respect to their corresponding β-actin control. Data obtained 24 h after ischemia in Cx**(A)**, CA1 **(B)**, CA3 **(C)** and 48 after ischemia in Cx **(D)**, CA1 **(E)** and CA3 **(F)** under the different conditions analysed: sham animals treated and untreated with salubrinal (S-Sal and S-V, grey columns and black columns, respectively) and injured animals treated and untreated with salubrinal (I/R-Sal and I/R-V, striped and white columns, respectively). Representative bands of both beclin-1 and its reference β-actin are shown at the bottom of each column. * represents significant differences between sham and ischemia, # significant differences elicited by salubrinal treatment and ¥ significant interaction between the factors ischemia and salubrinal treatment. Two way ANOVA followed by Bonferroni test (n=5, p<0.05).

LC3B immunofluorescence assays

The presence of LC3B puncta is a typical marker of the association of this protein with the phagophore, which indicates autophagy activity in the cells. The co-localization of LC3B with the neuronal marker NeuN allows this process to be studied selectively in neurons. After 48 h of reperfusion, the ischemic insult resulted in an increased number of LC3B puncta in Cx and CA1 neurons but no changes were observed in those of CA3. At this time, the treatment with salubrinal also significantly increased the number of LC3B puncta in the neurons of injured animals in all the structures studied (**Figure 23**).

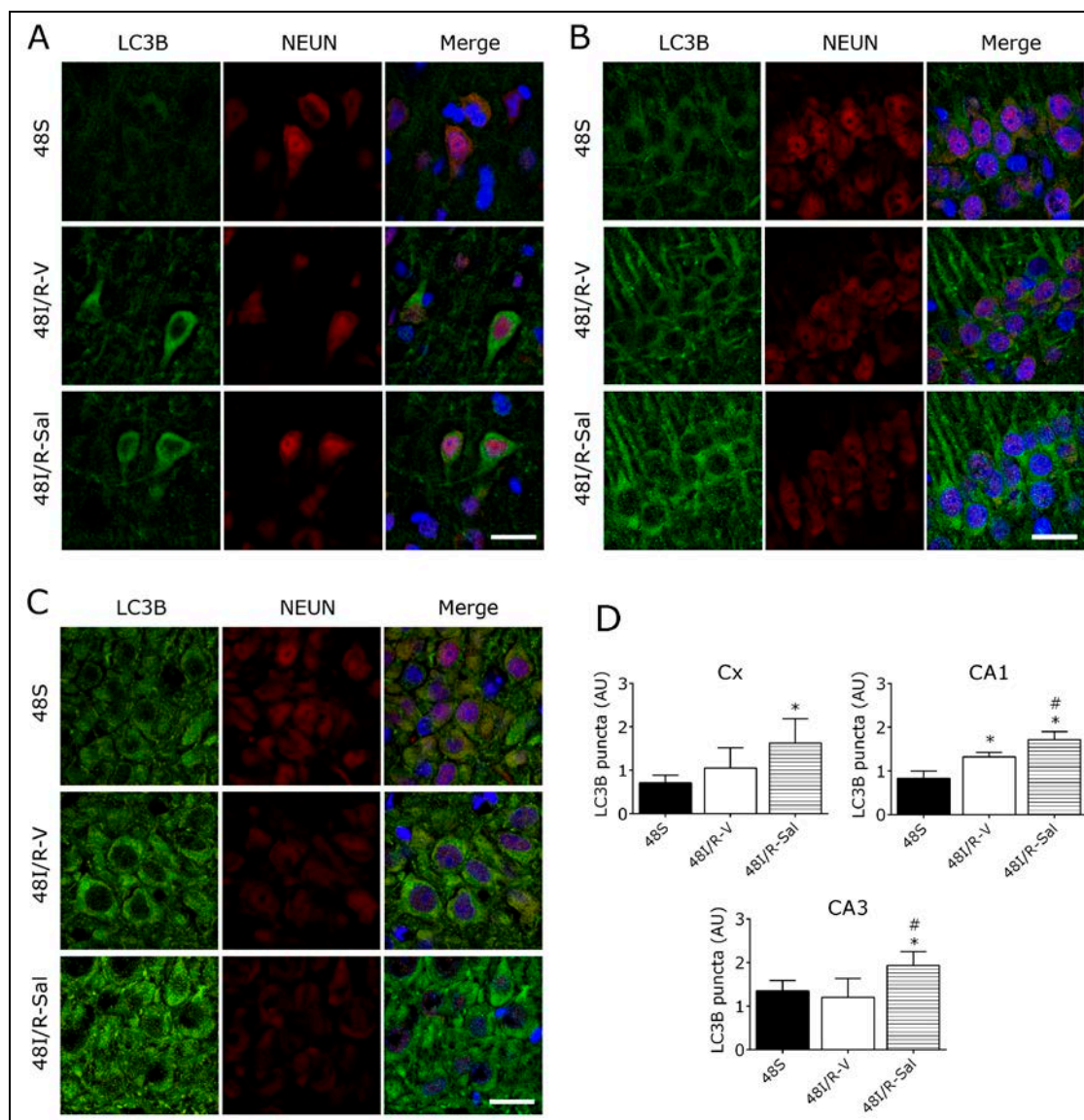**Figure 23. LC3B staining 48 hours after ischemia**. Pyramidal neurons showing LC3B puncta (stained in green) 48 hours after the ischemic insult in Cx **(A)**, CA1 **(B)** and CA3 **(C)**. The co-localization with the neuronal marker NeuN (stained in red) allows discrimination of autophagy in neurons (merged images) Bar = 20 μm. Plots **(D)** show the score of puncta (mean ± SEM) in sham animals (48S, black columns),

injured untreated (48I/R-V, white columns) and salubrinal treated injured animals (48I/R-Sal, striped columns) in Cx, CA1 and CA3. * represents significant differences between sham and ischemic animals and # significant differences between salubrinal-treated and untreated ischemic animals. Kruskal-Wallis test followed by the post-hoc Dunn test (p<0.05, n=4).

P62/SQSTM1 protein levels

The ischemic insult elicited significant decreases in P62/SQSTM1 levels at 24 h only in CA1. At 48 h, however, these levels appeared significantly increased compared with those observed in sham animals. The treatment with salubrinal did not trigger a significant effect 24 hours after ischemia but elicited a striking decrease in P62/SQSTM1 levels in CA1 48 h after the insult (**Figure 24, A-F)**
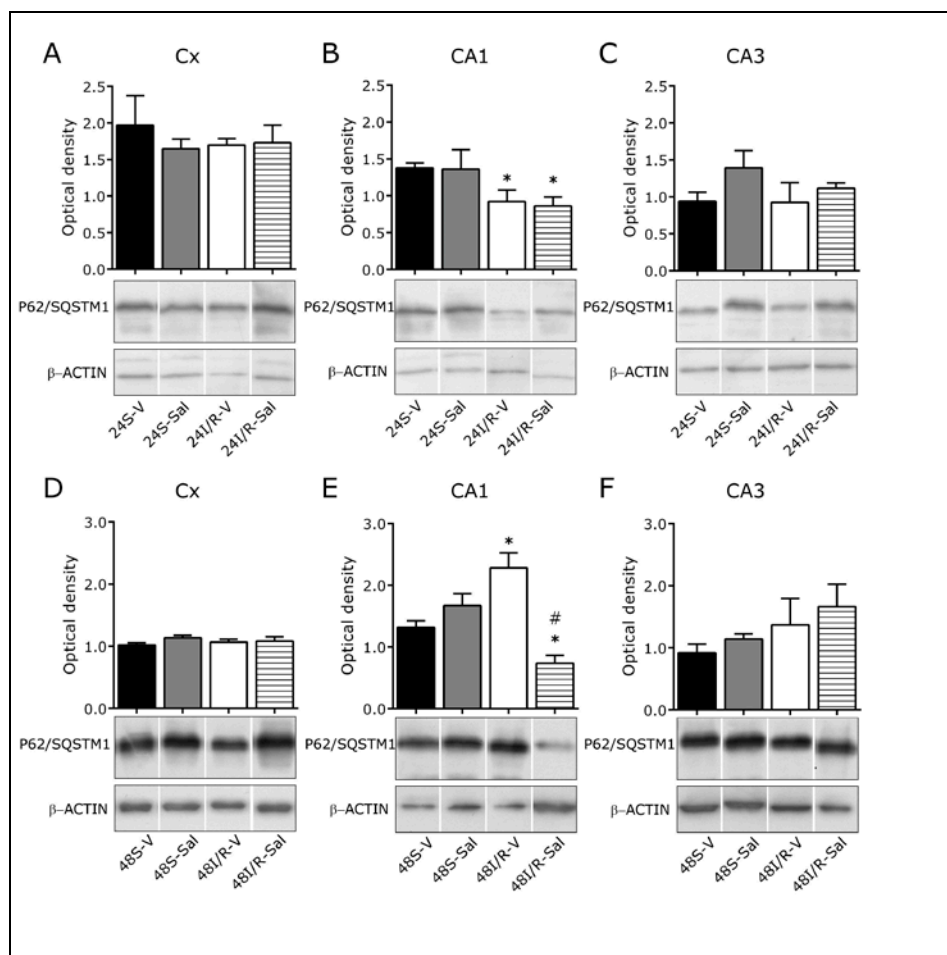
Figure 24. P62/SQSTM1 protein levels. Plot shows optical density values (mean ± SEM) obtained from Western blot bands normalized with respect to their corresponding β-actin. Data obtained 24 h after ischemia in Cx **(A)**, CA1 **(B)**, CA3 **(C)** and 48 h after ischemia in Cx **(D)**, CA1 **(E)** and CA3 **(F)** under the different conditions analysed: sham animals treated and untreated with salubrinal (S-Sal and S-V, grey columns and black columns, respectively) and injured animals treated and untreated with salubrinal (I/R-Sal and I/R-V, striped and white columns, respectively). Representative bands of both P62/SQSTM1 and its reference β-actin are shown at the bottom of each column. * represents significant differences between sham and ischemia, # significant differences elicited by salubrinal treatment and ¥ significant

interaction between the factors ischemia and salubrinal treatment. Two way ANOVA followed by Bonferroni test (n=5, p<0.05).

P62/SQSTM1 immunofluorescence assays

P62/SQSTM1 immunohistochemistry confirmed the ischemic-dependent increases observed in CA1 at 48 h and how the salubrinal treatment abolished this effect (**Figure 25 A**).The labelling with P62/SQSTM1 in 48I/R-V animals ranged from cells with a poor staining of scattered puncta located mainly in the somata (**Figure 25, A-D, arrows**) to cells with a strong labelling with puncta in large aggregates (**Figure 25, A-D, arrow heads**) located in the somata and the proximal apical prolongation. The strongest P62/SQSTM1 immunofluorescent labelling was observed in the neurons of the CA1 pyramidal layer of 48I/R-V, in a less degree in the Cx and non-detected in CA3 (**Figure 25**). Distribution of cells with strong labelling in the hippocampus ranged from small cell groups to a homogenous band along the whole CA1 pyramidal layer (**Figure 25 E**). We did not observe local differences in the distribution of this cell type along the different layers of Cx.

CA1 neurons presented a strong labelling in LC3B, which co-localized with neurons with low P62/SQSTM1/ labelling (**Figure 25 B, arrows**); however cells with a strong P62/SQSTM1 labelling did not present a corresponding increase in LC3B (**Figure 25 B, arrow heads**). LAMP2A labelling did not fit with P62/SQSTM1 labelling (**Figure 25 C**). However, a good co-localization as well as a positive correlation in the levels of polyubiquitin and P62/SQSTM1 labelling were observed (**Figure 25 D, arrow heads**).

The treatment with salubrinal decreased the labelling of P62/SQSTM1 in all the neurons and it was particularly relevant in the neurons with stronger labelling (**Figure 25 A**).
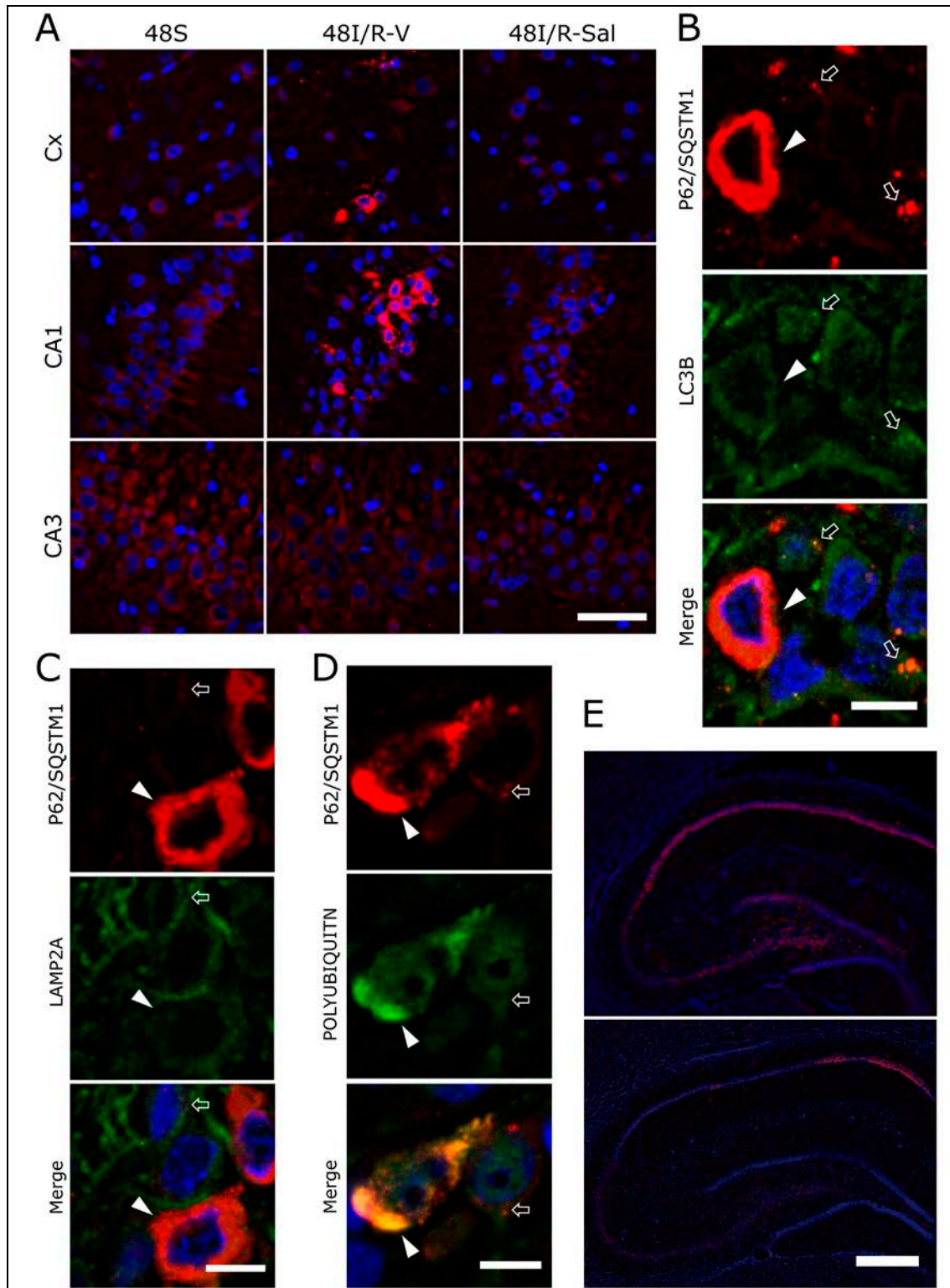
Figure 25. P62/SQSTM1 immunofluorescence. P62/SQSTM1 labelling (in red) after 48 hours of reperfusion **(A)** is shown in Cx, CA1 and CA3 pyramidal layers of sham animals (48S), untreated injured animals (48I/R-V) and salubrinal-treated injured animals (48I/R-Sal). Bar = 50 µm. Double labelling of P62/SQSTM1 and LC3B **(B)**, P62/SQSTM1 and LAMP2A **(C)** and P62/SQSTM1 and ubiquitin **(D)** in CA1 neurons of untreated injured animals. Arrows indicate type I neurons and arrowheads type II neurons. Type II neurons show ubiquitin and SQSTM1/p62 positive aggregates not included in autophagosomes (LC3B) or autolysosomes (LAMP2A). See text for additional explanation. Bar = 10 µm. Different patterns

of P62/SQSTM1 accumulation **(E)** in CA1 from untreated injured animals, ranging from the whole pyramidal layer (upper image) to groups of a few cells (lower image). Bar = 500 μm.

Degeneration of CA1 pyramidal layer 48 hours after ischemic insult

Untreated injured animals showed a significant increase in the staining of pyramidal neurons labelled with FJ-B in CA1 pyramidal layer after 48 hours of reperfusion which was significantly decreased by the treatment with salubrinal (**Figure 26 , A-B**). A double labelling of P62/SQSTM1 and FJ-B was performed in CA1 pyramidal layer of 48I/R-V animals to detect whether pyramidal neurons that accumulates P62/SQSTM1 were healthy or damaged (**Figure 26 C**). Most of these cells were FJ-B positive (**Fig. 26 C, arrow heads**) but some of them were FJ-B negative (**Figure 26 C, arrows**).
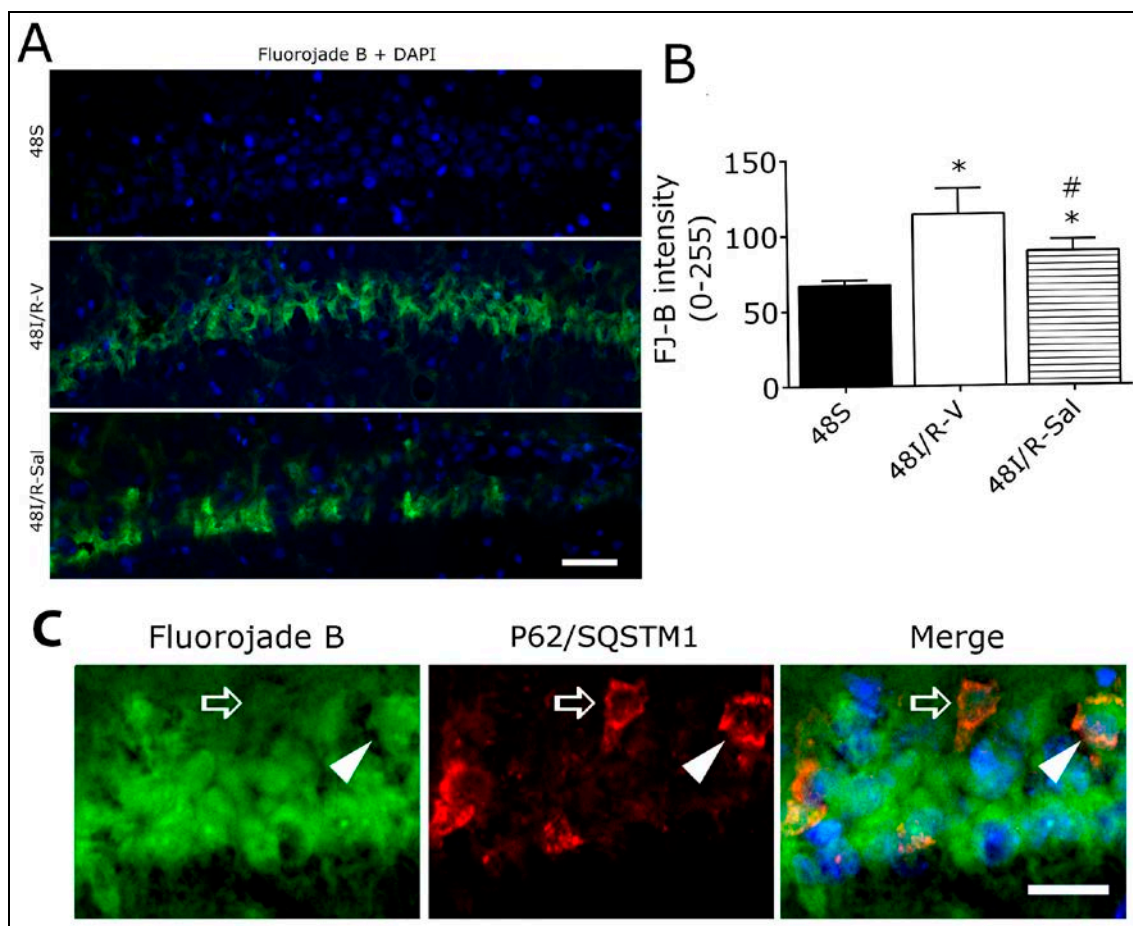
Figure 26.Neuronal damage in CA1 hippocampal region. Ischemia and salubrinal effects on neuronal damage 48 hours after ischemic insult. **A** shows representative Fluorojade-B (green) and DAPI (blue) staining from sections of CA1 pyramidal layer in sham (48S), untreated insulted (48I/R-V) and salubrinal treated injured animals (48I/R-Sal). Bar = 50 μm. Plots in **B** shows Fluorojade-B staining intensity (mean ± SEM) in the different experimental conditions. * represents significant differences between sham and ischemia and # significant differences elicited by salubrinal treatment. One-way ANOVA followed by Bonferroni test (n=5, p<0.05).Images in **C** correspond to the double labelling of Fluorojade-B (green) and

P62/SQSTM1 (red) of CA1 pyramidal neurons. Although most of cells with large SQSTM/p62 aggregates are FJ-B positives (arrow heads), some of them appear as FJB-B negative (arrows). Bar = 20 µm.

Discussion

Differential autophagy response between different brain structures

Differential vulnerability to ischemia has been described in different brain regions, particularly the higher vulnerability of CA1 pyramidal neurons compared with those from CA3 and Cx (Sarnowska, 2002; Kirino, 1982; Zhu *et al*., 2012). These differences in vulnerability observed 7 days after injury (Larsson *et al*., 2001; Anuncibay-Soto *et al*., 2016), can be detected in the first 48 hours as showed in this study. Many different cell processes follow ischemic damage, including oedema, necrosis and delayed cell death (Mehta *et al*., 2007), but the ultimate mechanisms responsible for the differential vulnerability remain unclear. Different molecules and mechanisms have been hypothesized to be responsible for this differential vulnerability, including differential kinase or phosphorylase activities (Pieper *et al*., 2001), differential susceptibility to calpain-caspase activation (Ayuso *et al*., 2010), variations in expression of hammartin (Papadakis *et al*., 2013), differential expression of glutamatergic (Stanika *et al*., 2010) and gabergic (Montori *et al*., 2012) receptors, excitoxicity (Fan *et al*., 2008,Ye *et al*., 2010) or even different properties in the neurovascular unit (Anuncibay-Soto *et al*., 2014). Interestingly, autophagy, in spite of being a well-known mechanism for controlling cell homeostasis (Thapalia *et al*., 2014), has scarcely been analysed as a factor responsible for this differential vulnerability (Ginet *et al*., 2009,Perez-Rodriguez *et al*., 2015).

Autophagy in cerebral cortex as a homeostatic mechanism

Our data revealed differences in the autophagy response in brain structures with differential vulnerability to ischemia, supporting the idea that autophagy could play a crucial role in the onset or the type of delayed cell death for these structures. In this study, we analysed both induction and autophagy flux markers in an attempt to discriminate whether the autophagy induced by ischemia in these areas is beneficial or detrimental. Thus, beneficial autophagy depends on balanced autophagosome

formation (autophagy induction) and substrate degradation (autophagy flux) that contributes to normal cell homeostasis (Viscomi and D'Amelio, 2012). In contrast, detrimental autophagy is mirrored by an imbalance between autophagy induction and autophagy flux, leading to an accumulation of autophagosomes in the cell that could drive a delayed cell death program (Sarkar *et al.*, 2014).

Transcript and protein expression of BECLIN1 and LC3B, considered representative markers of autophagy induction (Yang and Klionsky, 2010) indicated ischemic-dependent autophagy induction in Cx. Further support for the effect of ischemia on autophagy induction was provided by the consistently enhanced expression of the rest of the autophagy-related genes analysed in this structure. Autophagy flux was measured by quantifying P62/SQSTM1 protein clearance, the most accepted parameter since it mirrors the cargo degradation of autophagosomes by lysosomes (Mizushima and Yoshimori, 2007). We should notice that a specifically blocking of autophagy flux *in vivo*, which would confirm our data, require very complex assays. Situations where P62/SQSTM1 transcripts increase without changes in protein levels, as observed herein, have also been considered to reflect an increase in autophagy flux (Jain *et al.*, 2010). Moreover, the increased number of LC3B puncta observed in the immunofluorescence analysis supports this increased autophagy flux. Therefore, our data show that ischemia results in increased autophagy induction accompanied by increased autophagy flux, i.e, a beneficial autophagy, which provides strong support for the hypothesis that increased autophagy after ischemic insult plays a neuroprotective role in the cerebral cortex (Perez-Rodriguez *et al.*, 2015,Ginet *et al.*, 2009). These data are consistent with previous work in *ex vivo* assays demonstrating that blocking autophagy with 3MA after OGD increases the mortality in Cx (Perez-Rodriguez *et al.*, 2015).

Differential autophagy response in CA1 and CA3 hippocampal subfields

While CA1 presented ischemic-induced modifications in autophagy, CA3 did not, which could support a role for autophagy in the differential vulnerability considering only these structures. However, the different autophagic response in Cx (that increases autophagy), CA3 (which has no autophagic changes) and CA1 (that also increases autophagy but still presents high mortality) discards the hypothesis of autophagy as the

main responsible for the differential vulnerability. Thus, although autophagy response to global ischemia is structure-dependent, other mechanisms seem to be required to explain the differential vulnerability.

Surprisingly, the differences between CA1 and CA3 in the autophagic response here observed are opposite to those previously published using a model of neonatal ischemia, where autophagy was not modified in CA1 and increased in CA3 and Cx, although detrimental autophagy for CA3 and beneficial autophagy for Cx were described (Ginet *et al*., 2009). In light of these data, we think that, in the first 48 hours after global ischemia, autophagy activity could be age-dependent in the hippocampus but not in the cerebral cortex.

Autophagy data from CA1 are more consistent than those from cerebral cortex. Thus, increases in both induction and autophagy flux appear 24 h after ischemia on the basis of increased BECLIN1 protein levels, in agreement with decreased P62/SQSTM1 protein levels. This suggests a beneficial autophagy at this time. In contrast, this response was thoroughly modified 48 h after ischemia, when P62/SQSTM1 increases were observed. We wondered if P62/SQSTM1 accumulates as a consequence of decreased autophagosome clearance and this would be due to impaired autophagy flux leading to neural death, in a similar way to that reported in a model of traumatic brain injury (Sarkar *et al*., 2014). To prove this idea, we carried out double-labelling analyses of P62/SQSTM1 with markers of autophagosomes (LC3B) and lysosomes (LAMP2A). Accumulation of P62/SQSTM1 did not correlate with an accumulation of LC3B and therefore we discard accumulation of autophagosomes as a consequence of the ischemia at this time of analyisis. In the same way, LAMP2A levels did not correlate with P62/SQSTM1 levels and, together with the lack of co-localization, allows to state that P62/SQSTM1 accumulation is not related with autolysosomes. Therefore, we discarded the idea of autophagy flux impairment and we hypothesized that P62/SQSTM1 aggregates here observed are unable to be included in the autophagosome-lysosome pathway.

To test this hypothesis, we considered that P62/SQSTM1 is an adaptor protein required for the aggregation of ubiquitinated proteins, playing essential roles in its autophagic

clearance (Lippai and Low, 2014) and we found a consistent co-localization of P62/SQSTM1 and polyubiquitinated proteins. These characteristics meet the criteria to consider P62/SQSTM1 aggregates here observed as **sequestosomes**, defined as aggregated insoluble proteins in cytoplasmic bodies lacking enveloping membranes and apparently destined for autophagic clearance (Solcia *et al.*, 2014).

UPR-PERK pathway modulation and the autophagy response

The accumulation of insoluble protein aggregates at this time of reperfusion after ischemia suggests the presence of a strong ER stress that cannot be overcome by UPR. In fact, a greater vulnerability to ischemia of CA1 has been previously proposed to be consequence of a deficient UPR (Llorente *et al.*, 2013a). In light of our data, we hypothesized that neurons presenting an accumulation of P62/SQSTM1 aggregates are unable to elicit a level of autophagy sufficient to eliminate these ischemia-induced misfolded protein aggregates (sequestosomes) and this could be a consequence of an insufficient UPR. Cultured autophagy-deficient cells from a knock-out mouse strain showing the presence of P62/SQSTM1 and ubiquitin positive aggregates (Hara *et al.*, 2006) gives additional support to our idea.

To confirm this hypothesis, we assumed that enhancement of the UPR would help to overcome ischemic-induced ER-stress, preventing or reducing the presence of sequestosomes in some CA1 neurons. The use of salubrinal seemed to be an obvious choice as a promoter or the earlier UPR PERK-ATF4 pathway, given its ability to specifically inhibit the dephosphorylation of p-eIF2α (Boyce *et al.*, 2005), its capacity to cross the blood brain barrier (Sokka *et al.*, 2007) and its previously demonstrated neuroprotective effect (Nakka *et al.*, 2010). We demonstrated enhancement of the PERK pathway by salubrinal with a previous study showing an increased eIF2αP/eIF2α ratio in cerebral cortex, CA1 and CA3 as well as its ability of improve CA1 outcome 7 days after global ischemia (Anuncibay-Soto *et al.*, 2016).

PERK pathway, through ATF4 activation, has been reported to be a key pathway that links the UPR and autophagy in the resistance of cells to hypoxia (Rzymski *et al.*, 2010, Rzymski *et al.*, 2009). Of note, UPR pathways other than PERK-ATF4 also seem to be involved in the regulation of autophagy, at least modulating the transcription of some

autophagy-related genes (Deegan *et al.*, 2015,B'chir *et al.*, 2013). There is some controversy about the salubrinal effect on the autophagy response. Thus, a number of reports indicates that salubrinal treatment decreases the autophagy response (Ciechomska *et al.*, 2012, Chao *et al.*, 2013), but some reports support that UPR is able to increase the levels of autophagy in response to hypoxia and ER stress (B'chir *et al.*, 2013,Rzymski *et al.*, 2009,Deegan *et al.*, 2015). In fact, ATF4 pathway has been reported to elicit the so called ISR which includes a cytoprotective autophagy (Harding *et al.*, 2008). The different mechanisms involved in ISR seem to depend on the type and intensity of stress stimuli and the cellular environment (Pakos-Zebrucka *et al.*, 2016). In any case, our results support that it is possible to increase autophagy by enhancing the UPR through the PERK-ATF4 pathway up to levels able to eliminate the large P62/SQSTM1 aggregates the neurons of ischemic animals. These facts support our hypothesis that ischemic-induced autophagy in CA1 is itself unable to overcome the ER-stress, and enhancement of the UPR-PERK pathway would provide additional fuel for cell survival.

In this regard, salubrinal treatment decreased the amount of FJ-B positive cells in CA1 48 hours after the insult, giving additional support to our previous results on the neuroprotective effect of UPR-PERK pathway enhancement and indicating that this effect can already be detected 48 h after the treatment. On the other hand, although an overall decrease in the levels of P62/SQSTM1 correlates with a decrease in FJ-B staining, there is no a clear correlation between the amount of P62/SQSTM1 and the amount of FJ-Bstaining between individual cells. This suggests that more than one mechanism is involved in the neuroprotective effect of salubrinal. We think that one of the mechanisms seems to depend on an increase in the autophagy flux since salubrinal induces an increased clearance of P62/SQSTM1 aggregates. We could only demonstrate this neuroprotective effect of salubrinal on CA1, probably because this structure was more damaged by the ischemic insult, but it is probably modulating other structures since salubrinal treatment results in alterations in autophagy activity also in CA3 and Cx. Therefore, this study confirms that enhancement of the autophagy through UPR-PERK

pathway seems to be a putative therapeutic target since it can be modulated after the ischemic insult.

In summary, we conclude that the autophagy response to global ischemia is structure-dependent and hypothesize that some neurons, located mainly in CA1, are unable to elicit a protective autophagy response sufficient to counteract ischemia-induced ER-stress. In addition, salubrinal-induced cell survival to ischemic insult involves an increase in autophagy, revealing novel therapeutic targets to counteract neuronal injury induced by global ischemia

CHAPTER 3

Integrated stress response (ISR) in organotypic hippocampal cultures exposed to oxygen and glucose deprivation.

Background

OGD in an organotypic hippocampal slice culture (OHSC) is a well-established model to provide insight into the mechanisms that underlie stroke (Zamin et al., 2006; Ziemka-Nałecz et al., 2013), one of the most prevalent of human health disorders (Broderick, 2004; Hankey, 2013; Olesen et al., 2012). This model maintains cell architecture and interneuron connections but excludes the more complex parameters of *in vivo* models, such as blood supply and blood brain barrier (Buchs et al., 1993; Cimarosti et al., 2005; Xiang et al., 2000). Selective vulnerability to ischemia in the CA1 hippocampal area, observed in *in vivo* models (Petito et al., 1987; Zhu et al., 2012), is preserved in OHSC under OGD (Gerace et al., 2012). Understanding the mechanisms responsible for the higher vulnerability of CA1 neurons will provide useful targets for developing new therapeutic tools.

Ischemia unbalances the cell homeostasis in many ways (Mehta et al., 2007). One such way is by increasing the cargo of misfolded proteins in the cell – a condition known as ER stress (Hu et al., 2000; Raghubir et al., 2011; Xin et al., 2014). In this condition, the cell ignites the UPR, whose control seems to be crucial for neuronal survival (DeGracia and Montie, 2004; Sanderson et al., 2015; Yang and Paschen, 2016). The pathway mediated by PERK is the earliest of three canonical UPR pathways (Shin et al., 2015), characterized by a general protein synthesis inhibition (PSI) and selective translation of a number of proteins such as ATF4 (Ron and Walter, 2007). One of the hallmarks of this pathway is the phosphorylation eIF2α, whose dephosphorylation is mediated by the phosphatase PP1 (Kojima et al., 2003). Thus, the inhibition of PP1, which agents as salubrinal, is a mechanism of selectively enhancing this pathway (Boyce et al., 2005). Enhancement of this pathway has been reported to result in a neuroprotective effect *in*

vivo against excitotoxic stimuli (Sokka et al., 2007) as well as in focal (Nakka et al., 2010) and global cerebral ischemia (Anuncibay-Soto et al., 2016).

ATF4 is a bZIP transcription factor that promotes the expression of different prosurvival genes, eliciting the integrated stress response (ISR), which may increase the expression of autophagy-related genes (*atg*), anti-oxidant enzyme genes, and genes associated with amino acid metabolism (Harding et al., 2003; Pakos-zebrucka et al., 2016). Autophagy is a highly selective pathway that mediates the lysosomal degradation of damaged, long-lived proteins and organelles in the cell (Bernales et al., 2007; Weidberg et al., 2011; Yang and Klionsky, 2010). The role of autophagy in ischemia is not fully understood (Adhami et al., 2007; Balduini et al., 2009; Sheng and Qin, 2015), but its neuroprotective role in a model of OGD in brain slices seems to be structure-dependent and associated with ER-stress alleviation (Pérez-Rodríguez et al., 2015).

Energy failure, as a consequence of ischemia, causes the release of reactive oxygen species (ROS) and reactive nitrogen species (RNS) that impair the function of lipids, proteins, and nucleic acids. As a result, the affected cell promotes the expression of anti-oxidant enzymes to restore homeostasis. The imbalance between the cellular production of free radicals and the ability of cells to counteract them is referred to as oxidative stress (Radak et al., 2014), which is considered one of the main events that lead to brain damage after cerebral ischemia (Niizuma et al., 2009). Interestingly, although oxygen levels increase after the ischemia due to blood reperfusion, this increase actually exacerbates oxidative stress and contributes to further cell damage (Love, 1999).

The use of OGD models, where the tissue can be returned to normoxic conditions to replicate reperfusion, provide the advantage of analyzing the ISR during OGD and a reperfusion-like (RL) condition. In this study, we report the effect of modulating the UPR-PERK pathway on the ISR, first characterizing the time course of eIF2α phosphorylation and the effect of its enhancement on cell mortality, and the role of autophagy and anti-oxidative response.

Methods

Animals

All animal experiments were carried out in accordance with the ARRIVE guidelines, and the Guidelines of the European Union Council Directive (63/2010/EU) for the use of laboratory animals. The experimental protocols were approved by the Animal Care Committee of the Department of Health Sciences, University of Florence. All efforts were made to reduce the number of animals used.

Organotypic hippocampal slice culture

Hippocampal slice cultures were performed as previously described (Gerace et al., 2012). The brains of 8–10 day old Wistar rats (Harlan, MI, Italy) were rapidly removed, and the hippocampi were dissected. Hippocampal slices were created by cutting transversal sections (420 μm thickness) of hippocampi using a McIlwain tissue chopper (Ted Pella Inc., Altadena, CA, US) in a sterile environment. The hippocampal slices were transferred into a Hanks' balanced salt solution (supplemented with 5 mg/ml glucose and 3.75 μg/ml amphotericin B). They were then placed onto semi porous membrane inserts (30 mm diameter Millicell®, Millipore, Cat. No. PICM03050), four to five slices per insert. Inserts were placed into six-well tissue culture plates, with each well containing 1.2 ml of culture medium. The composition of the culture medium was 50% Eagle's minimal essential medium (MEM, Sigma-Aldrich, Cat. No. M2279), 25% heat-inactivated horse serum and 25% Hank's balanced salt solution (HBSS, Sigma-Aldrich, Cat. No. H9269). The medium was supplemented with 5 mg/ml glucose, 2 mM L-glutamine, and 3.75 mg/ml amphotericin B. Slices were maintained for two weeks at a temperature of 37 °C in a humidified environment with an atmospheric content of 5% CO_2. Culture medium changes were performed three times per week. Before starting the experiment, slice viability was checked under light microscopy, discarding those with symptoms of degeneration.

OGD assays

OGD assays were performed following (Gerace et al., 2012). Membrane inserts containing the slices were transferred to a six-well plate containing serum and glucose

free medium (75% MEM, 25% HBSS, 4 mM L-glutamine, and 3.75 mg/ml amphotericin B). Culture plates were then placed in a hypoxia chamber (Billups-Rothenberg Inc., San Diego, CA, US) filled with 95% N_2 / 5% CO_2 for 30 min at 37 °C. After the OGD period, serum-free and glucose-free medium were replaced for serum-free medium (75% MEM, 25% HBSS, 2 mM L-glutamine, 3.75 mg/ml amphotericin B, and 5 mg/ml glucose) and plates were placed in the incubator at 37 °C in a humidified environment with an atmospheric content of 5% CO_2. Control samples were maintained in all experiments by using parallel inserts maintained in serum-free medium and normoxic conditions.

Experimental conditions

Two sets of experiments were carried out. The first set of experiments tested the neuroprotective effect of 50 μM salubrinal (**Figure 27 A**). The experiment was replicated under different treatments, and cell mortality after 24 h was measured. The treatments were: normoxic conditions (Nmx); 30 min of OGD followed by 24 h in normoxic conditions (RL); 30 min of OGD followed by 24 h in normoxic conditions, with salubrinal present in the medium only during RL (RL-S); and 30 min of OGD followed by 24 h in normoxic conditions with salubrinal present in the medium during both OGD and RL (RL-SS).
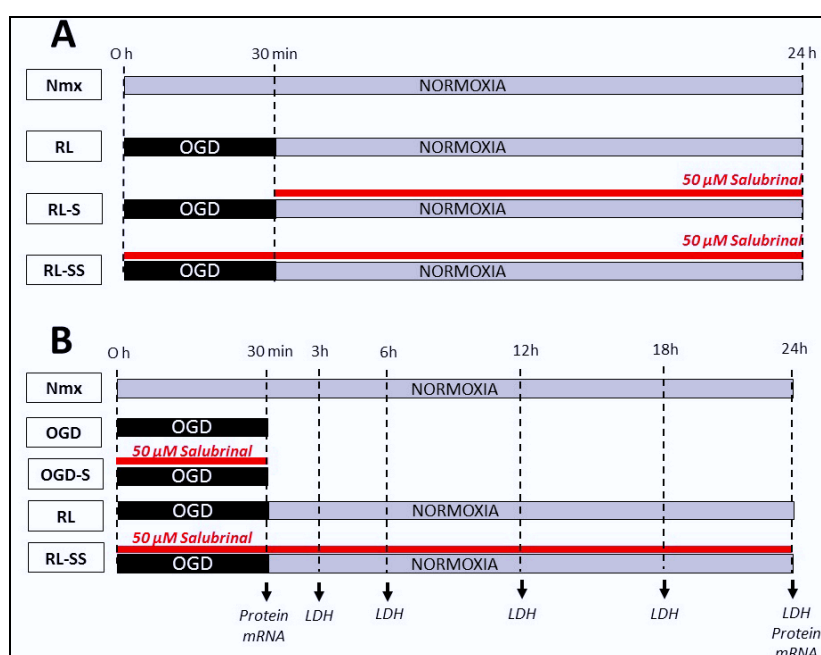

Figure 27. **Experimental conditions**. **A.** Experimental conditions for PI assays to test the salubrinal effect on OGD-induced cell mortality. **B.** Experimental conditions assayed for LDH, mRNA and protein sampling.

Once the neuroprotective effect of salubrinal was assessed, the second set of experiments were carried out to measure the cell mortality at different times after OGD and to analyze the different protein and mRNA markers associated with eIF2α phosphorylation, autophagy, and antioxidant enzymes (**Figure 27 B**). Additionally, the role of autophagy in slice viability was assessed by using 5 mM 3-MA (Acros Organics, Cat. No. 379791000) in the incubation media for 24 hours.

Propidium iodide assessment

The hippocampal slices were incubated for 20 min in 5 mg/ml propidium iodide (PI) in serum-free medium at 37 °C, 24 h after OGD. Fluorescence images (8-bit) were taken using an Olympus IX-50 microscope and a rhodamine filter set (Olympus, Hamburg, Germany). Illumination intensity, detector gain, and exposure time were kept constant between the different experimental conditions to avoid bias in quantification. Fluorescence intensity mean (0-255) in the CA1 pyramidal layer was obtained with ImageJ software (NIH, US). Results were expressed as a percentage of intensity over OGD condition in each experiment.

LDH quantification

Incubation medium samples (30 µl) were obtained at different times after OGD (1, 3, 6, 12, 18, and 24 h) and stored at 4 °C until the experiment had finished. LDH activity was spectrophotometrically quantified with a Cytotoxicity Detection Kit (Roche, Cat. No. 11644793001) following the manufacturer's instructions for use. Absorbance values at 492 nm, obtained in a Synergy-HT spectrophotometer (BioTek, Winooski, VT, US), were expressed as percent over the Nmx condition.

Real-time qPCR assays

To run real-time quantitative PCR assays, hippocampal slices were washed in ice-cold, sterile, PBS and snap-frozen in dry ice. RT-qPCR assays were performed according to the MIQE guidelines. Total RNA was isolated with Tripure® Isolation Reagent (Roche, Cat. No. 11667157001) following the manufacturer's instructions for use. Concentration and purity of RNA samples were analyzed in a NanoDrop ND-2200 spectrophotometer (NanoDrop Technologies, Wilmington, DE, US) and RNA integrity in 1% agarose gel

electrophoresis. Those samples showing low purity and/or integrity levels were discarded.

Equal amounts (600 ng) of each RNA sample were retrotranscripted for 2 h at 37 °C with random primers using a High Capacity cDNA Reverse Transcription Kit (Applied Biosystems, Cat. No. 4368813) following the manufacturer's instructions for use. The RT-qPCR was performed with SYBR Green PCR Master Mix (Applied Biosystems, Cat. No. 4309155) and custom designed oligos (**Table 5**) in a StepOnePlus thermocyler (Applied Biosystems, Foster City, CA, US) with the following cycling conditions: 10 min at 95 °C, 40 cycles of 15 s at 95 °C, and 1 min at 60 °C. Cycle threshold (Ct) values obtained for each gene were normalized with the corresponding Ct value of the housekeeping gene (*gapdh*). Results were expressed as fold change in gene expression relative to the control condition, following the ΔΔCt method (Livak and Schmittgen, 2001).

Table 5. Custom designed oligos used in RT-qPCR assays.

Gene	Primer Forward	Primer Reverse	Gene Bank
beclin1	5´ctgatggtggcaccatgga	5´gccagacatgatgtcaaaaag	NM_053739.2
p62/sqstm1	5' ccatgggtttctcggatgaa	5' ggagggtgctttgaatactgg	NM_175843.3
lc3b	5'ccatgggtttctcggatgaa	5'gtgctgctcccggatgag	NM_001014250.1
atg7	5' cgatggcttcctactgttatt	5' catgacaacaaaggtgbtcaaa	AY_206669.1
gadd34	5'cccccgcccggaat	5' agtgcacctttctacccttcaga	NM_133546.3
Gclm	5' cagtcaaatctggtggcatca	5' gcacaggtaaacccaatagtaatca	NM_017305
nqo1	5' gagtgggattcttctgcgcttct	5' caatgctgtacaccagttgaggtt	NM_017000.3
sod2	5' agcgcctcgtggtacttctc	5' gcacttaacggcgagatca	NM_017051.2
Gapdh	5'gggcagcccagaacatca	5'tgaccttgcccacagcct	NM_017008

Western blot assays

Western blot assays were conducted by washing hippocampal slices in ice-cold PBS and immediately homogenated in 1% SDS. Total protein was quantified with a DC Protein Assay Kit (BioRad, Cat. No. 500-0111) following the manufacturer's instructions for use. Then, 30 μg of each sample were resolved in SDS-PAGE for 2 h at 110 V using a Mini-

Protean II system (BioRad, Hercules, CA, US). Proteins were then transferred to 0.45 μm nitrocellulose membranes with an iBot Gel Transfer System (Invitrogen, Carlsbad, CA, USA). To detect LC3B, proteins resolved in the gel were transferred to 0.2 μm PVDF membranes (BioRad, Cat. No. 1620175). After transference, membranes were blocked with 5% bovine serum albumin (BSA) in 0.2% Tween20 and 50 mM Tris Buffered Saline pH 7.4 (TBS-T) and incubated with primary antibodies (**Table 6**) diluted in 2.5% BSA in TBS-T overnight at 4 °C. The presence of primary antibodies was detected with a chemiluminiscence reaction using HRP-conjugated secondary antibodies (**Table 6**) and Pierce ECL Western Blotting Substrate (Thermo, Cat. No. 32106). Resultant bands were digitalized with a GS-800 calibrated densitometer (BioRad, Hercules, CA, US) and the integrated optical density was calculated with ImageJ. Bands of each experimental condition were normalized against those of the loading control (βACTIN) and the results were expressed as percent over the control condition.

Table 6. Primary and secondary antibodies used.

Protein	Antibody type	Working dilution	Manufacturer	Cat. No.
LC3B	Rabbit polyclonal	1 μg/ml	NOVUS	NB-100-2220
P62/SQSTM 1	Mouse monoclonal	0.5 μg/ml	Abnova	H00008878-M01
BECLIN1	Rabbit polyclonal	1 μg/ml	MBL	PD017
Polyubiquitin	Rabbit polyclonal	1 μg/ml	Dako	Z0458
β-ACTIN	Mouse monoclonal	0.2 μg/ml	Sigma	A5316
Rabbit Ig	Goat polyclonal	0.2 μg/ml	Dako	P0447
Mouse Ig	Goat polyclonal	0.2 μg/ml	Dako	P0448

Protein carbonyl group detection

The oxidative status of protein lysates was assessed with Oxidized Protein Western Blot Kit (Abcam, Cat. No. ab178020) following Abcam's protocol. Carbonyl groups in the side protein chains were derivatized to 2,4-dinitrophenylhydrazone (DNP-hydrazone) by reaction with 2,4-dinitrophenylhydrazine (DNPH). Total protein content was isolated with 50 mM dithiothreitol in an extraction buffer to prevent protein oxidation, and

quantified with the BioRad Protein Assay Kit I (BioRad, Cat. No. 5000001). Next, 20 µg of each protein sample were used in the derivatization reaction. Another 20 µg of the same sample was subjected to the same derivatization without the DNPH reagent, to use as a negative control. The DNP-derivatized protein sample, as well as the negative control, were then separated in SDS-PAGE with a Mini-Protean II system (BioRad, Hercules, CA, US) and transferred to nitrocellulose membranes with an iBot Gel Transfer System (Invitrogen, Carlsbad, CA, USA). DNP-hydrazone was detected by the Western blot technique using specific primary antibody and HRP-conjugated secondary antibody. A chemiolumniscence reaction was performed with Pierce ECL Western Blotting Substrate (Thermo, Cat. No. 32106) and the films that were obtained were digitalized using a GS-800 Calibrated Densitometer (BioRad, Hercules, CA, US).

Statistical analysis

All results are expressed as the mean ± SEM of at least three experiments. Six to eight rat pups were used in each experiment. One-way ANOVA tests, followed by the post-hoc Tukey test, were conducted to test for differences of each parameter in the different experimental treatments. The significance was set at a 95% confidence level. The statistical analyses were carried out using Graph Pad Prism 6.0 (Graph Pad software, San Diego, CA, USA).

Results

Salubrinal effect on OGD-induced cell mortality

The effect of 50 µM of salubrinal on cell mortality was measured 24 h after OGD. The presence of salubrinal during OGD and RL (RL-SS condition) significantly reduced cell mortality, compared with its absence (RL condition). We did not observe any difference in cell mortality under the RL-S condition (**Figure 28 A, B**).

A progressive increase in cell mortality (measured as LDH release) during RL was observed along the time course series, compared with the Nmx condition. The presence of salubrinal seemed to decrease cell mortality (RL-SS condition) and this decrease seemed to be more pronounced in the last eight hours (**Figure 28 C**).
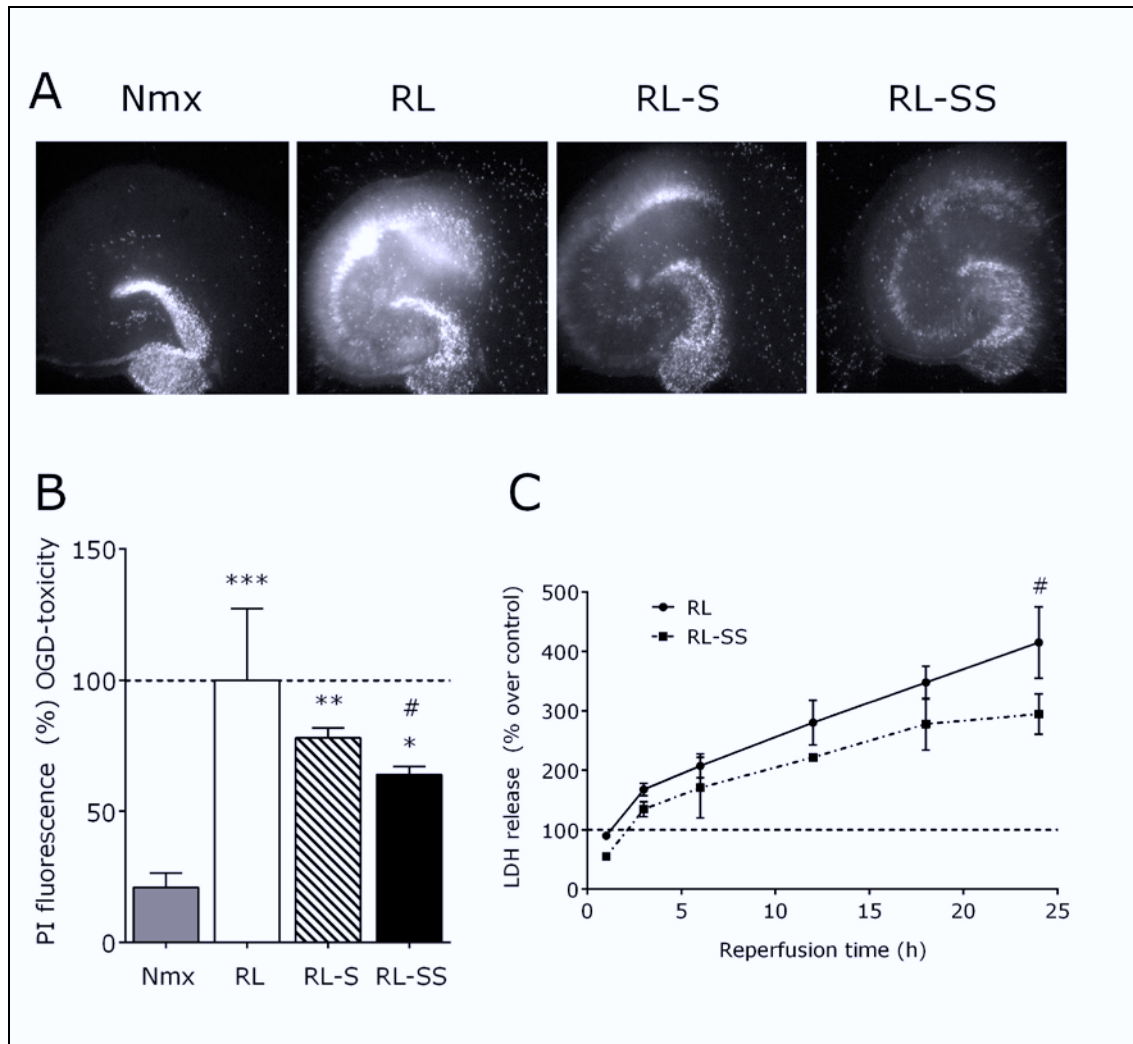
Figure 24. Cell mortality measurement. A. Representative images of PI staining following Nmx and RL conditions with and without salubrinal. **B.** PI intensity values in CA1 hippocampal area in the different experimental conditions. **C.** LDH levels along the RL time in the presence and in the absence of salubrinal. * represents significant differences between RL and Nmx conditions and # between RL and RL-SS conditions. One-way ANOVA followed by Tukey's test. One symbol $p<0.05$, Two symbols $p<0.01$, Three symbols $p<0.001$.

eIF2α phosphorylation and ATF4 pathway activity after OGD and reperfusion

Phosphorylation levels of eIF2α (measured as the ratio p-eIF2 α/eIF2α) presented similar values after 30 min OGD, and in its respective normoxic control. However, this phosphorylation was significantly lower after 24 h of RL. The presence of 50 µM salubrinal in RL (RL-SS) prevented the eIF2α phosphorylation decrease that was observed in RL and shows similar levels in OGD-S than in the OGD condition (**Figure 29 A, B**). Levels of p-eIF2α during OGD showed that, after 20 min, the levels of phosphorylation increase significantly, and the presence of salubrinal enhances the phosphorylation levels (**Figure 29 C**).

Transcript levels of the phosphatase PP1 inducible cofactor (*gadd34*), responsible for the eIF2α dephosphorylation, were significantly higher in OGD and OGD-S than in Nmx conditions. Tissues incubated in the RL condition showed a significant decrease in *gadd34* transcript levels compared to OGD, and similar levels to those of the Nmx conditions. In contrast, tissues in the RL-SS condition showed significantly higher levels with respect to those of the RL condition, and similar levels to those of OGD and OGD-S conditions (**Figure 29 D**).
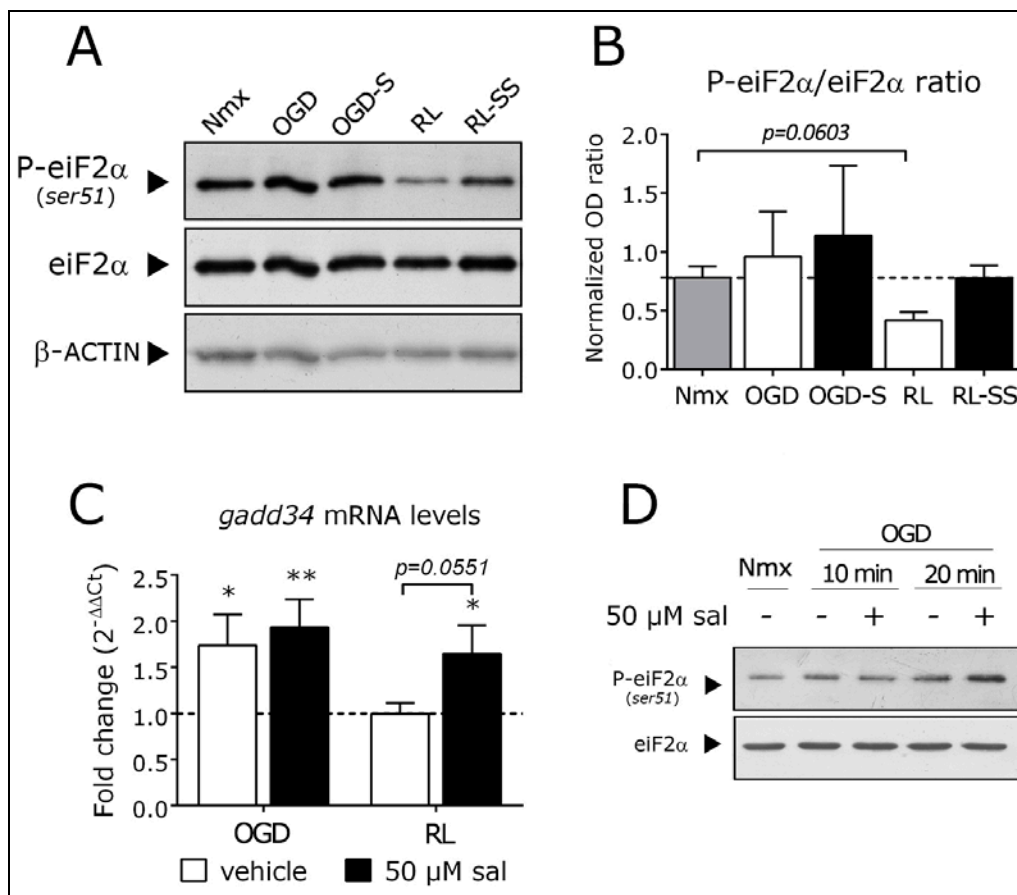

Figure 29. UPR-PERK activation in OGD and RL. A. Representative bands of p-eIF2α and eIF2α in the different experimental conditions assayed. **B**. Optical density ratio between p-eIF2α and eIF2α. **C**. Fold change in *gadd34* mRNA levels in OGD and RL with respect to Nmx condition (dotted line, value 1)**. D.** Representative bands of p-eIF2α after 10 and 20 min of OGD. * represents significant differences between RL and Nmx conditions. One-way ANOVA followed by Tukey's test. One symbol p<0.05, Two symbols p<0.01.

Autophagy activity following OGD and salubrinal treatment

LC3B is a protein widely used for detecting autophagy. The ratio LC3BII/LC3BI, considered one of the main autophagy activity hallmarks, displays a significant increase in the organotypic hippocampal cultured sections compare to fresh non-cultured

sections (**Figure 30 A, B**). The presence of the autophagy inhibitor 3-methyladenine (3-MA) for 24 h elicited high cell mortality in normoxic slices (**Figure 30 C**).
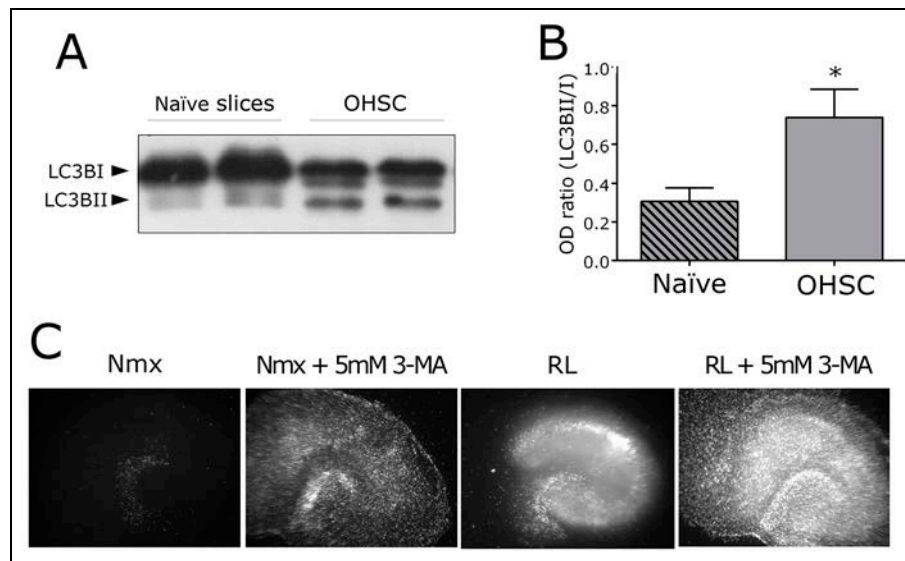

Figure 30. Autophagy levels in OHSC. A. Representative bands of LC3B Western blot comparing freshly obtained slices (naïve) with slices after 14 days in culture (OHSC). **B.** OD values of LC3BII / LC3BI ratio in naïve slices and OHSC. **C.** Slices stained with PI showing the effect of the presence of 3-MA in the incubation media. * represents significant differences between naïve slices and OHSC. Two tailed Student t test, $p<0.05$.

Transcript levels of *beclin1, lc3b, atg7*, and *p62* were not significantly modified by OGD but the presence of salubrinal increased the transcript levels of *beclin1* in the OGD-S condition. The analysis of the RL and RL-SS conditions showed no significant changes in the mRNA levels in any of these genes, both in the presence or absence of salubrinal (**Figure 31 A–D**).

Protein levels of BECLIN1, the ratio LC3BII/LC3B1, P62/SQSTM1 as well as levels of polyubiquitinated proteins presented similar levels in all conditions tested, except for significant increases in Beclin1 observed under the RL-SS treatment (24 h of RL in the tissues incubated in the presence of salubrinal) (**Figure 31 E–H**).
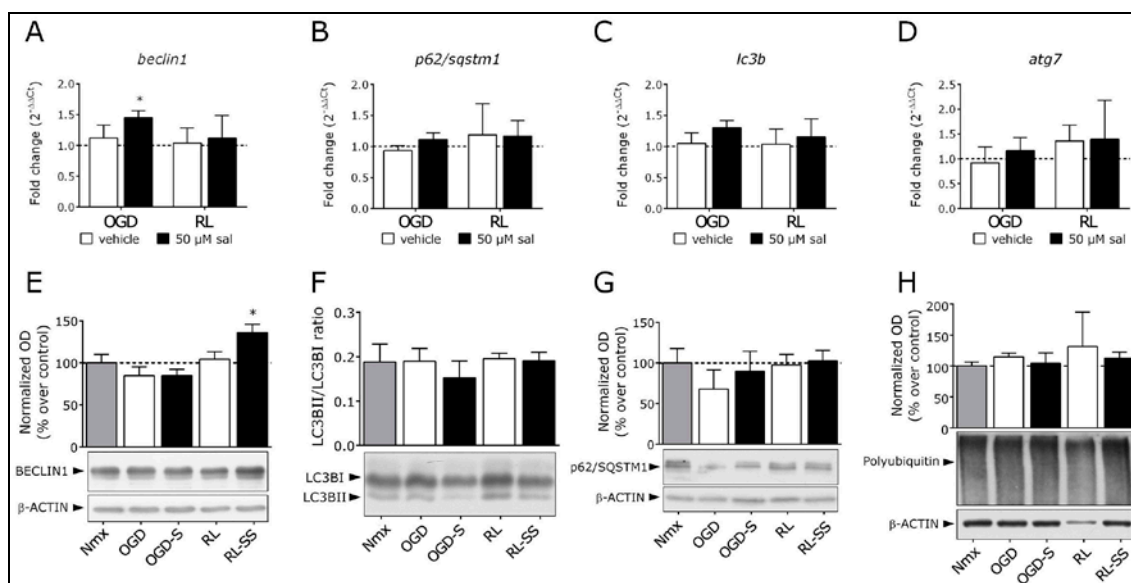
Figure 31. Effect of OGD and salubrinal on autophagy. *Upper part.* Fold change in *beclin1* (**A**)*, p62/sqstm1* (**B**)*, lc3b* (**C**) *and atg7* (**D**) mRNA levels in OGD and RL with respect to Nmx condition (dotted line, value 1). *Lower part.* Protein levels of BECLIN1 (**E**), LC3B (**F**), P62/SQSTM1 (**G**) and polyubiquitin (**H**) in the different experimental conditions. * represents significant differences with respect to Nmx conditions. One-way ANOVA followed by Tukey's test, p<0.05.

Oxidative stress after OGD and salubrinal treatment

In the presence or in absence of salubrinal, OGD does not elicit significant changes in the levels of mRNA of superoxide dismutase (*sod2*), hemoxygenase1 *(hmox1)*, and glutamate-cysteine ligase regulatory subunit *(gclm)* and promotes a non-significant decrease in NAD(P)H quinone dehydrogenase 1 (*nqo1)*. In the RL condition, the expression levels of *sod2*, *hmox1*, and *gclm* presented similar levels to those of the control; however, *nqo1* presented a significant increase in its transcripts levels. Interestingly, in the RL-SS condition, the presence of salubrinal significantly increased the transcript levels in all genes studied (**Figure 33 A–D**). The amount of protein carbonylation, measured as DNP-hydrazone formation in protein lysates, was higher in the RL and RL-SS treatments than that observed in the Nmx condition. The presence of salubrinal decreased the amount of carbonyl groups (RL-SS condition) when compared with the RL condition (**Figure 33 E, arrows**).
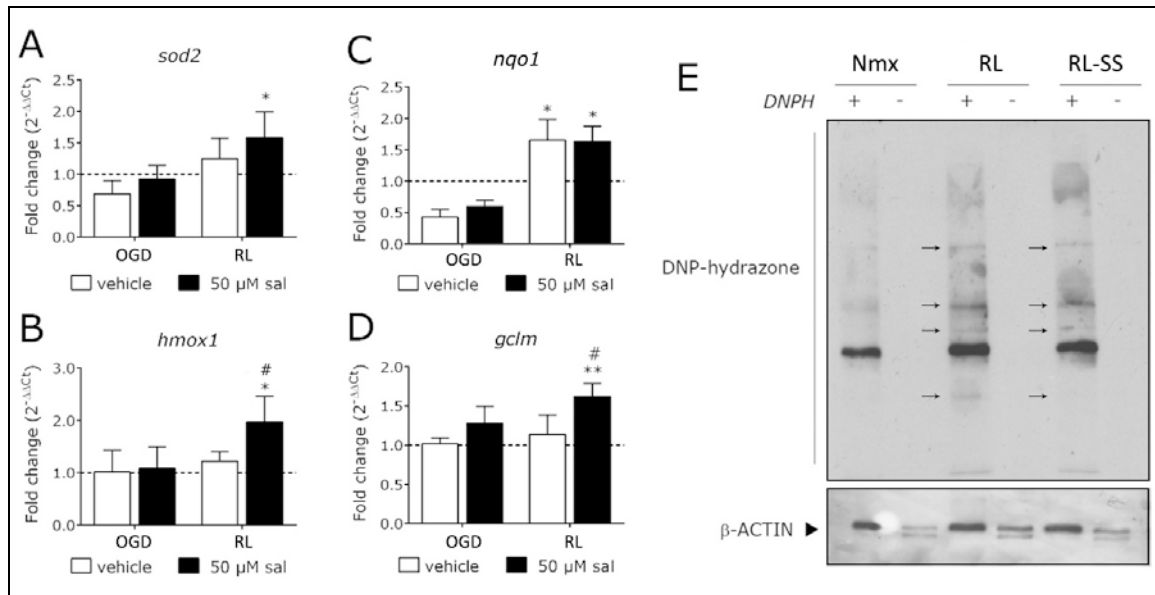
Figure 33. Effect of OGD and salubrinal on oxidative stress. Fold change in s*od2* (**A**), *nqo1 (B)*, *hmox1* (**C**) and *gclm* (**D**) mRNA levels in OGD and RL with respect to Nmx condition (value 1, dotted line). **E.** DNP-hydrazone levels in protein lysates of Nmx, RL and RL-SS. * represents significant differences with respect to Nmx condition and # significant differences with between RL and RL-SS groups. One symbol p<0.05, two symbols p<0.01. One-way ANOVA followed by Tukey's test.

Discussion

eIF2α phosphorylation, ATF4 activation and neuroprotection

Our results suggest that the presence of salubrinal after OGD is able to elicit an neuroprotective effect evidenced by decreased cell mortality. In addition, the early presence of salubrinal during OGD significantly increases the neuroprotective effect. The rapid eiF2α phosphorylation described for ischemia *in vivo* (DeGracia et al., 1999) and for OGD in cell cultures (Badiola et al., 2011) may be responsible for the stronger neuroprotective effect observed by the presence of salubrinal during OGD. Thus, a quick activation of ATF4 seems crucial in preventing cell death and demonstrates the key role of this pathway in the control of cell death.

The time course of eIF2α phosphorylation suggests the presence of a phosphorylation peak about 20 min after onset of OGD, with levels returning to normal 30 min after OGD onset. This peak seems to be increased by the presence of salubrinal, however, this agent cannot prevent the decrease of peIF2α at 30 min after OGD onset.

Consistent with the peak in the peIF2α during OGD, our data show increased *gadd34* transcript levels. ATF4 directly controls the expression of this gene whose product, the PP1 cofactor, has been reported to be responsible for eIF2α dephosphorylation, thus switching off the ATF4 pathway (Ameri and Harris, 2008; Kojima et al., 2003).

All these data show (1) a short activation of ATF4 promoted by a transient Eif2α phosphorylation during OGD, and (2) a long-term decrease on the peIF2α during reperfusion, mediated by the *gadd34* expression elicited by the short OGD-dependent ATF4 activation.

Salubrinal inhibits PP1 activity independently of GADD34 (Boyce et al., 2005). Our data indicate that the effects of salubrinal include the maintenance of eIF2α phosphorylation for at least 24 h of RL. Moreover, the increased *gadd34* expression levels at this time support the notion of a sustained activation of ATF4. Consistently, our data of LDH release in the supernatant show that salubrinal decreases the mortality along the RL period and reveal that its neuroprotective effect increases with time, mainly after 18 h of RL. The data do not, however, explain changes in this last period of RL.

The phosphorylation of eIF2α relies on the activity of four different kinases: GCN2, PKR, HRI and PERK (Pakos-zebrucka et al., 2016). However, PKR is specific for viral infection (García et al., 2007) and HRI is only expressed in erythrocytes (Han et al., 2001). Thus, PERK, which is activated by ER stress (Walter and Ron, 2011), and GCN2, which is activated by amino acid starvation (Bunpo et al., 2009), seem to be the only kinases involved in the OGD response. Although we cannot discard the GCN2 activity in this process, the role of UPR in *in vivo* assays of cerebral ischemia (DeGracia et al., 1999; Kumar et al., 2003; Llorente et al., 2013a; Yang and Paschen, 2016) and cell culture (Ibuki et al., 2012; Vavilis et al., 2016) supports the idea that PERK plays a crucial role in this response. In fact, GCN2 is thought to cooperate with PERK in phosphorylating eIF2α upon UPR activation in PC12 cells (Hamanaka et al., 2005). In addition, the quick PERK activation after 15 min of OGD and its inactivation during the following 15 min in cortical cultures (Badiola et al., 2011) gives additional support to the role of PERK in ATF4 activation. This proves that ER stress is a key therapeutic target to prevent cell damage by ischemia.

The integrated stress response after OGD

Phosphorylation of eIF2α results in a general PSI, allowing the translation of specific mRNAs such as ATF4. Persistent PSI has been reported to occur selectively in CA1 after ischemia, independently of eIF2α (Ayuso et al., 2010; DeGracia et al., 2002). In fact, persistent PSI is considered to be a marker for neurons destined to undergo programmed cell death subroutines in the reperfused brain (White et al., 2000) and we will discuss here the ATF4 downstream ISR which under some stress stimuli would involve cytoprotective autophagy as well as an antioxidant response (Pakos-zebrucka et al., 2016).

Autophagy

Our data did not detect OGD-dependent changes in autophagy in OHSC, contrasting with the increased CA1 autophagy observed in global cerebral ischemia which seems to play a neuroprotective role (Hwang et al., 2016). A high basal autophagy, as a consequence of the experimental procedure of obtaining and culturing brain slices, could mask the effect of OGD in autophagy markers. In this regard, we observed marked increases in LC3BII levels in OHSC compared with fresh hippocampal sections. This increased autophagy seems to be crucial for organotypic culture survival, since the presence of the 3-MA resulted in strong cell death. The use of LY294002, another autophagy inhibitor, has been also reported to increase cell damage in OHSC (Horn et al., 2005). Thus, this study shows how the neuroprotective effect of ATF4 pathway in this model seems to be independent of autophagy levels, in contrast with those observed in other models of hypoxia in cell cultures (Rzymski et al., 2009, 2010).

ATF4 forms homodimers and heterodimers with more than 20 interacting partners and regulates transcription by binding to C/EBP-ATF response element (CARE) sequences. This interaction network is reported to allow the fine-tuning of cell response to several types of stress stimuli (Pakos-zebrucka et al., 2016). Thus, ATF4 is only able to elicit the expression of some autophagy-related genes and other transcription factors are required for a full activation of autophagy (B'Chir et al., 2013; Rzymski et al., 2010). This could explain why the presence of salubrinal increases the expression of some autophagy related proteins such as *beclin1* but not the whole autophagy mechanism.

Oxidative stress

If autophagy does not play a relevant role, which responses mediate the ATF4-induced neuroprotection in this experimental model? ATF4 dimerizes with NRF2, promoting the transcription of a number of phase-2 anti-oxidant enzymes induced by oxidative stress (Cullinan and Diehl, 2006; Dey et al., 2015; He et al., 2001). In fact, UPR-PERK pathways have been demonstrated to activate NRF2, thus coordinating the ER and oxidative stress signalling (Cullinan and Diehl, 2006). In this regard, our data demonstrate that the neuroprotective effect of salubrinal would rely, at least partially, on the stimulation of the levels of a number of NRF2-dependent anti-oxidant enzymes such as GCLM, NQO1 and HMOX1 thus increasing anti-oxidant activity in the cell.

Another antioxidant enzyme that has not been linked so far with NRF2 is SOD2, but there is experimental support for an ATF4-dependent SOD2 increase (Fusakio et al., 2016). This would indicate that OGD-dependent ATF4 activation would elicit anti-oxidative pathways not only related with NRF2.

Our data, indicating an OGD-dependent increase in the oxytidized protein which can be reduced by salubrinal, demonstrate the role of this agent in counteracting oxidative stress, indicating a complementary neuroprotective mechanism. Other agents involved in reducing oxidative stress, such as lipid agents (2 hidroxiarachidonic or DHA) (Belayev et al., 2017; Ugidos et al., 2017) or polyphenols (such as resveratrol) (Dera et al., 2017) have been reported to exert a neuroprotective effect against ischemic damage.

In summary, the OGD-induced eIF2α phosphorylation in the OHSC model presents a quick and short response. In contrast with other hypoxia models, an early enhancement of this phosphorylation promotes a significant neuroprotective effect that seems to be mediated by the ATF4 control of oxidative stress rather than autophagy. Thus, the relevance of the different components of the ISR seem to depend on the cellular context and the experimental model.

CONCLUSIONS

Conclusions

1) Basal levels of autophagy are higher in hippocampal than in cerebral cortical slices, indicating the structure-dependent autophagy.

2) Cerebral cortical slices present OGD-induced increases in both autophagy induction and autophagy flux. The modulation of this response suggests that autophagy plays a neuroprotective role and is responsible for the OGD clearance of polyubiquitinated substrates.

3) Global cerebral ischemia confirms the conclusions obtained in the brain slices model, supporting a neuroprotective role for autophagy in the cerebral cortex that is not raised in the CA1 hippocampal area.

4) CA1 hippocampal autophagy induced by global cerebral ischemia is unable to counteract the ischemia-induced ER stress, as indicated by the presence of sequestosomes.

5) The enhancement of the UPR-PERK pathway increases autophagy activity in both the cerebral cortex and hippocampus, clearing the sequestosomes and indicating the crosslinking between these homeostatic responses.

6) Organotypic hippocampal slice culture increases basal autophagy, which seems to be required for the slice survival.

7) Organotypic hippocampal slice culture deprived of oxygen and glucose present a quick and transient peak in eIF2α phosphorylation, revealing the activation of the UPR-PERK pathway. The inhibition of eIF2α phosphorylation increases this peak.

8) In line with conclusions obtained in the global cerebral ischemia model, the UPR-PERK enhancement results in a neuroprotective effect in organotypic hippocampal slice culture, however, the work window to elicit neuroprotection *ex vivo* is earlier and shorter than that observed in the *in vivo* model.

9) The integrated stress response downstream of the UPR-PERK pathway seems to rely on anti-oxidant activity rather than the autophagy response, suggesting that the relevance of the autophagy depends on the experimental model.

REFERENCES

References

Adhami F., Liao G., Morozov Y. M., Schloemer A., Schmithorst V. J., Lorenz J. N., Dunn R. S., Vorhees C. V., Wills-Karp M., et al. **2006**. Cerebral ischemia-hypoxia induces intravascular coagulation and autophagy. *American J Pathol*. 169(2):566-83.

Adhami F., Schloemer A. and Kuan, C. Y. **2007**. The roles of autophagy in cerebral ischemia. *Autophagy*. 3(1):42-4.

Al Dera H. Neuroprotective effect of resveratrol against late cerebral ischemia reperfusion induced oxidative stress damage involves upregulation of osteopontin and inhibition of interleukin-1beta. J Physiol Pharmacol. 68(1):47-56.

Althausen S., Mengesdorf T., Mies G., Oláh L., Nairn A. C., Proud C. G. and Paschen W. **2001**. Changes in the phosphorylation of initiation factor eIF-2alpha, elongation factor eEF-2 and p70 S6 kinase after transient focal cerebral ischaemia in mice. *J Neurochem*. 78(4):779-87.

Ameri K. and Harris A. L. **2008**. Activating transcription factor 4. *Int J Biochem Cell Biol*. 40(1):14-21.

Anuncibay-Soto B., Pérez-Rodríguez D., Llorente I. L., Regueiro-Purriños M., Gonzalo-Orden J. M. and Fernández-López A. **2014**. Age-dependent modifications in vascular adhesion molecules and apoptosis after 48-h reperfusion in a rat global cerebral ischemia model. *Age*. 36(5):9703.

Anuncibay-Soto B., Pérez-Rodríguez D., Santos-Galdiano M., Font E., Regueiro-Purriños M. and Fernández-López A. **2016**. Post-ischemic salubrinal treatment results in a neuroprotective role in global cerebral ischemia. *J Neurochem*. 138(2):295-306.

Arundine M. and Tymianski M. **2004**. Molecular mechanisms of glutamate-dependent neurodegeneration in ischemia and traumatic brain injury. *Cell Mol Life Sci*. 61(6):657-68.

Ayuso M. I., Garcia-Bonilla L., M. E. Martin, and Salinas M. **2010**. Assessment of protein expression levels after transient global cerebral ischemi a using an antibody microarray analysis. *Neurochem Res*. 35(8):1239-47.

B'chir W., Maurin A. C., Carraro V., Averous J., Jousse C., Muranishi Y., Parry L., Stepien G., Fafournoux P. and Bruhat A. **2013**. The eIF2alpha/ATF4 pathway

is essential for stress-induced autophagy gene expression. *Nucleic Acids Res*. 41(16):7683-99.

Baba M., Osumi M. and Ohsumi Y. **1995**. Analysis of the membrane structures involved in autophagy in yeast by freeze-replica method. *Cell Struct Funct*. 20(6):465–71.

Baba M., Osumi M., Scott S. V., Klionsky DJ. and Ohsumi Y. **1997**. Two distinct pathways for targeting proteins from the cytoplasm to the vacuole/lysosome. *J Cell Biol*. 139(7):1687-95.

Baba M., Takeshige K., Baba N. and Ohsumi Y. **1994**. Ultrastructural analysis of the autophagic process in deast: detection of autophagosomes and their characterization. *J Cell Biol*. 124(6):903-13.

Badiola N., Penas C., Miñano-Molina A., Barneda-Zahonero B., Fadó R., Sánchez-Opazo G., Comella J. X., Sabriá J., Zhu C. et al. **2011** Induction of ER stress in response to oxygen-glucose deprivation of cortical cultures involves the activation of the PERK and IRE-1 pathways and of caspase-12. *Cell Death Dis*. 2(4):e149.

Balduini W., Carloni S. and Buonocore G. **2009**. Autophagy in hypoxia-ischemia induced brain injury: evidence and speculations. *Autophagy*. 5(2):221-23.

Baltan S., Besancon E. F., Mbow B., Ye Z., Hamner M. A. and Ransom B.R. **2008**. White matter vulnerability to ischemic injury increases with age because of enhanced excitotoxicity. *J Neurosci*. 28(6):1479-89.

Baron J. C. **2017**.Mapping the ischaemic penumbra with PET: implications for acute stroke treatment. *Cerebrovasc Dis*. 9(4):193–201.

Beckman J. S., Beckman T. W., Chen J., Marshall P. A., and Freeman B. A. **1990**. Apparent hydroxyl radical production by peroxynitrite: implications for endothelial injury from nitric oxide and superoxide. *Proc Natl Acad Sci U S A*. 87(4):1620–24.

Béjot Y., Daubail B., Sensenbrenner B., Legris N., Durier J. and Giroud M. **2015**. iScore for predicting institutional care after ischemic stroke: a population-based study. *J Stroke Cerebrovasc Dis*. 24(3):694-98.

Belayev L., Mukhuerjee P. K., Balaszczuk V., Calandria J. M., Obenaus A., Khoutorova L., Hong S. H. and Bazan N. G. **2017**. Neuroprotectin D1 upregulates Iduna expression and provides protection in cellular uncompensated oxidative stress and in experimental ischemic stroke. *Cell Death Differ*. 24(6):1091-1099.

Bernales S., Schuck S., and Walter P. **2007**. Selective autophagy of the endoplasmic reticulum. *Autophagy.* 3(3):285-7.

Birch P.J., Rogers H., Hayes A. G., Hayward N. J., Tyers M. B., Scopes D. I., Naylor A. and Judd D. B. **1991**. Neuroprotective actions of GR89696, a highly potent and selective kappa-opioid receptor agonist. *Br J Pharmacol*. 103(3):1819-23.

Bjørkøy G., Lamark T., Brech A., Outzen H., Perander M., Overvatn A., Stenmark H. and Johansen T. **2005**. p62/SQSTM1 forms protein aggregates degraded by autophagy and has a protective effect on huntingtin-induced cell death. *J Cell Biol*. 171(4):603-14.

Bodalia A., Li H. and Jackson M. F. **2013**. Loss of endoplasmic reticulum Ca2+ homeostasis: contribution to neuronal cell death during cerebral ischemia. *Acta Pharmacol Sin*. 34(1):49-59.

Bonapace L., Bornhauser B. C., Schmitz M., Cario G., Ziegler U., Niggli F. K., Schäfer B. W., Schrappe M., Stanulla M. and Bourquin J. P. **2010**. Induction of autophagy-dependent necroptosis is required for childhood acute lymphoblastic leukemia cells to overcome glucocorticoid resistance. *J Clin Invest*. 120(4):1310-23.

Boyce M., Bryant K. F., Jousse C., Long K., Harding H. P., Scheuner D., Kaufman R. J., Ma D., Coen D. M., Ron D. and Yuan J. **2005**. A selective inhibitor of eIF2alpha dephosphorylation protects cells from ER stress. *Science.* 307(5711):935-9.

Broderick J. P. **2004**. William M. Feinberg Lecture: stroke therapy in the year 2025: burden, breakthroughs, and barriers to progress. *Stroke*. 35(1):205-11.

Broussalis E., Killer M., McCoy M., Harrer A., Trinka E. and Kraus J. **2012a**. Current therapies in ischemic stroke. Part A. Recent developments in acute stroke treatment and in stroke prevention. *Drug Discov Today*. 17(7–8):296-309.

Broussalis E., Trinka E., Killer M., Harrer A., McCoy M. and Kraus J. **2012b**. Current therapies in ischemic stroke. Part B. Future candidates in stroke therapy and experimental studies. *Drug Discov Today*. 17(13–14):671-84.

Buchs P. A., Stoppini L. and Muller D. **1993**. Structural modifications associated with synaptic development in area CA1 of rat hippocampal organotypic cultures. *Brain Res*. 71(1):81-91.

Bunpo P., Dudley A., Cundiff J. K., Cavener D. R., Wek R. C. and Anthony T. G. **2009**. GCN2 protein kinase is required to activate amino acid deprivation responses in mice treated with the anti-cancer agent L-asparaginase. *J Biol Chem*. 284(47):32742-9.

Burman C. and Ktistakis N. T. **2010**. Autophagosome formation in mammalian cells. *Semin Immunopathol.* 32(4):397-413.

Carloni S., Buonocore G. and Balduini W. **2008**. Protective role of autophagy in neonatal hypoxia-ischemia induced brain injury. *Neurobiol Dis.* 32(3):329-39.

Carloni S., Girelli S., Scopa C., Buonocore G., Longini M., Balduini W. **2010**. Activation of autophagy and Akt/CREB signaling play an equivalent role in the neuroprotective effect of rapamycin in neonatal hypoxia-ischemia. *Autophagy*. 6(3):366-77.

Carloni S., Albertini M. C., Galluzzi L., Buonocore G., Proietti F. and Balduini W. **2014**. Increased autophagy reduces endoplasmic reticulum stress after neonatal hypoxia-ischemia: role of protein synthesis and autophagic pathways. *Exp Neurol*. 255:103-12.

Cavaglia M., Dombrowski S. M., Drazba J., Vasanji A., Bokesch P. M. And Janigro D. **2001**. Regional variation in brain capillary density and vascular response to ischemia. *Brain Res*. 910(1-2):81-93.

Caudle W. M. and Zhang J. **2009**. Glutamate, excitotoxicity, and programmed cell death in Parkinson disease. *Exp Neurol*. 220(2):230-33.

Chaabane W., User S. D., El-Gazzah M., Jaksik R., Sajjadi E., Rzeszowska-Wolny J. and Los M. J. **2013**. Autophagy, apoptosis, mitoptosis and necrosis: interdependence between those pathways and effects on cancer. *Arch Immunol Ther Exp (Warsz)*. 61(1):43-58.

Chan E. Y. **2012**. Regulation and function of uncoordinated-51 like kinase proteins. *Antioxid Redox Signal*. 17(5):775-85.

Chao, Y.M., Lai, M.D., Chan, J.Y. **2013.** Redox-sensitive endoplasmic reticulum stress and autophagy at rostral ventrolateral medulla contribute to hypertension in spontaneously hypertensive rats. *Hypertension*. 61: 1270-80.

Chapman R., Sidrauski C., and Walter P. **1998**. Intracellular signaling from the endoplasmic reticulum to the nucleus. *Annu Rev Cell Dev Biol*. 14(1):459-85.

Chen J. H., Kuo H. C., Lee K. F. and Tsai T. H. **2015**. Global proteomic analysis of brain tissues in transient ischemia brain damage in rats. *Int J Mol Sci*. 16(6):11873-91.

Ciechomska, I.A., Gabrusiewicz, K., Szczepankiewicz, A.A. and Kaminska, B., **2013**. Endoplasmic reticulum stress triggers autophagy in malignant glioma cells undergoing cyclosporine a-induced cell death. *Oncogene*. 32: 1518-29.

Cimarosti H., Zamin L. L., Frozza R., Nassif M., Horn A. P., Tavares A., Netto C. A. and Salbego C. **2005**. Estradiol protects against oxygen and glucose deprivation in

rat hippocampal organotypic cultures and activates Akt and inactivates GSK-3beta. *Neurochem Res*. 30(2):191-9.

Creutzfeldt C. J. and Holloway R. G. **2012**. Treatment decisions after severe stroke: uncertainty and biases. *Stroke*. 43(12):3405-8.

Cui D. R., Wang L., Jiang W., Qi A. H., Zhou Q. H. and Zhang X. L. **2013**. Propofol prevents cerebral ischemia-triggered autophagy activation and cell death in the rat hippocampus through the NF-κB/p53 signaling pathway. *Neuroscience* 246:117-32.

Cullinan S. B., and Diehl J. A. **2006**. Coordination of ER and oxidative stress signaling: The PERK/Nrf2 signaling pathway. *Int J Biochem Cell Biol.* 38(3):317-332.

Das I., Krzyzosiak A., Schneider K., Wrabetz L., D'Antonio M., Barry N., Sigurdardottir A. and Bertolotti A. **2015**. Preventing proteostasis diseases by selective inhibition of a phosphatase regulatory subunit. *Science.* 348(6231):239-242.

Decker T. and Lohmann-Matthes M. L. **1988**. A quick and simple method for the quantitation of lactate dehydrogenase release in measurements of cellular cytotoxicity and tumor necrosis factor (TNF) activity. *J Immunol Methods*. 115(1):61-69.

Deegan, S., Koryga, I., Glynn, S.A., Gupta, S., Gorman, A.M. and Samali, A. **2015**. A close connection between the PERK and IRE arms of the UPR and the transcriptional regulation of autophagy. *Biochem. Biophys. Res. Commun*. 456: 305-311.

DeGracia D. J., Adamczyk S., Folbe A. J., Konkoly L. L., Pittman J. E., Neumar R. W., Sullivan J. M., Scheuner D., Kaufman R. J., White B. C. and Krause G. S. **1999**. Eukaryotic initiation factor 2alpha kinase and phosphatase activity during postischemic brain reperfusion. *Exp Neurol*. 155(2):221-7.

DeGracia D. J., Kumar R., Owen C. R., Krause G. S. and White, B. C. **2002**. Molecular pathways of protein synthesis inhibition during brain reperfusion: implications for neuronal survival or death. *J Cereb Blood Flow Metab.* 22(2):127-41.

DeGracia D. J. and Montie H. L. **2004**. Cerebral ischemia and the unfolded protein response. *J Neurochem*. 91(1):1-8.

Denton D., Nicolson S. and Kumar S. **2012**. Cell death by autophagy: facts and apparent artefacts. *Cell Death Differ*. 19(1):87-95.

Descloux C., Ginet V., Clarke P. G., Puyal J. and Truttmann A. C. **2015**. Neuronal death after perinatal cerebral hypoxia-ischemia: Focus on autophagy-mediated cell death. *Int J of Dev Neurosci*. 45:75-85.

Deter R. L., Baudhuin P. and De Duve C. **2014**. Participation of lysosomes in cellular autophagy induced in rat liver by glucagon. *J Cell Biol*. 35(2):C11-6.

Devenish R. J. and Klionsky D. J. **2012**. Autophagy: mechanism and physiological relevance 'brewed' from yeast studies. *Front Biosci (Schol Ed)*. 4:1354-63.

Dey S., Sayers C. M., Verginadis I. I., Lehman S. L., Cheng Y., Cerniglia G. J., … Koumenis, C. **2015**. ATF4-dependent induction of heme oxygenase 1 prevents anoikis and promotes metastasis. *J Clin Invest.* 125(7):2592-2608.

Dice J.F., Walker C. D., Byrne B. and Cardiel A. **1978**. General characteristics of protein degradation in diabetes and starvation. Proc Nat Acad Sci U S A. 75(5):2093-97.

Dirnagl U., Iadecola C., and Moskowitz M. A. **1999**. Pathobiology of ischaemic stroke: an integrated view. *Trends Neurosci*. 22(9):391-7.

Dos-Anjos S., Martínez-Villayandre B., Montori S., Salas A., Pérez-García C. C. and Fernández-López A. **2008**. Quantitative gene expression analysis in a brain slice model: influence of temperature and incubation media. *Anal Biochem*. 378(1):99-101.

Dos-Anjos S., Martínez-Villayandre B., Montori S., Pérez-García C. C., and Fernández-López A. **2009**. Early modifications in N-methyl-D-aspartate receptor subunit mRNA levels in an oxygen and glucose deprivation model using rat hippocampal brain slices. *Neuroscience.* 164(3):1119-26.

Dudney T. M. and Elliott C. G. 1994. Pulmonary embolism from amniotic fluid, fat, and air. *Prog Cardiovas Dis*. 36(6):447-74.

Ehara, A. and Ueda, S. **2009**. Application of Fluoro-Jade C in acute and chronic neurodegeneration models: utilities and staining differences*. Acta Histochem. Cytochem*. 42: 171-179.

Eisenberg-Lerner A., Bialik S., Simon H. U. and Kimchi A. **2009**. Life and death partners: apoptosis, autophagy and the cross-talk between them. *Cell Death Differ*. 16(7):966-75.

Eklöf B. and Siesjö B. K. **1972**. The effect of bilateral carotid artery ligation upon the blood flow and the energy state of the rat brain. *Acta Physiol Scand*. 86(2):155-65.

Elkind M. S. **2010**. Inflammatory mechanisms of stroke. *Stroke*. 41(10 Suppl):S3-8.

Eskelinen E. L. **2005**. Maturation of autophagic vacuoles in Mammalian cells. *Autophagy*. 1(1):1-10.

Fakharnia F., Khodagholi F., Dargahi L. and Ahmadiani A. **2017**. Prevention of cyclophilin D-mediated mPTP opening using cyclosporine-A alleviates the elevation of necroptosis, autophagy and apoptosis-related markers following global cerebral ischemia-reperfusion. *J Mol Neurosci*. 61(1):52-60.

Fan, Y., Deng, P., Wang, Y.C., Lu, H.C., Xu, Z.C. and Schulz, P.E. **2008**. Transient cerebral ischemia increases CA1 pyramidal neuron excitability. *Exp. Neurol*. 212, 415-421.

Fass E., Shvets E., Degani I., Hirschberg K. and Elazar Z. **2006**. Microtubules support production of starvation-induced autophagosomes but not their targeting and fusion with lysosomes. *J Biol Chem*. 281(47):36303-16.

Feigin V. L., Mensah G. A., Norrving B., Murray C. J., Roth G. A. and GBD 2013 Stroke Panel Experts Group. **2015**. Atlas of the global burden of stroke (1990-2013): the GBD 2013 study. *Neuroepidemiology*. 45(3):230-36.

Fernández-López D., Martínez-Orgado J., Casanova I., Bonet B., Leza J. C., Lorenzo P., Moro M. A. and Lizasoain I. **2005**. Immature rat brain slices exposed to oxygen-glucose deprivation as an in vitro model of neonatal hypoxic-ischemic encephalopathy. *J Neurosci Methods*. 145(1-2):205-12.

Fisher M. and Bastan B. **2008**. Treating acute ischemic stroke. *Curr Opin Drug Discov Devel*. 11(5):626-32.

Florey O., Kim S. E., Sandoval C. P., Haynes C. M. and Overholtzer M. **2011**. Autophagy machinery mediates macroendocytic processing and entotic cell death by targeting single membranes. *Nat Cell Biol*. 13(11):1335-43.

Fraser P. A. **2011**. The role of free radical generation in increasing cerebrovascular permeability. *Free Radic Biol Med*. 51(5):967-77.

Fujita N., Morita E., Itoh T., Tanaka A., Nakaoka M., Osada Y., Umemoto T., Saitoh T., Nakatogawa H., Kobayashi S., Haraguchi T., Guan J. L., Iwai K., Tokunaga F., Saito K., Ishibashi K., Akira S., Fukuda M., Noda T., Yoshimori T. **2013**. Recruitment of the autophagic machinery to endosomes during infection is mediated by ubiquitin. *J Cell Biol*. 203(1):115-28.

Furuichi T., Liu W., Shi H., Miyake M. and Liu K. J. **2005**. Generation of hydrogen peroxide during brief oxygen-glucose deprivation induces preconditioning neuronal protection in primary cultured neurons. *J Neurosci Res*. 79(6):816-24.

Furuta N., Fujita N., Noda T., Yoshimori T. and Amano A. **2010**. Combinational soluble N-ethylmaleimide-sensitive factor attachment protein receptor proteins VAMP8 and Vti1b mediate fusion of antimicrobial and canonical autophagosomes with lysosomes. *Mol Biol Cell*. 21(6):1001-10.

Fusakio M. E., Willy J. A., Wang Y., Mirek E. T., Al Baghdadi R. J., Adams C. M., Anthony T. G. and Wek R. C. **2016**. Transcription factor ATF4 directs basal and select induced gene expression in the unfolded protein response and cholesterol metabolism in liver. *Mol Biol Cell*. 27(9):1536-51.

Galluzzi L., Bravo-San Pedro J. M., Vitale I., Aaronson S. A., Abrams J. M. et al. **2014**. Essential versus accessory aspects of cell death: recommendations of the NCCD 2015. *Cell Death Differ*. 22(1):58-73.

Galluzzi L., Bravo-San Pedro J. M., Blomgren K. and Kroemer G. **2016**. Autophagy in acute brain injury. *Nat Rev Neurosci*. 17(8):467-84.

Gao C., Cai Y., Zhang X., Huang H., Wang J., Wang Y., Tong X., Wang J. and Wu J. **2015**. Ischemic preconditioning mediates neuroprotection against ischemia in mouse hippocampal CA1 neurons by inducing autophagy. PLoS One. 10(9):1-13.

García M. A., Meurs E. F. and Esteban M. **2007**. The dsRNA protein kinase PKR: Virus and cell control. *Biochimie*. 89(6-7):799-811.

Gardner B. M. and Walter P. **2011**. Unfolded proteins are Ire1-activating ligands that directly induce the unfolded protein response. *Science*. 333(6051):1891-94.

Geeraert C., Ratier A., Pfisterer S. G., Perdiz D., Cantaloube I., Rouault A., Pattingre S., Proikas-Cezanne T., Codogno P. and Poüs C. **2010**. Starvation-induced hyperacetylation of tubulin is required for the stimulation of autophagy by nutrient deprivation. *J Biol Chem*. 285(31):24184-94.

Gerace E., Landucci E., Scartabelli T., Moroni F. and Pellegrini-Giampietro D. E. **2012**. Rat hippocampal slice culture models for the evaluation of neuroprotective agents. *Methods Mol Biol.* 846:343-54.

Ginet V., Puyal J., Clarke P. G. and Truttmann A. C. **2009**. Enhancement of autophagic flux after neonatal cerebral hypoxia-ischemia and its region-specific relationship to apoptotic mechanisms. *Am J Pathol*. 175(5):1962-74.

Gump J. M. and Thorburn A. **2011**. Autophagy and apoptosis: what is the connection?. *Trends Cell Biol*. 21(7):387-92.

Guo Y., Wang J., Wang Z., Yang Y., Wang X. and Duan Q. **2010**. Melatonin protects N2a against ischemia/reperfusion injury through autophagy enhancement. *J Huazhong Univ Sci Technolog Med Sci*. 30(1):1-7.

Hacke W., Kaste M., Fieschi C., Toni D., Lesaffre E., et al. **1995**. Intravenous thrombolysis with recombinant tissue plasminogen activator for acute

hemispheric stroke. The European Cooperative Acute Stroke Study (ECASS). *JAMA.* 274(13):1017-25.

Hamanaka R. B., Bennett B. S., Cullinan S. B. and Diehl J. A. **2005**. PERK and GCN2 contribute to eIF2alfa phosphorylation and cell cycle arrest after activation of the unfolded protein response pathway. *Mol BiolCell*. 16(12):5493-501.

Han A. P., Yu C., Lu L., Fujiwara Y., Browne C., Chin G., Chin G., Fleming M., Leboulch P., Orkin S. H. and Chen J. J. **2001**. Heme-regulated eIF2alpha kinase (HRI) is required for translational regulation and survival of erythroid precursors in iron deficiency. *EMBO J.* 20(23):6909-18.

Hankey G. J. **2013**. The global and regional burden of stroke. *Lancet Glob Health*. 1(5):e239–40.

Hara, T., Nakamura, K., Matsui, M., Yamamoto, A., Nakahara, Y., Suzuki-Migishima, R., Yokoyama M., Mishima, K., Saito, I., Okano, H. and Mizuhima, N. **2006**. Supression of basal autophagy in neural cells causes neurodegenerative disease in mice. *Nature*. 441, 885-889.

Hardie D. G. **2007**. AMP-activated/SNF1 protein kinases: conserved guardians of cellular energy. *Nat Rev Mol Cell Biol*. 8(10):774-85.

Harding H. P., Zhang Y., Zeng H., Novoa I., Lu P. D., Calfon M., Sadri N., Yun C., Popko B., Paules R., Stojdl D. F., Bell J. C., Hettmann T., Leiden J. M. and Ron D. **2003**. An integrated stress response regulates amino acid metabolism and resistance to oxidative stress. *Mol Cell.* 11(3):619-33.

Harding T. M., Morano K. A., Scott S. V. and Klionsky D. J. **1995**. Isolation and characterization of yeast mutants in the cytoplasm to vacuole protein targeting pathway. *J Cell Biol*. 131(3):591-602.

Hatakeyama T., Matsumoto M., Brengman J. M. and Yanagihara T. **1988**. Immunohistochemical investigation of ischemic and postischemic damage after bilateral carotid occlusion in gerbils. *Stroke*. 19(12):1526-34.

He C. H., Gong P., Hu B., Stewart D., Choi M. E., Choi A. M. K. and Alam, J. **2001**. Identification of activating transcription factor 4 (ATF4) as an Nrf2-interacting protein. Implication for heme oxygenase-1 gene regulation. *J Biol Chem*. 276(24):20858-65.

He C. and Klionsky D. J. **2009**. Regulation mechanisms and signaling pathways of autophagy. *Ann Rev Genet*. 43:67-93.

Hetz C. **2012**. The unfolded protein response: controlling cell fate decisions under ER stress and beyond. *Nat Rev Mol Cell Biol*. 13(2):89-102.

Hinzen D. H., Müller U., Sobotka P., Gebert E., Lang R. and Hirsch H. **1972**. Metabolism and function of dog's brain recovering from longtime ischemia. *Am J Physiol*. 223(5):1158-64.

Holen I., Gordon P. B. and Seglen P. O. **1992**. Protein kinase-dependent effects of okadaic acid on hepatocytic autophagy and cytoskeletal integrity. *Biochem J*. 284 (Pt 3):633-6.

Holen I., Gordon P. B. and Seglen P. O. **1993**. Inhibition of hepatocytic autophagy by okadaic acid and other protein phosphatase inhibitors. *Eur J Biochem*. 215(1):113–22.

Horn A. P., Gerhardt D., Geyer A. B., Valentim L., Cimarosti H., Tavares A., Horn F., Lenz G. and Salbego C. **2005**. Cellular death in hippocampus in response to PI3K pathway inhibition and oxygen and glucose deprivation. *Neurochem Res*. 30(3):355-61.

Hossmann K. A. **1993**. Disturbances of cerebral protein synthesis and ischemic cell death. *Prog Brain Res*. 96:161-77.

Hossmann K. A. **1994**. Viability thresholds and the penumbra of focal ischemia. *Ann Neurol*. 36(4):557-65.

Hossmann V. and Hossmann K. A. **1973**. Return of neuronal functions after prolonged cardiac arrest. *Brain Res.* 60(2):423-38.

Hu B. R., Martone M. E., Jones Y. Z. and Liu C. L. **2000**. Protein aggregation after transient cerebral ischemia. *J Neurosci*. 20(9):3191-9.

Huang W. C., Qiao Y., Xu L., Kacimi R., Sun X., Giffard R. G. and Yenari M. A. **2010**. Direct protection of cultured neurons from ischemia-like injury by minocycline. *Anat Cell Biol*. 43(4):325-31.

Hwang J. Y., Gertner M., Pontarelli F., Court-Vazquez, B., Bennett M. V. L. Ofengeim D. and Zukin R. S. **2016.** Global ischemia induces lysosomal-mediated degradation of mTOR and activation of autophagy in hippocampal neurons destined to die. *Cell Death and Diff*. 24(1):1-13.

Ibuki T., Yamasaki Y., Mizuguchi H. and Sokabe M. **2012**. Protective effects of XBP1 against oxygen and glucose deprivation/reoxygenation injury in rat primary hippocampal neurons. *Neurosci Lett*. 518(1):45-8.

Ichimura Y., Kominami E, Tanaka K. and Komatsu M. **2008**. Selective turnover of p62/A170/SQSTM1 by autophagy. *Autophagy*. 4(8):1063-6.

Itakura E., Kishi C., Inoue K. and Mizushima N. **2008**. Beclin 1 forms two distinct phosphatidylinositol 3-kinase complexes with mammalian Atg14 and UVRAG. *Mol Biol Cell*. 19(12):5360-72.

Jackson D. L. and Dole W. P. **1979**. Total cerebral ischemia: a new model system for the study of post-cardiac arrest brain damage. *Stroke*. 10(1):38-43.

Jackson R. J., Hellen C. U. T. and Pestova T. V. **2010**. The mechanism of eukaryotic translation initiation and principles of its regulation. *Nat Rev Mol Cell Bio.*10, 113-127.

Jäger S. Bucci C., Tanida I., Ueno T., Kominami E., Saftig P. and Eskelinen E. L. **2004**. Role for Rab7 in maturation of late autophagic vacuoles. *J Cell Sci*. 117(Pt 20):4837-48.

Jahreiss L., Menzies F. M. and Rubinsztein D. C. **2008**. The itinerary of autophagosomes: from peripheral formation to kiss-and-run fusion with lysosomes. *Traffic*. 9(4):574-87.

Jain A., Lamark T., Sjøttem E., Larsen K. B., Awuh J. A., Øvervatn A., McMahon M., Hayes J. D. and Johansen T. **2010**. p62/SQSTM1 is a target gene for transcription factor NRF2 and creates a positive feedback loop by inducing antioxidant response element-driven gene transcription. *J Biol Chem*. 285(29):22576-91. Jiang X., Mu D., Manabat C., Koshy A. A., Christen S., Täuber M. G., Vexler Z. S. and Ferriero D. M. **2004**. Differential vulnerability of immature murine neurons to oxygen-glucose deprivation. *Exp Neurol*. 190(1):224-32.

Jiang Y., Zhu J., Wu L., Xu G., Dai J., Liu X. **2012**. Tetracycline inhibits local inflammation induced by cerebral ischemia via modulating autophagy. *PLoS One.* 7(11):1-9.

Jin Z., Li Y., Pitti R., Lawrence D., Pham V. C., Lill J. R. and Ashkenazi A. **2009**. Cullin3-based polyubiquitination and p62-dependent aggregation of caspase-8 mediate extrinsic apoptosis signaling. *Cell*. 137(4):721-35.

Jovićević M., Divjak I., Slankamenac P., Jovanović A., Ruzicka S. and Dickov A. **2010**. Non-atherosclerotic arteriopathy as the cause of ischemic stroke among young adults. *Medi Pregl*. 63(5-6):324-32.

Kabat H. and Schadewald M. **1941**. The relative susceptibility of the synaptic terminals and of the perikaryon to arrest of the circulation of the brain. *Am J Pathol*. 17(6):833-840.1.

Kaminskyy V. and Zhivotovsky B. **2012**. Proteases in Autophagy. *Biochim Biophys Acta.* 1824(1):44-50.

Kaneko M., Niinuma Y. and Nomura Y. **2003**. Activation signal of nuclear factor-kappa B in response to endoplasmic reticulum stress is transduced via IRE1 and tumor necrosis factor receptor-associated factor 2. *Biol Pharm Bull*. 26(7):931-5.

Karsy M., Brock A., Guan J., Taussky P., Kalani M. Y., Park M. S. **2017**. Neuroprotective strategies and the underlying molecular basis of cerebrovascular stroke. *Neurosurg Focus.* 42(4):1-15.

Kojima E., Takeuchi A., Haneda M., Yagi A., Hasegawa T., Yamaki K., Takeda K., Akira S., Shimokata K. and Isobe K. **2003**. The function of GADD34 is a recovery from a shutoff of protein synthesis induced by ER stress: elucidation by GADD34-deficient mice. *FASEB J.* 17(11):1573-5.

Kaufman R. J. **1999**. Stress signaling from the lumen of the endoplasmic reticulum: coordination of gene transcriptional and translational controls. *Genes Dev*. 13(10):1211-33.

Kim J., Kundu M., Viollet B. and Guan K. L. **2011**. AMPK and mTOR regulate autophagy through direct phosphorylation of Ulk1. *Nat Cell Biol*. 13(2):132-41.

Kimelberg H. K. **2005**. Astrocytic swelling in cerebral ischemia as a possible cause of injury and target for therapy. *Glia*. 50(4):389-97.

Kirino T. **1982**. Delayed neuronal death in the gerbil hippocampus following ischemia. *Brain Res*. 239(1):57-69.

Klionsky D. J., Abdelmohsen K., Abe A., Abedin M. J., Abeliovich H., et al. **2016**. Guidelines for the Use and Interpretation of Assays for Monitoring Autophagy (3rd Edition). *Autophagy*. 12(1):1-222.

Klionsky D. J., Cregg J. M., Dunn W. A. Jr, Emr S. D., Sakai Y., Sandoval I. V., Sibirny A., Subramani S., Thumm M., Veenhuis M. and Ohsumi Y. **2003**. A unified nomenclature for yeast autophagy-related genes. *Dev Cell*. 5(4):539-45.

Klionsky D. J. **2008**. Autophagy revisited: a conversation with Christian de Duve. *Autophagy*. 4(6):740-3.

Klionsky D. J., Eskelinen E. L. and Deretic V. **2014**. Autophagosomes, phagosomes, autolysosomes, phagolysosomes, autophagolysosomes... wait, I'm confused. *Autophagy*. 10(4):549-51.

Kofler J., Hattori K., Sawada M., DeVries A. C., Martin L. J., Hurn P. D., Traystman R. J. **2004**. Histopathological and behavioral characterization of a novel model of cardiac arrest and cardiopulmonary resuscitation in mice. *J Neurosci Methods*. 136(1):33-44.

Kohno K., Higuchi T., Ohta S., Kohno K., Kumon Y. and Sakaki S. **1997**. Neuroprotective nitric oxide synthase inhibitor reduces intracellular calcium accumulation following transient global ischemia in the gerbil. *Neurosci Lett.* 224(1):17-20.

Komatsu M., Waguri S., Chiba T., Murata S., Iwata J., Tanida I., Ueno T., Koike M., Uchiyama Y., Kominami E. and Tanaka K. **2006**. Loss of autophagy in the central nervous system causes neurodegeneration in mice. *Nature*. 441(7095):880-4.

Kozutsumi Y., Segal M., Normington K., Gething M. J. and Sambrook J. **1988**. The presence of malfolded proteins in the endoplasmic reticulum signals the induction of glucose-regulated proteins. *Nature*. 332(6163):462-4.

Kuma A., Mizushima N., Ishihara N. and Ohsumi Y. **2002**. Formation of the 350-kDa Apg12-Apg5.Apg16 multimeric complex, mediated by Apg16 oligomerization, is essential for autophagy in yeast." *J Biol Chem*. 277(21):18619-25.

Kumar R., Krause G. S., Yoshida H., Mori K. and DeGracia D. J. **2003**. Dysfunction of the unfolded protein response during global brain ischemia and reperfusion. *J Cereb Blood Flow Metab.* 23(4):462-71.

Larsson, E., Lindvall, O. and Kokaia, Z., **2001**. Stereological assessment of vulnerability of immunocytochemically identified striatal and hippocampal neurons after global cerebral ischemia in rats. *Brain Res*. 913: 117-132.

Laurin N., Brown J. P., Morissete J. and Raymond V. **2002**. Recurrent mutation of the gene encoding sequestosome 1 (SQSTM1/p62) in Paget disease of bone. *Am J Hum Genet*. 70(6):1582-88.

Ler C. K. 2015. Hypoxic preconditioning and cell death from oxygen/glucose deprivation co-opt a subset of the unfolded protein response in hippocampal neurons. *Neuroscience*. 310, 306-21

Li H., Gao A., Feng D., Wang Y., Zhang L., Cui Y., Li B., Wang Z. and Chen G. **2014**. Evaluation of the protective potential of brain microvascular endothelial cell autophagy on blood-brain barrier integrity during experimental cerebral ischemia-reperfusion injury. *Trans Stroke Res*. 5(5):618-26.

Li Q., Li H., Roughton K., Wang X., Kroemer G., Blomgren K. and Zhu C. **2010.** Lithium reduces apoptosis and autophagy after neonatal hypoxia-ischemia. *Cell Death Dis*. 1:e56.

Liang C., Lee J. S., Inn K. S., Gack M. U., Li Q., Roberts E.A., Vergne I., Deretic V., Feng P., Akazawa C. and Jung J. U. **2008**. Beclin1-binding UVRAG targets the class C Vps complex to coordinate autophagosome maturation and endocytic trafficking. *Nat Cell Biol*. 10(7):776-87.

Lippai M. and Low P. **2014**. The role of the selective adaptor p62 and ubiquitin-like proteins in autophagy. *BioMed Res Int* 2014:832704.

Liu C., Gao Y., Barrett J. Hu B. **2010**. Autophagy and protein aggregation after brain ischemia. *J Neurochem*. 115(1):68-78.

Liu R., Yuan H., Yuan F. and Yang S. H. **2012**. Neuroprotection targeting ischemic penumbra and beyond for the treatment of ischemic stroke. *Neurol Res*. 34(4):331–37.

Liu Y. and Levine B. **2015**. Autosis and autophagic cell death: the dark side of autophagy. *Cell Death Differ*. 22(3):367-76.

Liu Y., Liu X. J. and Sun D. **2009.** Ion transporters and ischemic mitochondrial dysfunction. *Cell Adh Migr*. 3(1):94-98.

Liu Y., Shoji-Kawata S., Sumpter R. Mm, Wei Y., Ginet V., Zhang L., Posner B., Tran K. A., Green D. R., Xavier R. J., Shaw S. Y., Clarke P. G. H., Puyal J., and Levinea B. **2013.** Autosis is a Na+,K+-ATPase-regulated form of cell death triggered by autophagy-inducing peptides, starvation, and hypoxia-ischemia. *Proc Natl Acad Sci*. 110(51):20364–71.

Livak K. J. and Schmittgen T. D. **2001**. Analysis of relative gene expression data using real-time quantitative PCR and the 2(-Delta Delta C(T)) Method. *Methods*. 25:402-8.

Llorente I. L., Burgin T. C., Pérez-Rodríguez D., Martínez-Villayandre B., Pérez-García C. C. and Fernández-López A. **2013a**. Unfolded protein response to global ischemia following 48 h of reperfusion in the rat brain: the effect of age and meloxicam. *J Neurochem*. 127(5):701-10.

Llorente I. L., Pérez-Rodríguez D., Martínez-Villayandre B., Dos-Anjos S., Darlison M. G., Poole A. V. and Fernández-López A. **2013b**. GABA(A) receptor chloride channels are involved in the neuroprotective role of GABA following oxygen and glucose deprivation in the rat cerebral cortex but not in the hippocampus. *Brain Res*. 1533:141-51.

Lobo A. C., Gomes J. R., Catarino T., Mele M., Fernandez P., Inácio A. R., Bahr B. A., Santos A. E., Wieloch T., Carvalho A. L. and Duarte C. B. **2011**. Cleavage of the vesicular glutamate transporters under excitotoxic conditions. *Neurobiol Dis*. 44(3):292-303.

Love S. **1999**. Oxidative stress in brain ischemia. *Brain Pathol*. 9(1):119-31.

Luccini E., Romei C., Di Prisco S., Raiteri M. and Raiteri L. **2010**. Ionic dysregulations typical of ischemia provoke release of glycine and GABA by multiple mechanisms. *J Neurochem*. 114(4):1074-84.

Luo, T., Liu, G., Ma, H., Lu, B., Xu, H., Wang, Y., Wu, J., Ge, P. and Liang, J. **2014**. Inhibition of autophagy via activation of PI3K/Akt pathway contributes to the protection of ginsenoside Rb1 against neuronal death caused by ischemic insults. *Int. J. Mol. Sci.* 15: 15426-15442.

Ma L., Gao P. Y., Hu Q. M., Lin Y., Jing L. N., Xue J., Chen Z. J., Wang Y. J., Liu M. L. and Cai Y. F. **2011**. Effect of baseline magnetic resonance imaging (MRI) apparent diffusion coefficient lesion volume on functional outcome in ischemic stroke. *Neurol Res* 33(5):494-502.

Matsunaga K., Saitoh T., Tabata K., Omori H., Satoh T., Kurotori N., Maejima I., Shirahama-Noda K., Ichimura T., Isobe T., Akira S., Noda T. and Yoshimori T. **2009.** Two Beclin 1-binding proteins, Atg14L and Rubicon, reciprocally regulate autophagy at different stages. *Nat Cell Biol* 11(4):385-96

Mayer S. A. **2003**. Ultra-early hemostatic therapy for intracerebral hemorrhage. *Stroke* 34(1):224-29.

Mehta S. L., Manhas N. and Raghubir R. **2007.** Molecular targets in cerebral ischemia for developing novel therapeutics. *Brain Res Rev*. 54(1):34-66.

Mijaljica D., Prescott M. and Devenish R.J. **2011**. Microautophagy in mammalian cells: revisiting a 40-year-old conundrum. *Autophagy*. 7(7):673-82.

Miracco C., Cosci E., Oliveri G., Luzi P., Pacenti L., Monciatti I., Mannucci S., De Nisi M. C., Toscano M., Malagnino V., Falzarano S. M., Pirtoli L. and Tosi P. **2007**. Protein and mRNA expression of autophagy gene Beclin 1 in human brain tumours. *Int J Oncol*. 30(2):429-36.

Mizushima N. and Yoshimori T. 2007. How to interpret LC3 immunoblotting. Autophagy. 3(6):542-45.

Montori, S., Dos Anjos, S., Poole, A., Regueiro-Purrinos, M.M., Llorente, I.L., Darlison, M.G., Fernandez-Lopez, A. and Martinez-Villayandre, B. **2012**. Differential effect of transient global ischaemia on the levels of gamma-aminobutyric acid type A (GABA(A)) receptor subunit mRNAs in young and older rats. *Neuropathol. Appl. Neurobiol*. 38, 710-722.

Moreau K., Renna M. and Rubinsztein D.C. **2013**. Connections between SNAREs and autophagy. *Trends Biochem Sci*. 38(2):57-63.

Moro M. A., De Alba J., Leza J. C., Lorenzo P., Fernández A. P., Bentura M. L., Boscá L., Rodrigo J. and Lizasoain I. **1998**. Neuronal expression of inducible nitric oxide synthase after oxygen and glucose deprivation in rat forebrain slices. *Eur J Neurosci*. 10(2):445-56.

Mori K., Sant A., Kohno K., Normington K., Gething M. J. and Sambrook J. F. **1992**. A 22 bp cis-acting element is necessary and sufficient for the induction of the yeast KAR2 (BiP) gene by unfolded proteins. *EMBO J*. 11(7):2583-93.

Morishima N., Nakanishi K. and Nakano A. **2011**. Activating Transcription Factor-6 (ATF6) mediates apoptosis with reduction of Myeloid Cell Leukemia Sequence 1 (Mcl-1) protein via induction of WW domain binding protein 1. *J Biol Chem*. 286(40):35227–35.

Moscat J. and Diaz-Meco M. T. **2012**. p62: a versatile multitasker takes on cancer. Trends *Biochem Sci*. 37(6):230-36.

Mozes E., Hunya A., Posa A., Penke B. and Datki Z. **2012**. A novel method for the rapid determination of beta-amyloid toxicity on acute hippocampal slices using MTT and LDH assays. *Brain Res Bull.* 87(6):521-25.

Murray C. J. **1994**. Quantifying the burden of disease: the technical basis for disability-adjusted life years. *Bull World Health Organ*. 72(3):429-45.

Murray C. J., Vos T., Lozano R., Naghavi M., Flaxman A. D. et al. **2012.** Disability-adjusted life years (DALYs) for 291 diseases and injuries in 21 regions, 1990-2010: a systematic analysis for the Global Burden of Disease Study 2010. *Lancet.* 380(9859):2197-2223.

Nagy P., Hegedus K., Pircs K., Varga A. and Juhász G. **2014.** Different effects of Atg2 and Atg18 mutations on Atg8a and Atg9 trafficking during starvation in Drosophila. *FEBS Lett*. 588(3):408-13.

Nakatogawa H., Ichimura Y. and Ohsumi Y. **2007.** Atg8, a ubiquitin-like protein required for autophagosome formation, mediates membrane tethering and hemifusion. *Cell*. 130(1):165-78.

Nakka V. P., Gusain A. and Raghubir R. **2010**. Endoplasmic reticulum stress plays critical role in brain damage after cerebral ischemia/reperfusion in rats. *Neurotox Res.* 17(2):189-202.

Nickischer D., Laethem C., Trask O. J. Jr., Williams R. G., Kandasamy R., Johnston P. A. and Johnston P. A. **2006**. Development and implementation of three mitogen-activated protein kinase (MAPK) signaling pathway imaging assays to provide MAPK module selectivity profiling for kinase inhibitors: MK2-EGFP translocation, c-Jun, and ERK activation. *Methods Enzymol*. 414:389-418.

Nicole O, Docagne F, Ali C, Margaill I, Carmeliet P, MacKenzie ET, Vivien D, Buisson A. **2001**. The Proteolytic Activity of Tissue-Plasminogen Activator Enhances NMDA Receptor-Mediated Signaling. *Nat Med*. 7(1):59–64

Nihira K., Miki Y., Ono K., Suzuki T. and Sasano H. **2014.** An inhibition of p62/SQSTM1 caused autophagic cell death of several human carcinoma cells. *Cancer Sci.* 105(5):568-75.

Niizuma K., Endo H. and Chan P. H. **2009**. Oxidative stress and mitochondrial dysfunction as determinants of ischemic neuronal death and survival. *J Neurochem*. 109(1):133-8.

Ning M., Furie K. L., Koroshetz W. J., Lee H., Barron M., Lederer M., Wang X., Zhu M., Sorensen A. G., Lo E. H., and Kelly P. J. **2006**. Association between tPA therapy and raised early matrix metalloproteinase-9 in acute stroke. *Neurology*. 66(10):1550-55.

Nitatori T., Sato N., Waguri S., Karasawa Y., Araki H., Shibanai K., Kominami E. and Uchiyama Y. **1995.** Delayed neuronal death in the CA1 pyramidal cell layer of the gerbil hippocampus following transient ischemia is apoptosis. *J Neurosci*. 15(2):1001-11.

Nowicki J. P., Assumel-Lurdin C., Duverger D. and MacKenzie E.T. **1988**. Temporal evolution of regional energy metabolism following focal cerebral ischemia in the rat. *J Cereb Blood Flow Metab*. 8(4):462–73

O'Collins V. E., Macleod M. R., Donnan G. A., Horky L. L., van der Worp B. H. and Howells D. W. **2006**. 1,026 experimental treatments in acute stroke. *Ann Neurol*. 59(3):467-77.

O'Donnell M. J., Chin S. L., Rangarajan S., Xavier D., Liu L. et al. **2016**. Global and regional effects of potentially modifiable risk factors associated with acute stroke in 32 countries (INTERSTROKE): a case-control study. Lancet. 388(10046):761-75.

Ohsumi Y. **2001**. Molecular dissection of autophagy: two ubiquitin-like systems. *Nat Rev Mol Cell Biol*. 2(3):211-16.

Ohsumi Y. **2014**. Historical landmarks of autophagy research. *Cell Res*. 24(1):9-23.

Olesen J., Gustavsson A., Svensson M., Wittchen H. U., Jönsson B., CDBE2010 study group and European Brain Council. **2012**. The economic cost of brain disorders in Europe. *Eur J Neurol*. 19(1):155-62.

Osada N., Kosuge Y., Ishige K. and Ito Y. **2010**. Characterization of neuronal and astroglial responses to ER stress in the hippocampal CA1 area in mice following transient forebrain ischemia. *Neurochem Int*. 57(1):1-7.

Pakos-Zebrucka K., Koryga I., Mnich K., Ljujic M., Samali A. and Gorman A. M. **2016**. The integrated stress response. *EMBO Rep*. 17(10):1-22.

Pankiv S., Lamark T., Bruun J., Øvervatn A., Bjørkøy G. and Johansen T. **2010**. Nucleocytoplasmic shuttling of p62/SQSTM1 and its role in recruitment of nuclear polyubiquitinated proteins to promyelocytic leukemia bodies. *J Biol Chem*. 285(8):5941-53.

Papadakis P., Hadley G., Xilouri M., Hoyte L. C. and Nagel S. **2013**. Tsc1 (Hamartin) confers neuroprotection against ischemia by inducing autophagy. *Nat Med*. 19(3):351-57.

Parés-Badell O., Barbaglia G., Jerinic P., Gustavsson A., Salvador-Carulla L. and Alonso J. **2014** Cost of disorders of the brain in Spain. *PLoS ON*E 9(8):e105471.

Parsons J. T., Churn S. B. and DeLorenzo R. J. **1997**. Ischemia-induced inhibition of calcium uptake into rat brain microsomes mediated by Mg2+/Ca2+ ATPase. J. Neurochem. 68(3):1124-34.

Paschen W., Aufenberg C., Hotop S. and Mengesdorf T. **2003**. Transient cerebral ischemia activates processing of xbp1 messenger RNA indicative of endoplasmic reticulum stress. *J Cereb Blood Flow Metab*. 23(4):449-61.

Pasquier B. **2016**. Autophagy inhibitors. Cell Mol Life Sci. 73(5):985-1001.

Pellegrini-Giampietro, D. E., Zukin R. S., Bennett M. V., Cho S. and Pulsinelli W. A. **1992**. Switch in glutamate receptor subunit gene expression in CA1 subfield of hippocampus following global ischemia in rats. *Proc Natl Acad Sci*. 89(21):10499-503.

Pérez-Rodríguez D., Anuncibay-Soto B., Llorente I. L., Pérez-García C. C. and Fernández-López, A. **2015**. Hippocampus and cerebral cortex present a different autophagic response after oxygen and glucose deprivation in an ex vivo rat brain slice model. *Neuropathol Appl Neurobiol.* 41(4):e68-79.

Petito C. K., Feldmann E., Pulsinelli W. A. and Plum F. **1987**. Delayed hippocampal damage in humans following cardiorespiratory arrest. *Neurology*. 37(8):1281-6.

Petito C. K. and Pulsinelli W. A. **1984**. Sequential development of reversible and irreversible neuronal damage following cerebral ischemia. *J Neuropathol Exp Neurol*. 43(2):141-53.

Pfeifer U. and Strauss P. **1981**. Autophagic vacuoles in heart muscle and liver. a comparative morphometric study including circadian variations in meal-fed rats. J Mol Cell Cardiol. 13(1):37–49.

Pieper A. A., Brat D. J., O'Hearn E., Krug D. K., Kaplin A. I., Takahashi K., Greenberg J. H., Ginty D., Molliver M. E. and Snyder S. H. 2001. Differential neuronal localizations and dynamics of phosphorylated and unphosphorylated type 1 inositol 1,4,5-trisphosphate receptors. *Neurosci.* 102(2):433-44.

Polson H. E., de Lartigue J., Rigden D. J., Reedijk M., Urbé S., Clague M. J. and Tooze S. A. **2010**. Mammalian Atg18 (WIPI2) localizes to omegasome-anchored phagophores and positively regulates LC3 lipidation. *Autophagy*. 6(4):506-22.

Prieto-Arribas R., Moreno-Gutiérrez A., Simal-Hernández P., Pascual-Garvi J. M., Matías-Guiu J., Roda J. M. and Barcia-Albacar J. A. **2008.** Experimental Models of Cerebral Ischemia. *Rev Neurol*. 47(8):414–26.

Prieto-Arribas R., Pascual-Garvi J. M., González-Llanos F. and Roda J. M. **2011**. ¿Cómo reparar el daño cerebral isquémico? Utilidad de los modelos experimentales en la búsqueda de respuestas. *Neurología*. 26(2):65-73.

Pulsinelli W. A. and Brierley J. B. **1979.** A new model of bilateral hemispheric ischemia in the unanesthetized rat. Stroke 10(3):267-72.

Pulsinelli W. A., Brierley J. B. and Plum F. **1982.** Temporal profile of neuronal damage in a model of transient forebrain ischemia. Ann Neurol. 11(5):491-98.

Pundik S., Xu K. and Sundararajan S. **2012.** Reperfusion brain injury focus on cellular bioenergetics. Neurology. 79(13 SUPPL. 1):S44-51.

Putcha G. V., Le S., Frank S., Besirli C. G., Clark K., Chu B., Alix S., Youle R. J., LaMarche A., Maroney A. C. and Johnson E. M. Jr. **2003.** JNK-mediated BIM phosphorylation potentiates BAX-dependent apoptosis. Neuron. 38(6):899-914.

Puyal J. and Clarke P. G. **2009**. Targeting autophagy to prevent neonatal stroke damage. *Autophagy*. 5(7):1060-61.

Qin A. P., Liu C. F., Qin Y. Y., Hong L. Z., Xu M., Yang L., Liu J., Qin Z. H. and Zhang H. L. **2010**. Autophagy was activated in injured astrocytes and mildly decreased cell survival following glucose and oxygen deprivation and focal cerebral ischemia. *Autophagy*. 6(6):738-53.

Radak D., Resanovic I. and Isenovic E. R. **2014.** Link between oxidative stress and acute brain ischemia. *Angiology*. 65(8):667-76.

Raghubir R., Nakka V. P. and Mehta S. L. **2011**. Endoplasmic reticulum stress in brain damage. *Methods Enzymol.* 489:259-75.

Rami A. and Kogel D. **2008**. Apoptosis meets autophagy-like cell death in the ischemic penumbra: Two sides of the same coin? *Autophagy*. 4(4):422-6.

Rami A., Langhagen A. and Steiger S. **2008**. Focal cerebral ischemia induces upregulation of Beclin 1 and autophagy-like cell death. *Neurobiol Dis*. 29(1):132-41.

Rao R. V., Hermel E., Castro-Obregon S., del Rio G., Ellerby L. M., Ellerby H. M. and Bredesen D. E. **2001**. Coupling endoplasmic reticulum stress to the cell death program. Mechanism of caspase activation. *J Biol Chem.* 276(36):33869-74.

Romero-Ramírez L., Nieto-Sampedro M., Barreda-Manso M. A. **2017**. Integrated stress response as a therapeutic target for CNS injuries. *BioMed Res Int.* 2017: 1-7.

Ron D. and Walter P. **2007**. Signal integration in the endoplasmic reticulum unfolded protein response. *Nat Rev Mol Cell Biol.* 8(7):519-29.

Reggiori F., Komatsu M., Finley K. and Simonsen A. **2012**. Autophagy: more than a nonselective pathway. *Int J Cell Biol*. 2012:1-18.

Richard M. J., Saleh T. M., El Bahh B. and Zidichouski J. A. **2010**. A novel method for inducing focal ischemia in vitro. *J Neurosci Methods*. 190(1):20-27.

Ruan Y. W., Han X. J., Shi Z. S., Lei Z. G. and Xu Z. C. **2012**. Remodeling of synapses in the CA1 area of the hippocampus after transient global ischemia. *Neuroscience*. 218:268-77.

Rzymski T., Milani M., Pike L., Buffa F., Mellor H. R., Winchester L., Pires I., Hammond E., Ragoussis I. and Harris, A. L. **2010**. Regulation of autophagy by ATF4 in response to severe hypoxia. *Oncogene*. 29(31):4424-35.

Rzymski T., Milani M., Singleton D. C. and Harris A. L. **2009**. Role of ATF4 in regulation of autophagy and resistance to drugs and hypoxia. *Cell Cycle.* 8(23):3838-47.

Sanderson T. H., Gallaway M. and Kumar R. **2015**. Unfolding the unfolded protein response: unique insights into brain ischemia. *Int J Mol Sci.* 16(4):7133-42.

Sanganalmath S. K., Gopal P., Parker J. R., Downs R. K., Parker J. C. Jr and Dawn B. **2017**. Global cerebral ischemia due to circulatory arrest: insights into cellular pathophysiology and diagnostic modalities. *Mol Cell Biochem.* 426(1-2):111-27.

Sanz L., Sanchez P., Lallena M. J., Diaz-Meco M. T. and Moscat J. **1999**. The interaction of p62 with RIP links the atypical PKCs to NF-κB activation. *EMBO J.* 18(11):3044-53.

Sarkar C., Zhao Z., Aungst S., Sabirzhanov B., Faden A. I. and Lipinski M. M. **2014**. Impaired autophagy flux is associated with neuronal cell death after traumatic brain injury. *Autophagy*. 10(12):2208-22.

Sarnowska, A. **2002**. Application of organotypic hippocampal culture for study of selective neuronal death. *Folia Neuropathol*. 40: 101-106.

Schmidt-Kastner R. **2015**. Genomic approach to selective vulnerability of the hippocampus in brain ischemia-hypoxia. *Neuroscience*. 309:259-79.

Schmued, L.C. and Hopkins, K.J. **2000**. Fluoro-Jade B: a high affinity fluorescent marker for the localization of neuronal degeneration. *Brain Res*. 874: 123-130.

Seglen P. O. and Gordon P. B. **1982**. 3-Methyladenine: specific inhibitor of autophagic/lysosomal protein degradation in isolated rat hepatocytes. *Proc Natl Acad Sci U S A.* 79(6):1889-92.

Seshadri S. and Wolf P. A. **2007**. Lifetime risk of stroke and dementia: current concepts, and estimates from the Framingham Study. *Lancet Neurol*. 6(12):1106-14.

Shanware N. P., Bray K. and Abraham R. T. **2013**. The PI3K, metabolic, and autophagy networks: interactive partners in cellular health and disease. *Annu Rev Pharmacol Toxicol*. 53(1):89-106.

Sheng R. and Qin, Z. **2015**. The divergent roles of autophagy in ischemia and preconditioning. *Acta Pharmacol Sin*. 36(4):411-20.

Shi R., Weng J., Zhao L., Li X. M., Gao T. M. and Kong J. **2012**. Excessive autophagy contributes to neuron death in cerebral ischemia. *CNS Neurosci Ther.* 18(3):250-60.

Siemkowicz E. and Hansen A. J. **1978**. Clinical restitution following cerebral ischemia in hypo-, normo- and hyperglycemic rats. *Acta Neurol Scand*. 58(1):1-8.

Simonsen A. and Tooze S. A. **2009**. Coordination of membrane events during autophagy by multiple class III PI3-kinase complexes. *J Cell Biol*. 186(6):773-82.

Sims N. R. and Muyderman H. **2010**. Mitochondria, oxidative metabolism and cell death in stroke. *Biochim Biophys Acta.* 1802(1):80-91.

Slemmer J. E., Shacka J. J., Sweeney M. I. and Weber J. T. **2008**. Antioxidants and free radical scavengers for the treatment of stroke, traumatic brain injury and aging." *Curr Med Chem*. 15(4):404-14.

Smith M. L., Auer R. N. and Siesjö B. K. **1984**. The density and distribution of ischemic brain injury in the rat following 2-10 min of forebrain ischemia. *Acta Neuropathol.* 64(4):319-32.

Smith C. M., Chen Y., Sullivan M. L., Kochanek P. M. and Clark R. S. **2011**. Autophagy in acute brain injury: feast, famine, or folly?. *Neurobiol Dis*. 43(1):52-59.

Sokka A. L., Putkonen N., Mudo G., Pryazhnikov E., Reijonen S., Khiroug L., Belluardo N., Lindholm D. and Korhonen L. **2007**. Endoplasmic reticulum stress inhibition protects against excitotoxic neuronal injury in the rat brain. *J Neurosci*. 27(4):901-8.

Solcia, E., Sommi, P., Necchi, V., Vitali, A., Manca, R. and Ricci, V. **2014**. Particle-rich cytoplasmic structure (PaCS): identification, natural history, role in cell biology and pathology. *Biomolecules* 4: 848-861.

Stanika, R.I., Winters, C.A., Pivovarova, N.B. and Andrews, S.B. **2010**. Differential NMDA receptor-dependent calcium loading and mitochondrial dysfunction in CA1 vs. CA3 hippocampal neurons. *Neurobiol Dis*. 37, 403-411.

Sternberg S.R. **1983**. Biomedical Image Processing. *Comput. J.* 16: 22-34.

Su J., Zhang T., Wang K., Zhu T. and Li X. **2014**. Autophagy activation contributes to the neuroprotection of remote ischemic perconditioning against focal cerebral ischemia in rats. *Neurochem Res*. 39(11):2068-77.

Suzuki T., Franchi L., Toma C., Ashida H., Ogawa M., Yoshikawa Y., Mimuro H., Inohara N., Sasakawa C. and Nuñez G. **2007**. Differential regulation of caspase-1 activation, pyroptosis, and autophagy via Ipaf and ASC in Shigella-infected macrophages. *PLoS Pathog.* 3(8):e111.

Tajiri S., Oyadomari S., Yano S., Morioka M., Gotoh T., Hamada J. I., Ushio Y. and Mori M. **2004**. Ischemia-induced neuronal cell death is mediated by the endoplasmic reticulum stress pathway involving CHOP. *Cell Death Differ.* 11(4):403-15.

Takeshige K., Baba M., Tsuboi S., Noda T. and Ohsumi Y. **1992**. Autophagy in yeast demonstrated with proteinase-deficient mutants and conditions for its induction. *J Cell Biol.* 119(2):3-8.

Tanida I., Ueno T. and Kominami E. **2004**. LC3 conjugation system in mammalian autophagy. *Int J Biochem Cell Biol*. 36(12):2503-18.

Tanida I., Ueno T. and Kominami E. **2008**. LC3 and autophagy. *Methods Mol Biol*. 445(2):77-88.

Taniuchi S., Miyake M., Tsugawa K., Oyadomari M. and Oyadomari S. **2016.** Integrated stress response of vertebrates is regulated by four eIF2α kinases. *Sci Rep.* 6, 32886.

Tanoue T. and Nishida E. **2002**. Docking interactions in the mitogen-activated protein kinase cascades. *Pharmacol Ther.* 93(2–3):193-202.

Taylor S., Wakem M., Dijkman G., Alsarraj M. and Nguyen M. **2010**. A practical approach to RT-qPCR-publishing data that conform to the MIQE guidelines. *Methods*. 50(4):S1-5.

Thapalia, B.A., Zhou, Z. and Lin, X. **2014**. Autophagy, a process within reperfusion injury: an update. *Int. J. Clin. Exp. Pathol*. 7, 8322-8341.

Thumm M., Egner R., Koch B., Schlumpberger M., Straub M., Veenhuis M. and Wolf DH. **1994**. Isolation of autophagocytosis mutants of *Saccharomyces cerevisiae*." *FEBS Lett.* 349:275c80.

Tirasophon, W., Welihinda A. A. and Kaufman R. J. **1998**. A stress response pathway from the endoplasmic reticulum to the nucleus requires a novel bifunctional protein kinase/endoribonuclease (Ire1p) in mammalian cells. *Genes Dev*. 12(12):1812-24.

Traystman R. J. **2003**. Animal models of focal and global cerebral ischemia." *ILAR J.* 44(2):85-95.

Tsukada M. and Ohsumi Y. **1993**. Isofation and charactization of autophagy-defective mutants of *Saccharomyces cerevisiae*. *FEBS Lett*. 333(1):169-74.

Ugidos IF, Santos-Galdiano M, Pérez-Rodríguez D, Anuncibay-Soto B, Font-Belmonte E, López DJ, Ibarguren M, Busquets X and Fernández-López A. **2017**. Neuroprotective effect of 2-hydroxy arachidonic acid in a rat model of transient middle cerebral artery occlusion. *Biochim Biophys Acta*. doi:10.1016/j.bbamem.2017.03.009

Vavilis T., Delivanoglou N., Aggelidou E., Stamoula E., Mellidis K., Kaidoglou A., Cheva A., Pourzitaki C., Chatzimeletiou K., Lazou A., Albani M. and Kritis, A. **2016**.Oxygen and Glucose Deprivation (OGD) Modulates the Unfolded Protein Response (UPR) and Inflicts Autophagy in a PC12 Hypoxia Cell Line Model. *Cell Mol Neurobiol*. 36(5):701-12.

Vieira, M., Fernandes, J., Carreto, L., Anuncibay-Soto, B., Santos, M., Han, J., Fernandez-Lopez, A., Duarte, C.B., Carvalho, A.L., Santos, A.E. **2014**. Ischemic

insults induce necroptotic cell death in hippocampal neurons through the up-regulation of endogenous RIP3. *Neurobiol Dis*. 68: 26-36.

Viscomi, M.T. and D'Amelio, M. **2012**. The "Janus-faced role" of autophagy in neuronal sickness: focus on neurodegeneration. *Mol Neurobiol*. 46: 513-521.

Vornov J. J., Tasker R. C. and Coyle J. T. **1994**. Delayed protection by MK-801 and tetrodotoxin in a rat organotypic hippocampal culture model of ischemia. *Stroke.* 25(2):457-64-5.

Walter P. and Ron D. **2011**. The unfolded protein response: from stress pathway to homeostatic regulation. *Science*. 334(6059):1081-86.

Wang J. Y., Xia Q., Chu K. T., Pan J., Sun L. N., Zeng B., Zhu Y. J., Wang Q., Wang K. and Luo B. Y. **2011**. Severe global cerebral ischemia-induced programmed necrosis of hippocampal CA1 neurons in rat is prevented by 3-methyladenine: a widely used inhibitor of autophagy. *J Neuropathol Exp Neurol*. 70(4):314-22.

Wang P., Xu T. Y., Wei K., Guan Y. F., Wang X., Xu H., Su D. F., Pei G. and Miao C. Y. **2014**. ARRB1/beta-arrestin-1 mediates neuroprotection through coordination of BECN1-dependent autophagy in cerebral ischemia. *Autophagy.* 10(9):1535-48.

Way S. W., Podojil J. R., Clayton B. L., Zaremba A. Collins T. L., Kunjamma R. B., Robinson A. P., Brugarolas P., Miller R. H., Miller S. D. and PopkoB. **2015**. Pharmaceutical integrated stress response enhancement protects oligodendrocytes and provides a potential multiple sclerosis therapeutic. *Nat Commun.* 6:6532.

Weidberg H., Shvets E., Shpilka T., Shimron F., Shinder V. and Elazar Z. **2010**. LC3 and GATE-16/GABARAP subfamilies are both essential yet act differently in autophagosome biogenesis. *EMBO J*. 29(11):1792-802.

Weidberg H., Shvets E. and Elazar Z. **2011**. Biogenesis and cargo selectivity of autophagosomes. *Annu Rev Biochem*. 80:125-56.

Weis S. N., Toniazzo A. P., Ander B. P., Zhan X., Careaga M., Ashwood P., Wyse A. T., Netto C. A. and Sharp F. R. **2014**. Autophagy in the brain of neonates following hypoxia-ischemia shows sex- and region-specific effects*. Neuroscience.* 256:201-9.

White B. C., Daya A., DeGracia D. J., O'Neil B. J., Skjaerlund J. M., Trumble S., Krause G. S. and Rafols J. A. **1993**. Fluorescent histochemical localization of lipid peroxidation during brain reperfusion following cardiac arrest. *Acta Neuropathol*. 86(1):1-9.

White B. C., Sullivan J. M., DeGracia D. J., O'Neil B. J., Neumar R. W., Grossman L. I., Rafols J. A. and Krause G. S. **2000**. Brain ischemia and reperfusion: molecular mechanisms of neuronal injury. *J Neurol Sci*. 179(S 1-2): 1-33.

Whittingham T. S., Lust W. D. and Passonneau J. V. **1984**. An in vitro model of ischemia: metabolic and electrical alterations in the hippocampal slice. *J Neurosci*. 4(3):793-802.

Wiebking, N., Maronde, E. and Rami, A. **2013**. Increased neuronal injury in clock gene Per-1 deficient-mice after cerebral ischemia. *Curr. Neurovasc Res*. 10, 112-125.

Wu Y. T., Tan H. L., Shui G., Bauvy C., Huang Q., Wenk M. R., Ong C. N., Codogno P. and Shen H. M. **2010**. Dual role of 3-methyladenine in modulation of autophagy via different temporal patterns of inhibition on class I and III phosphoinositide 3-kinase. *J Biol Chem*. 285(14):10850-61.

Wu C. X., Liu R., Gao M., Zhao G., Wu S., Wu C. F. and Du G. H.. **2013**. Pinocembrin protects brain against ischemia/reperfusion injury by attenuating endoplasmic reticulum stress induced apoptosis. *Neurosci Lett*. 546:57-62.

Xiang Z., Hrabetova S., Moskowitz S. I., Casaccia-Bonnefil P., Young S. R., Nimmrich V. C., Tiedge H., Einheber S., Karnup S., Bianchi R. and Bergold P. J. **2000**. Long-term maintenance of mature hippocampal slices in vitro. *J Neurosci Methods.* 98(2):145-54.

Xie Z., Nair U. and Klionsky D. J. **2008**. Atg8 controls phagophore expansion during autophagosome formation. *Mol Biol Cell.* 19(8):3290-98.

Xin Q., Ji B., Cheng B., Wang C., Liu H., Chen X., Chen J. and Bai B. **2014**. Endoplasmic reticulum stress in cerebral ischemia. *Neurochem Int*. 68:18–27.

Xin X. Y., Pan J., Wang X. Q., Ma J. F., Ding J. Q., Yang G. Y. and Chen S. D. **2011**. 2-Methoxyestradiol attenuates autophagy activation after global ischemia. Can J Neurol Sci. 38(4):631-38.

Xu F., Gu J. H. and Qin Z.H. **2012**. Neuronal autophagy in cerebral ischemia. *Neurosci Bull*. 28(5):658-66.

Xu F., Li J., Ni W., Shen Y. W., Zhang X. P. **2013.** Peroxisome proliferator-activated receptor-γ agonist 15d-prostaglandin J2 mediates neuronal autophagy after cerebral ischemia-reperfusion injury. PLoS ONE 8(1):1-10.

Yamashima T. and Oikawa S. **2009.** The role of lysosomal rupture in neuronal death. Prog Neurobiol. 89(4):343-58.

Yang W. and Paschen W. **2016**. Unfolded protein response in brain ischemia: A timely update. *J Cereb Blood Flow Metab.* 36(12):2044-50.

Yang Z. and Klionsky D. J. **2010**. Mammalian autophagy: core molecular machinery and signaling regulation. Curr Opin Cell Biol. 22(2):124-31.

Ye, H., Jalini, S., Zhang, L., Charlton, M. and Carlen, P.L. **2010**. Early ischemia enhances action potential-dependent, spontaneous glutamatergic responses in CA1 neurons. *J. Cereb. Blood Flow Metab*. 30, 555-565.

Yin, B., Liang, H., Chen, Y., Chu, K., Huang, L., Fang, L., Matro, E., Jiang, W. and Luo, B. **2013**. EGB1212 post-treatment ameliorates hippocampal CA1 neuronal death and memory impairment induced by transient global cerebral ischemia/reperfusion. *Am. J. Chin. Med*. 41, 1329-1341.

Young S. K. and Wek R. C. **2016.** Upstream open reading frames differentially regulate genespecific translation in the integrated stress response. J Biol Chem. 291(33):16927-35.

Yu S. and Melia J. **2017.** The coordination of membrane fission and fusion at the end of autophagosome maturation. Curr Opin Cell Biol. 47:92-98.

Zamin L. L., Dillenburg-Pilla P., Argenta-Comiran R., Horn A. P., Simão F., Nassif M., Gerhardt D., Frozza R. L. and Salbego C. **2006**. Protective effect of resveratrol against oxygen-glucose deprivation in organotypic hippocampal slice cultures: Involvement of PI3-K pathway. *Neurobiol Dis.* 24(1):170-82.

Zhang L., Wang T. and Valle D. **2015.** Reduced PLP2 expression increases er-stress-induced neuronal apoptosis and risk for adverse neurological outcomes after hypoxia ischemia injury. Hum Mol Genet. 24(25):7221–26.

Zhang X., Yan H., Yuan Y., Gao J., Shen Z., Cheng Y. et al. **2013a.** Cerebral ischemia-reperfusion-induced autophagy protects against neuronal injury by mitochondrial clearance. Autophagy. 9(9):1321-33.

Zhao G., Zhang W., Li L., Wu S. and Du G. **2014.** Pinocembrin protects the brain against ischemia-reperfusion injury and reverses the autophagy dysfunction in the penumbra area. Molecules 19(10):15786-98.

Zheng C., Han J., Xia W., Shi S., Liu J., Ying W. **2012**. NAD (+) administration decreases ischemic brain damage partially by blocking autophagy in a mouse model of brain ischemia. *Neurosci Lett*. 512(2):67-71.

Zhou L., Wang H. F., Ren H. G., Chen D., Gao F., Hu Q. S., Fu C., Xu R. J., Ying Z. and Wang G. H. **2013**. Bcl-2-dependent upregulation of autophagy by sequestosome 1/p62 in vitro. *Acta Pharmacol Sin*. 34(10):651-56.

Zhu C., Wang X., Xu F., Bahr B. A., Shibata M., Uchiyama Y., Hagberg H. and Blomgren K. **2005**. The influence of age on apoptotic and other mechanisms of cell death after cerebral hypoxia-ischemia. *Cell Death Differ*. 12(2):162-76.

Zhu H., Yoshimoto T., Imajo-Ohmi S., Dazortsava M., Mathiyanan A. and Yamashima T. **2012**. Why are hippocampal CA1 neurons vulnerable but motor cortex neurons resistant to transient ischemia?. *J Neurochem*. 120(4):574-85.

Ziemka-Nałecz M., Stanaszek L. and Zalewska T. **2013**. Oxygen-glucose deprivation promotes gliogenesis and microglia activation in organotypic hippocampal slice culture: Involvement of metalloproteinases. *Acta Neurobiol Exp*. 73(1):130-42.

Zientara-Rytter K. and Suresh S. **2016**. Autophagic degradation of peroxisomes in mammals. *Biochem Soc Trans.* 44(2):431-40.

del Zoppo G., Ginis I., Hallenbeck J. M., Iadecola C., Wang X. and Feuerstein G. Z. **2000**. Inflammation and stroke: putative role for cytokines, adhesion molecules and iNOS in brain response to ischemia. *Brain Pathol*. 10(1):95-112.